



**NTNU – Trondheim**  
Norwegian University of  
Science and Technology

# Modelling of Metocean Conditions for the Purpose of Planning Marine Operations

**Edward Laverton**

Marine Technology

Submission date: July 2015

Supervisor: Sverre Kristian Haver, IMT

Norwegian University of Science and Technology  
Department of Marine Technology



NORWEGIAN UNIVERSITY OF SCIENCE AND TECHNOLOGY

---

MASTER THESIS

MODELLING OF METOCEAN CONDITIONS  
FOR THE PURPOSE OF PLANNING MARINE  
OPERATIONS

---

*Author:*

Edward LAVERTON

*Supervisor:*

Sverre HAVER

July 22, 2015

## Preface

This is a report for a master thesis carried out at the Department for Marine Technology at the Norwegian University of Science and Technology (NTNU). The outline of the thesis (found in appendix A) as well as guidance was conducted by Professor Sverre Haver.

The work which is reported is in essence an establishment of the sea environment in two areas, which is then utilized in order to investigate the possibility of conducting marine operations, among other topics. The first part of the report presents a description of the sea environment, while the second part utilizes some of the first part to investigate certain marine operations.

Almost all of the work is based on a Hindcast data file. These data files have been handed to me by the Norwegian Meteorological Insititue via Professor Sverre Haver. Most of the analysis has been carried out using a software called *MATLAB*, a mathematical computer tool which can effectively handle large data samples such as the Hindcast data.

I would like to thank Professor Sverre Haver for his help and guidance throughout the project. By helping me in situations where I have found the theory and application of this to be difficult I have had the possibility to reach my goals. Furthermore, it has been encouraging to work with him due to his eagerness to conduct frequent guidance meetings and always being available to answer any question at any time. Secondly, I would like to thank my family: my brother, Christian, for all the help regarding *Latex*, my father, Bernard, for helping me with grammar and structure, and my girlfriend, Tone, for being supportive. Thirdly, I would like to thank Professor Sverre Steen for producing and handing me the Response Amplitude Operators at such short notice. Lastly, I would like to thank all my classmates who have helped me solve various issues during both the project thesis and the master thesis.

Edward Laverton

Trondheim, July 22, 2015

## Abstract

The sea conditions of two areas, Haltenbanken and the Barents Sea, have been established in this project. Furthermore, a few cases of marine operations have been evaluated, among other topics.

The first part establishes the sea conditions by creating a so-called Metocean Design Basis. This is a basis for determining the feasibility of e.g. a marine operation. The report focuses on sea states in terms of waves and the duration of good and bad weather windows. Current and wind is neglected. Sea states, in terms of  $H_s$  and  $T_p$ , are presented by scatter diagrams, where tendencies of the sea environment can be observed. It is also described by mathematical models, which have been established through different techniques. The subject of probability and statistics plays a central part in establishing such a report. Extreme sea states have been obtained by using the same mathematical models along with a contour plot. The duration of good and bad weather windows have been established through simple considerations and mathematical distributions. Results show that sea conditions are more severe at Haltenbanken than in the Barents Sea.

The Metocean report constitutes a basis for investigation of marine operations, which is presented in the second part. There are two cases in this part, and the first case investigates limiting conditions in terms of the heave motion of a drill ship. Results are shown in Figure 1, which illustrates the acceptable sea states together with relevant severe sea states. The empty pocket in-between the contour plot and the acceptable values illustrates critical sea states. This has been achieved by establishing the response spectrum, a method which assumes a linear relationship between the waves and the response of the vessel, an assumption which is probably valid for the heave response.

The feasibility of marine operations have been considered by employing the distribution for the duration of the longest good weather windows. Additionally, the feasibility of marine operations have been looked at by simulation. Two different methods were considered, and the one which employs data directly seems to yield the most accurate results. The other method, which employs the distribution of duration of good and bad weather windows, seems to have a potential, and could be improved in further work. Its strength lies in the ability to employ Monte Carlo simulation, while its weakness lies in

its inflexibility of handling different thresholds.

The second case is a study of the roll motion of a vessel. The purpose of the case is to investigate what kind of effect the roll motion of the ship, due to swell sea, has on the usability of good weather windows. Results are given in Figure 2. These show a drastic reduction in the average duration of good weather windows due roll motion caused by swell sea. Reductions seem too significant, and this is most likely because the damping of the roll motion is not sufficiently incorporated in the analysis. Although the results are probably not sufficiently accurate, they show that the swell sea has a significant effect on weather conditions which otherwise are considered as more than suitable. This could possibly confirm that the swell sea should be given more attention during the process of planning of a marine operation.

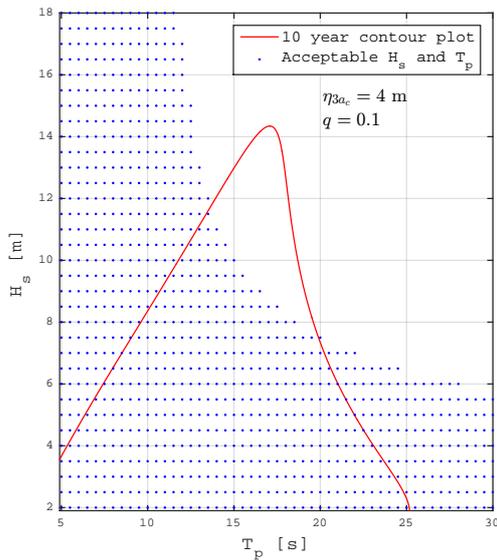


Figure 1: Acceptable sea states for drill ship

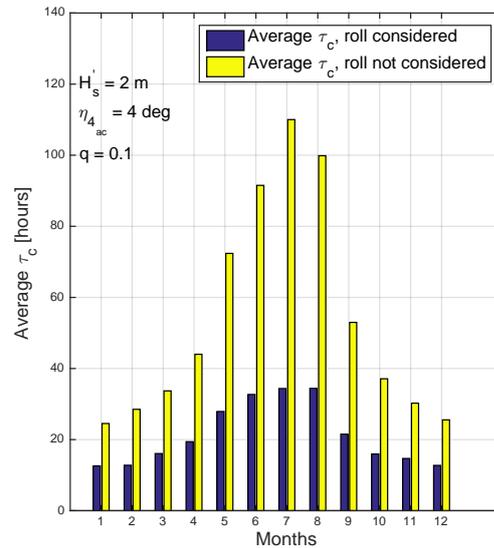


Figure 2: Usability of good weather windows

## Sammendrag

En beskrivelse av havmiljøene i Haltenbanken og Barentshavet har blitt produsert i dette prosjektet. I tillegg har forskjellige marine operasjoner blitt analysert, blant annet ved bruk av denne havmiljøbeskrivelsen.

Havmiljøbeskrivelsen, som er presentert i del én, har sitt fokus på bølger og varighet av gode og dårlige værvinduer. Strømninger og vind er ikke tatt med. Sjøtilstander, gitt ved  $H_s$  og  $T_p$ , er presentert ved tabeller. Disse tabellene kan gi et godt overblikk over karakteristikken til sjøtilstanden i et område. Det har også blitt etablert sannsynlighetsfordelinger (matematiske modeller) som beskriver sjøtilstanden. Forskjellige metoder har blitt brukt, deriblant "Method of Moments". Sannsynlighet og statistikk spiller en viktig rolle ved etableringen av en slik havmiljøbeskrivelse. Ekstreme sjøtilstander har blitt estimert ved bruk av sannsynlighetsfordelinger og contour plott. Varigheten av gode og dårlige værvinduer har blitt etablert. Dette har også blitt modellert ved en sannsynlighetsfordeling. Alle resultater viser at forholdene er mer vanskelig i Haltenbanken enn i Barentshavet.

Denne havmiljøbeskrivelsen utgjør en basis for å vurdere utførelsen av marine operasjoner. Slike vurderinger er presentert i del to. Først ble det sett på en case med et drillskip, hvor målet var å estimere begrensende sjøtilstander for skipet. En øvre terskel for hivbevegelsen ble satt, og ved hjelp av responsspekter-metoden ble akseptable sjøtilstander etablert. Disse er plottet sammen med et contour plot, se Figur 3, som viser relevante og vanskelige sjøtilstander, en såkalt 10-års sjøtilstand. Mellom de akseptable sjøtilstandene og denne finnes de kritiske sjøtilstandene for skipet.

Gjennomførbarheten av generiske marine operasjoner har blitt sett på ved å bruke fordelingen til det lengste gode værvinduet. På denne måten har det blitt produsert tabeller med forskjellige terskler og varighet av operasjon som gir et sannsynlighetsestimat på gjennomførbarheten. Videre har gjennomførbarheten av operasjoner blitt sett på ved bruk av simulering. Den ene metoden bruker sannsynlighetsfordelingene for varighet av gode og dårlige værvindu sammen med Monte Carlo-simulering. Denne metoden er interessant og utradisjonell. Den har en styrke ved at den kan simulere mange operasjoner, og en svakhet ved at det er vanskelig å simulere en operasjon med forskjellige terskler.

Den andre metoden bruker hindcast data direkte. Det vil si at den går igjennom all data og simulerer hvordan en operasjon ville utfoldet seg. Begge metodene gir et estimat på en gjennomsnittlig varighet av operasjon, avhengig av måned.

Til slutt ble det sett på rullebevegelsen til et skip på grunn av dønningsjø. Dette fordi det har vist seg at dønningsjø kan skape store problemer selv om sjøtilstanden totalt sett er antatt å være god. Resultatene er illustrert i Figur 4. Denne viser at gjennomsnittlig varighet av gode værvinde har blitt mer enn halvert. Dette resultatet er nok for stort, og dette er meget sannsynlig på grunn av at rulledemping ikke blir godt nok estimert ved bruk av metoden som ble brukt, nemlig responspekter-metoden. Denne metoden antar et lineært forhold mellom bølger og respons, noe som ikke stemmer godt nok for rullebevegelsen. Uansett, så viser resultatene en så sterk tendens at rullebevegelsen på grunn av dønningsjø bør vurderes videre, gjerne i et dataprogram hvor en kan ta godt nok hensyn til rulledemping.

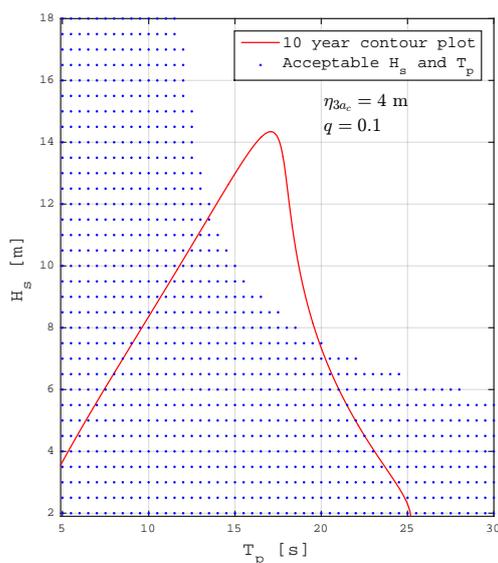


Figure 3: Akseptable sjøtilstander for drillskip

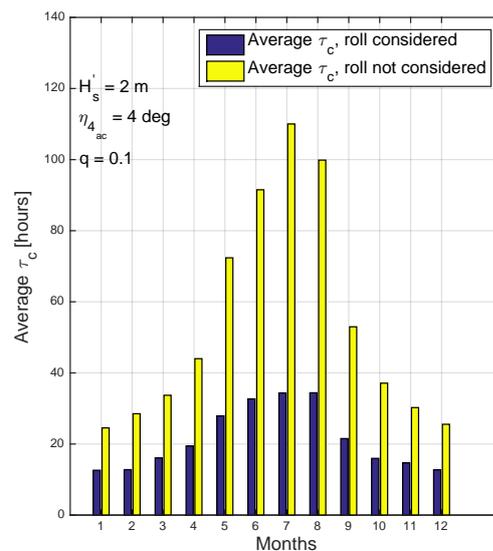


Figure 4: Brukbarheten av gode værvinde med rullebevegelse på grunn av dønningsjø tatt i betraktning

# Contents

Nomenclature	ix
List of Tables	xiii
List of Figures	xv
1 Introduction	1
2 Metocean Design Basis	3
2.1 Work prior to the master thesis . . . . .	3
2.2 What is a Metocean Design Basis, why do we need it, and how is it produced? . . . . .	3
2.3 Data, Hindcasting and Scatter Diagrams . . . . .	4
2.3.1 Some relevant definitions: wave spectrum, significant wave height and spectral peak period . . . . .	5
2.3.2 Modification of data . . . . .	7
2.3.3 Scatter Diagram . . . . .	9
2.3.4 Directional Scatter Diagrams . . . . .	10
2.4 Long Term Joint Distribution of $H_s$ and $T_p$ . . . . .	11
2.4.1 Establishing parameters . . . . .	14
2.4.2 Monthly long term <i>JPDF</i> 's . . . . .	16
2.5 Monthly marginal distributions of $H_s$ . . . . .	17
2.6 Extreme Sea States . . . . .	24
2.7 Determining extreme response by a contour plot . . . . .	28
2.8 Duration of good and bad weather windows . . . . .	33
2.8.1 Average Duration of Calms . . . . .	33
2.8.2 Average Duration of a Storm . . . . .	40
2.8.3 Describing the duration of calms and storms by a 2-parameter Weibull distribution . . . . .	40
3 Marine Operations	54
3.1 Establishing a limiting pair of $H_s$ and $T_p$ from a critical heave motion . .	54
3.1.1 Background . . . . .	54

3.1.2	Theory . . . . .	55
3.1.3	Case . . . . .	61
3.1.4	Results and Discussion . . . . .	67
3.2	Assessing the feasibility of a marine operation by using the distribution of the longest calm . . . . .	73
3.2.1	Theory and examples . . . . .	73
3.2.2	$P[\tau_{c_{max}} > t]$ for various values of $H'_s$ and $t$ . . . . .	77
3.3	Assessing the feasibility of a generic marine operation by simulation . .	80
3.3.1	Utilizing the distributions of the duration of calms and storms and Monte Carlo simulation . . . . .	80
3.3.2	Utilizing the Hindcast data directly . . . . .	82
3.3.3	Comments . . . . .	87
3.4	Rolling, a challenge in marine operations . . . . .	88
3.4.1	Background . . . . .	88
3.4.2	Roll damping and roll stabilization equipment . . . . .	89
3.4.3	Case . . . . .	95
4	Conclusion	110
5	Recommendations for Further Work	112
	References	113
	Appendices	i
A	Outline of Master Thesis	i
B	Response Amplitude Operators	v
B.1	RAO, heave, drill ship . . . . .	vi
B.2	RAO, roll, PSV . . . . .	vii
C	Matlab scripts	viii
D	Flowcharts for <i>MATLAB</i> scripts	ix

D.1	Flowchart for feasibility of marine operation by distribution of longest calm . . . . .	ix
D.2	Flowchart for <i>mar_op_weibull.m</i> . . . . .	x
D.3	Flowchart for <i>rolling_calm.m</i> . . . . .	xi
E	Confidence Interval	xii
F	Scatter Diagrams	xiii

# Nomenclature

## Acronyms & Abbreviations:

ALS	Accidental Limit State
CDF	Cumulative distribution function
DSM	Design Spectrum Method
DWM	Design Wave Method
IFORM	Inverse First Order Reliability Method
JPDF	Joint probability distribution function
PSV	Platform Supply Vessel
PDF	Probability distribution function
RAO	Response Amplitude Operator
ULS	Ultimate Limit State

## Greek Symbols:

$\delta$	2 parameter Weibull scale parameter
$\gamma$	2 parameter Weibull shape parameter
$\eta_{3ac}$	Critical heave amplitude
$\eta_{4ac}$	Critical roll amplitude
$\rho$	Density of water
$\eta_3$	Displacement in heave
$\eta_4$	Displacement in roll
$\tau_c$	Duration of a calm

$\tau_s$	Duration of a storm
$\omega$	Frequency
$\Gamma$	Gamma function
$\eta_{3a}$	Heave amplitude
$\theta$	Lognormal location parameter
$\alpha$	Lognormal scale parameter
$\eta$	LoNoWe parameter
$\mu$	Mean value
$\eta_{4a}$	Roll amplitude
$\phi_A$	Roll amplitude
$\omega_p$	Spectral peak frequency
$\sigma$	Standard deviation
$\sigma^2$	Variance
$\lambda$	Wave length
$\lambda$	Weibull location parameter
$\rho$	Weibull scale parameter
$\beta$	Weibull shape parameter

### **Symbols:**

$A_{44}$	Added mass moment in roll
$q$	Annual exceedance probability
$b_{BK}$	Breadth of bilge keel
$G$	Centre of gravity

$a_1$	coefficient in eq. for determining mean of lognormal distribution
$a_2$	coefficient in eq. for determining mean of lognormal distribution
$a_3$	coefficient in eq. for determining mean of lognormal distribution
$b_1$	coefficient in eq. for determining variance of lognormal distribution
$b_2$	coefficient in eq. for determining variance of lognormal distribution
$b_3$	coefficient in eq. for determining variance of lognormal distribution
$K_{ta}$	Coefficient in eq. of moment, due to anti roll tank
$F$	Cumulative distribution function
$B_{BK}$	Damping due to bilge keel
$B_{44}$	Damping in roll
$C_P$	Distribution of pressure difference coefficient
$d$	Draft
$F_4$	Excitation moment, roll
$E$	Expected value
$g$	Gravitational acceleration
$B_{BKH}$	Hull pressure damping due to bilge keel
$r$	Mean distance from G to to bilge keel
$l_0$	Moment lever
$I_{44}$	Moment of inertia
$m_n$	n'th spectral moment
$B_{BKN}$	Normal force damping of bilge keel
$N$	Number of zero up-crossing cycles during 3 hours

$f$	Probability distribution function
$P$	Probability
$S_{\eta_3}$	Response spectrum for heave
$S_{\eta_4}$	Response spectrum for roll
$I_{44}$	Restoring coefficient
$H_s'$	Significant wave height threshold
$H_s$	Significant wave height
$T_p$	Spectral peak period
$STD$	Standard deviance
$VAR$	Variance
$f$	Velocity increment ratio
$B_{BKW}$	Wave damping of bilge keel
$k$	Wave number
$T$	Wave period
$S$	Wave Spectrum
$T_{m02}$	Zero up-crossing period

## List of Tables

1	Omnidirectional Scatter Diagram for Haltenbanken . . . . .	10
2	Unidirectional Scatter Diagram, sector 1(north), $-15^\circ$ to $15^\circ$ , for Haltenbanken . . . . .	12
3	Estimated parameters in connection with establishing long term <i>JPDF</i> of $H_s$ and $T_p$ . . . . .	16
4	Monthly long term <i>JPDF</i> 's . . . . .	18
5	Moments of a distribution . . . . .	19
6	Estimated parameters for monthly marginal distributions of $H_s$ . . . . .	21
7	Extreme Values of $H_s$ from LoNoWe Distribution . . . . .	27
8	Monthly Extreme Values of $H_s$ from 3-parameter Weibull distribution . . . . .	27
9	Extreme Values of $H_s$ from 3-parameter Weibull distribution . . . . .	27
10	Table found in Nielsen [24, p. 31]: Approximate operational limits for some marine operations . . . . .	34
11	Values of $H_s$ for 1959, sorted by month . . . . .	36
12	Cumulative Distribution Function of Calms . . . . .	46
13	Comparing results from data and Weibull, parameters found by probability plot . . . . .	46
14	Comparing results from data and Weibull, parameters found by Method of Moments . . . . .	49
15	Estimated parameters for monthly distributions of the duration of a calm, $\tau_c$ . . . . .	51
16	Estimated parameters for monthly distributions of the duration of a storm, $\tau_s$ . . . . .	52
17	Definition of Response Amplitude Operator . . . . .	64
18	$P[\tau_{c_{max}} > t]$ , threshold value $H'_s = 1\text{m}$ . . . . .	78
19	$P[\tau_{c_{max}} > t]$ , threshold value $H'_s = 1.5\text{m}$ . . . . .	78
20	$P[\tau_{c_{max}} > t]$ , threshold value $H'_s = 2\text{m}$ . . . . .	79
21	$P[\tau_{c_{max}} > t]$ , threshold value $H'_s = 2.5\text{m}$ . . . . .	79
22	$P[\tau_{c_{max}} > t]$ , threshold value $H'_s = 3\text{m}$ . . . . .	79
23	Simulations of generic operation, constant threshold $H'_s$ , 10 000 simulations . . . . .	82

24	Simulation of generic operation, two intervals, two thresholds . . . . .	86
25	Simulation of generic operation, constant threshold $H'_s$ . . . . .	86
26	Average values of standard deviation of roll due to swell sea. $\eta_{4ac} = 4^\circ$ .	99
27	Distribution of adjusted swell angles for large values of $\sigma_{\eta_4}$ . . . . .	108
28	Omni Directional Scatter Diagram for Haltenbanken . . . . .	xiv
29	Omni Directional Scatter Diagram for Barents Sea . . . . .	xv
30	Scatter Diagram, sector 1(north), $-15^\circ$ to $15^\circ$ , for Haltenbanken . . . . .	xvi
31	Scatter Diagram, sector 7(south), $165^\circ$ to $195^\circ$ , for Haltenbanken . . . . .	xvii
32	Scatter Diagram, sector 4(east), $75^\circ$ to $105^\circ$ , for Haltenbanken . . . . .	xviii
33	Scatter Diagram, sector 10(west), $235^\circ$ to $265^\circ$ , for Haltenbanken . . . . .	xix
34	Scatter Diagram, sector 1(north), $-15^\circ$ to $15^\circ$ , for Barents Sea . . . . .	xx
35	Scatter Diagram, sector 7(south), $165^\circ$ to $195^\circ$ , for Barents Sea . . . . .	xxi
36	Scatter Diagram, sector 4(east), $75^\circ$ to $105^\circ$ , for Barents Sea . . . . .	xxii
37	Scatter Diagram, sector 10(west), $235^\circ$ to $265^\circ$ , for Barents Sea . . . . .	xxiii

## List of Figures

1	Acceptable sea states for drill ship . . . . .	iii
2	Usability of good weather windows . . . . .	iii
3	Akseptable sjøtilstander for drillskip . . . . .	v
4	Brukbarheten av gode værvinduer med rullebevegelse på grunn av dønningssjø tatt i betraktning . . . . .	v
5	Hindcast data file . . . . .	5
6	Definition of $H_s$ . . . . .	7
7	Connection between surface elevation $\zeta(t)$ and wave spectrum $S(\omega)$ . . . . .	8
8	Wave Height - Regular wave . . . . .	8
9	$T_p$ before modification . . . . .	9
10	$T_p$ after modification . . . . .	9
11	Sectors . . . . .	11
12	Distribution of waves among sectors . . . . .	12
13	Distribution of waves in sectors for Haltenbanken and Barents Sea . . . . .	13
14	Establishing parameters for LoNoWe distribution . . . . .	15
15	Complete LoNoWe distribution . . . . .	15
16	Establishing parameters for Lognormal distribution . . . . .	16
17	Long Term Joint Probability Distribution of $H_s$ and $T_p$ . . . . .	17
18	Estimation of $\beta$ of 3-parameter Weibull distribution, Haltenbanken . . . . .	21
19	Monthly 3-parameter Weibull distributions of $H_s$ for Haltenbanken . . . . .	22
20	Monthly 3-parameter Weibull distributions of $H_s$ for Barents Sea . . . . .	22
21	Probability plot, 3-parameter Weibull, July in Haltenbanken . . . . .	23
22	Probability plot, 3-parameter Weibull, July in Barents Sea . . . . .	23
23	Gaussian pdf . . . . .	30
24	Gaussian space . . . . .	30
25	Contour plot, Haltenbanken . . . . .	31
26	Contour plot, Barents Sea . . . . .	32
27	Definition of storms and calms . . . . .	35
28	Average duration of calms for Haltenbanken (left) and the Barents Sea (right), using a threshold of $H_s = 2\text{m}$ . . . . .	37

29	Worst, average and best duration of calms, Haltenbanken (left) and the Barents Sea (right), using a threshold of $H_s = 2\text{m}$ . . . . .	38
30	Average duration of calms for Haltenbanken (left) and the Barents Sea (right), using a threshold of $H_s = 5\text{m}$ . . . . .	38
31	Worst, average and best calms, Haltenbanken (left) and the Barents Sea (right), using a threshold of $H_s = 5\text{m}$ . . . . .	39
32	Values of $H_s$ , December 2009 . . . . .	39
33	Average duration of storms for Haltenbanken and the Barents Sea, using a threshold of $H_s = 2\text{m}$ . . . . .	41
34	Worst, average and best duration of storms, Haltenbanken and the Barents Sea, using a threshold of $H_s = 2\text{m}$ . . . . .	41
35	Average duration of storms for Haltenbanken and the Barents Sea, using a threshold of $H_s = 5\text{m}$ . . . . .	41
36	Worst, average and best duration of storms, Haltenbanken and the Barents Sea, using a threshold of $H_s = 5\text{m}$ . . . . .	42
37	Probability plot and curve fit . . . . .	45
38	2-parameter Weibull <i>PDF</i> for the duration of calms, Haltenbanken . . .	45
39	2-parameter Weibull <i>CDF</i> for the duration of calms, Haltenbanken . . .	47
40	Estimation of $\beta$ using Method of Moments . . . . .	50
41	Yearly <i>PDF</i> of the duration of calms, parameters estimated by method of moments . . . . .	51
42	Weibull <i>CDF</i> for the duration of calms, January, Haltenbanken . . . . .	52
43	Weibull <i>CDF</i> for the duration of calms, July, Haltenbanken . . . . .	53
44	Weibull <i>PDF</i> for the duration of calms, January and July, Haltenbanken	53
45	Structure in Waves . . . . .	56
46	Wave Process and Response Process . . . . .	57
47	Figure found in Faltinsen [7, p. 41]: Rigid-body motions modes and wave propagation . . . . .	58
48	Probability distribution functions . . . . .	59
49	Wave Spectrum, $H_s = 1\text{m}$ and $T_p = 5\text{s}$ . . . . .	63
50	<i>RAO</i> for Drill Ship . . . . .	65
51	<i>RAO</i> for Drill Ship . . . . .	65
52	<i>RAO</i> ( $\omega$ ) versus $\omega$ . . . . .	66

53	<i>RAO</i> ( $\omega$ ) versus $\omega$ , interpolated . . . . .	66
54	Acceptable pairs of $H_s$ and $T_p$ together with severe sea states (10 year contour plot) . . . . .	70
55	Wave frequencies. Large and small heave displacements. . . . .	71
56	Frequency domains . . . . .	71
57	Small Response Spectrums . . . . .	72
58	<i>CDF</i> of longest calm in July . . . . .	75
59	<i>PDF</i> of longest calm in July . . . . .	76
60	Simulations of a generic operation, July . . . . .	83
61	Simulations of a generic operation, January . . . . .	83
62	Generic Marine Operations . . . . .	84
63	Monthly duration of operation, both methods . . . . .	86
64	Anti-rolling devices . . . . .	92
65	Figure found in Ikeda [16, p. 10]. Damping coefficient $B_N$ due to the normal force of bilge keels . . . . .	94
66	Figure found in Ikeda [17, p. 9]. Change in hull pressure due to bilge keels . . . . .	94
67	Figure found in Ikeda [17, p. 10]. Roll damping coefficient $B_{BK}$ due to bilge keels . . . . .	95
68	<i>RAO</i> without anti-roll tank . . . . .	96
69	<i>RAO</i> with anti-roll tank . . . . .	97
70	Adjusted swell direction versus $\sigma_{\eta_4}$ . . . . .	100
71	Distribution of adjusted swell sea direction . . . . .	101
72	Distribution of $\sigma_{\eta_4}$ . . . . .	101
73	Distribution of swell sea $T_p$ . . . . .	101
74	Distribution of swell sea $H_s$ . . . . .	101
75	Calms, total sea and roll motion considered . . . . .	104
76	Worst, average and best calms, total sea and roll motion considered . . .	105
77	Average duration of a calm, both with and without roll response taken into consideration . . . . .	106
78	Swell Sea $\omega_p$ , corresponding to critical values of $\sigma_{\eta_4}$ . . . . .	108
79	The effect of the size of $H_s$ on the wave spectrum . . . . .	109
80	Swell Sea $H_s$ , corresponding to critical values of $\sigma_{\eta_4}$ . . . . .	109

81	Flowchart for script mar_op_weibull.m . . . . .	ix
82	Flowchart for script mar_op_weibull.m . . . . .	x
83	Flowchart for script rolling_calm.m . . . . .	xi
84	Confidence Intervals . . . . .	xii

# 1 Introduction

In connection to planning marine operations, it is of the utmost importance to have knowledge of the environment in which the operation will take place. Due to this fact there exist several techniques for recording values of certain characteristics which are important for a climate such as an area of sea. One of these techniques is hindcasting. This method utilizes real registrations of the wind in the relevant area and uses these in an algorithm in order to produce realistic values of the wave height. The produced values are thus artificial. These values are found in a data sample, a hindcast data file.

This data can be used to establish a report which describes the wave climate of the area which the data represent. Elements of such a report is produced in this project. This is done by employing theory and methods in probability and statistics.

Additionally, the data can be used to investigate the response of a marine structure. The sea state, given by data, can be described by a wave spectrum, and this can be further used to estimate the response of a vessel by the response spectrum. This method has been used in two cases, which are presented in the second part of the report. One can also estimate extreme wave heights (and therefore also extreme responses) by the use of probability distribution functions. Such functions are established in the first part.

The purpose of the project is to establish elements of a report which describes the sea environment, and use this in the evaluation of marine operations.

The report consists of the following main parts:

**Section 2:** Presentation of a Metocean design basis and relevant theory:

- Presenting data by scatter diagrams
- Long term joint distributions: description of the long term variation of a climate
- Monthly marginal distributions, hereunder extreme sea states
- Establishing extreme sea states by a contour plot
- Establishing the duration of good and bad weather windows

**Section 3:** Investigation of marine operations, establishing weather windows and generic tools, together with relevant theory:

- Establishing critical sea states from a critical heave motion
- Assessing the feasibility of marine operations by employing the distribution of the longest calms
- Assessing the feasibility of marine operations by simulation
- Investigating the effect that swell sea has on the roll motion of a vessel

Every part of the thesis is solved by the use of a mathematical computer software called *MATLAB*. It can be used as a simple calculator or as a programming tool where scripts use functions and algorithms in order to solve problems. Writing the *MATLAB* scripts and functions constitutes a significant amount of work in this project, and the relevant files are to be found in the attached file (*vedlegg.zip*). The scripts and functions are referred to throughout this report.

## 2 Metocean Design Basis

In this part a Metocean Design Basis with the emphasis on waves and weather windows is presented.

This section presents hindcast data in scatter diagrams, the short and long term variations of the wave climate, extreme sea states and the duration of good and bad weather windows. Relevant theory is presented throughout the section.

### 2.1 Work prior to the master thesis

Prior to the master thesis, a project thesis ([19]) was carried out, partly with an intention of being a pre-phase to this master thesis. In this project, parts of a Metocean Design Basis was produced. Some of the work which was performed during the project thesis was not satisfactory and therefore some of it has been improved during the master thesis. Elements of this report together with elements produced during the master thesis are presented in part one. This lays a foundation for the latter part of the master thesis, where generic and specific marine operations are investigated.

### 2.2 What is a Metocean Design Basis, why do we need it, and how is it produced?

Metocean is an abbreviation of Meteorology and Oceanography (see [21]), and a metocean design basis is a report which describes the characteristics of the environment of a certain area covered with sea. This is then a basis which is used in order to design structures which are to operate in the area which the report describes. Sea behaviour (described by waves, current, swell, etc.) and wind are particularly interesting (hence Meteorology and Oceanography). It is of the utmost importance to secure the integrity of a structure, and in order to do this one needs a very good understanding of the sea environment. Two of the most popular methods which are used when analysing the response of a marine vessel are the Design Wave Method (*DWM*) and the Design Spectrum Method (*DSM*). Both methods have been looked at in this thesis.

In order to use these methods, a metocean design basis can be used. Such a report is built on the data which represents the characteristics of an area. Several techniques exist for recording such data, and in this case the technique of hindcasting is used. This is a method which uses an algorithm, taking past events as input and producing new output (see [15]). The algorithm exploits real values of wind which are recorded, and produces estimates of waves. This is practical due to the fact that the wave data is scarce, while the wind data is plentiful. The result is a hindcast data file which includes several characteristic values such as wind, wave and current. This is explained in the next section.

*DWM* is typically used in a fashion where one makes certain assumptions so that one can express the behaviour of the sea in terms of a mathematical distribution function. In this manner one can establish estimates of e.g. the largest wave during ten years. *DSM* on the other hand, is a method where one utilizes the wave spectrum and a Response Amplitude Operator (*RAO*) in order to produce the response spectrum. The wave spectrum can be determined from the significant wave height, which describes a certain sea state, while the *RAO* is usually established through model tests or computer software. The characteristic value which is typically sought for is then the standard deviation of the response spectrum. These concepts are explained in greater detail later on in the report.

### 2.3 Data, Hindcasting and Scatter Diagrams

As previously mentioned the data is generated by the use of a technique termed hindcasting. Figure 5 shows the top part of a hindcast data file. The first entry corresponds to the year of 1957, and the last entry is from the end of 2014. In total there are 166053 entries. Every entry is an artificial registration, meaning that it is not a real time registration but a value generated by a mathematical model. This data file has been handed to the author by the Norwegian Meteorological Institute via Professor Sverre Haver. As we can see, the three blocks of columns to the right in the file are divided into total sea, wind sea and swell. This is because some of the sea is locally generated by the wind, while some of it is called swell sea, which means that it is sea that is not locally generated. Total sea has been employed in the majority of the analyses in this project.

Section 2.3.1 presents relevant theory, Section 2.3.2 discusses the topic of modifying hindcast data while Section 2.3.3 and Section 2.3.4 presents scatter diagrams and directional scatter diagrams, respectively.

WAM WIND AND WAVES																
LATITUDE: 65.29, LONGITUDE: 7.32																
WIND																
TOTAL SEA																
WIND SEA																
SWELL																
YEAR	M	D	H	WSP	DIR	HS	TP	TM	DIRP	DIRM	HS	TP	DIRP	HS	TP	DIRP
1957	9	1	6	7.0	33.	1.1	5.2	4.3	36.	26.	0.7	5.2	36.	0.8	5.2	351.
1957	9	1	9	7.9	21.	1.1	5.2	4.2	21.	27.	0.9	5.2	21.	0.6	6.3	66.
1957	9	1	12	8.4	26.	1.2	5.7	4.3	21.	26.	1.1	5.2	21.	0.6	6.9	351.

Figure 5: Hindcast data file

### 2.3.1 Some relevant definitions: wave spectrum, significant wave height and spectral peak period

The following definitions are found in Myrhaug [23].

One of the most interesting entries in the hindcast data (see Figure 5) is found in column seven and eight:  $H_s$ , significant wave height and  $T_p$ , spectral peak period. These two values can describe a sea state, which is often described by a wave spectrum  $S(\omega)$ . Such a wave spectrum is shown in Figure 6.

In order to define  $S(\omega)$ , one can start with the surface elevation of the sea. A surface elevation of an irregular sea consists of many separate wave components  $\zeta_{An} \cos(\omega_n t - k_n x + \epsilon_n)$ . If we consider a fixed position ( $x=0$ ) it is reduced to  $\zeta_{An} \cos(\omega_n t + \epsilon_n)$ . The surface elevation  $\zeta(t)$  is then given by

$$\zeta(x, t) = \sum_{n=1}^N \zeta_{An} \cos(\omega_n t - k_n x + \epsilon_n) \quad (1)$$

$$= \sum_{n=1}^N \zeta_{An} \cos(\omega_n t + \epsilon_n) \quad (2)$$

This is illustrated in Figure 7.  $\zeta_A$  is the wave amplitude,  $\omega_n$  is the wave frequency,  $k$  is the wave number and  $\epsilon$  is the phase angle. The wave number  $k$  is given as  $k = \frac{2\pi}{\lambda}$ , where  $\lambda$  is the wave length. Furthermore, the energy per unit length, which is completely

described by the amplitude of the wave and the length of the wave, can be expressed as

$$E_n = \frac{1}{2} \rho g \zeta_{An}^2 \quad (3)$$

Energy at different frequencies can be expressed through the wave spectrum  $S(\omega)$  by combining Equations 1 and 3:

$$\frac{E}{\rho g} = \sum_{n=1}^N \frac{1}{2} \zeta_{An}^2 = \sum_{n=1}^N S(\omega_n) \Delta\omega \quad (4)$$

A relation between the  $n$ 'th wavelet can be written as

$$\zeta_{An}^2(\omega_n) = \sqrt{2S(\omega_n)\Delta\omega} \quad (5)$$

As stated above, the  $S(\omega)$  can be established through  $H_s$  and  $T_p$ . As an example, the *Pierson Moskowitz* spectrum can be used. This spectrum is a so-called standardized spectra, which is based on data from the North Atlantic sea. The spectrum is valid for fully developed sea states in an open sea. It can be written as

$$S(\omega) = \frac{A}{\omega^5} \exp \left[ -\frac{B}{\omega^4} \right] \quad (6)$$

$$A = 0.11 H_s^2 \quad B = \frac{5}{4} \omega_p^4$$

By this we can understand how  $H_s$  and  $T_p$  can describe a sea state.  $H_s$  is in some literature defined as the average of the third largest wave heights during a relatively short time interval (usually between 20 minutes and 3 hours), and the definition of a wave height is shown in Figure 8. Another definition is  $H_s = 4\sqrt{m_0}$ , which is seen in Figure 6. As we can see, the value of  $H_s$  is determined by the wave spectrum  $S(\omega)$  via the moment  $m_0$  of the spectrum.  $m_0$  is equal to the area under the curve of  $S(\omega)$ .  $T_p$  or  $\omega_p$  (see Figure 6), which is the wave period/wave frequency with the highest energy in the sea state, can be defined as  $T_p \approx 5.3H_s^{1/2}$ . The relation between the period and frequency is  $T_p = \frac{2\pi}{\omega_p}$ .

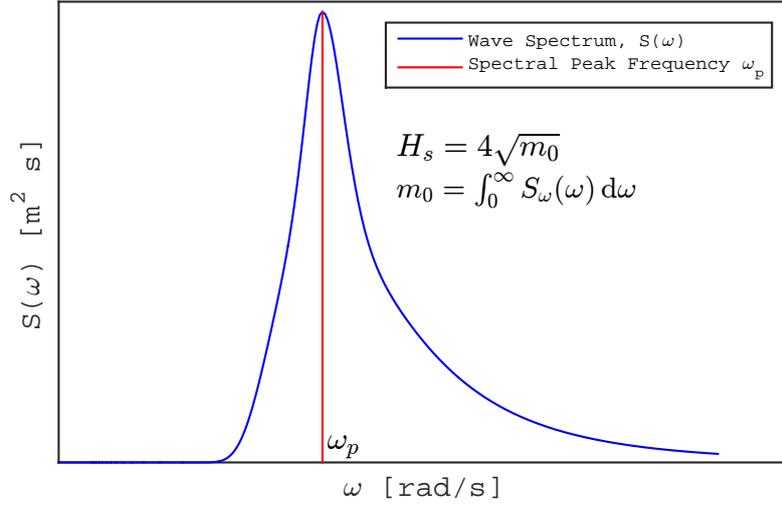


Figure 6: Definition of  $H_s$

### 2.3.2 Modification of data

Prior to using the hindcast data, some adjustments had to be done. Due to polarized values of the spectral peak period,  $T_p$ , modifications were needed. Figure 9 illustrates the problem. Instructions and reasoning behind these modifications are given in Andersen [1]. According to Andersen [1, p. 3], the problem is due to the fact that "the [...] spectral peak period (original values found in Hindcast data) is discrete with a logarithmic spacing". The equations used to modify the  $T_p$  values are given below (see [1]):

$$i = \text{ROUND} \left[ 1 + \frac{\ln(T_p^*/3.244)}{0.09525} \right] \quad (7)$$

$$T_p = 3.244 \cdot \exp(0.09525 \cdot (i - 0.5 - \text{rand})) \quad (8)$$

Equation 7 determines  $i$  based on the original value of  $T_p$ ,  $T_p^*$ . Next, the modified value of  $T_p$  is calculated by equation 8.  $\text{rand}$  is a random number generating function, generating a random number between 0 and 1. The result is the noisy distribution of  $T_p$ , illustrated in Figure 10.

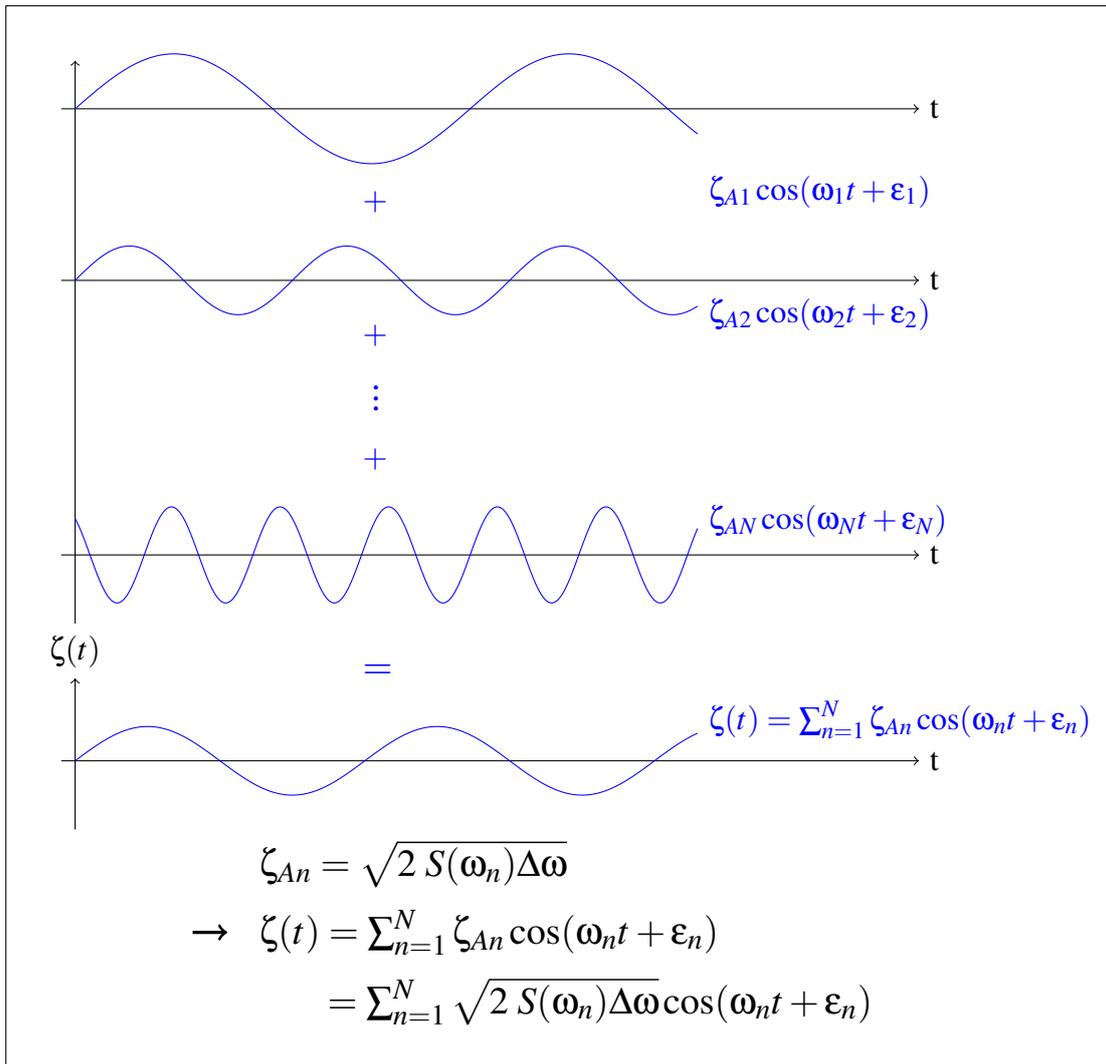


Figure 7: Connection between surface elevation  $\zeta(t)$  and wave spectrum  $S(\omega)$

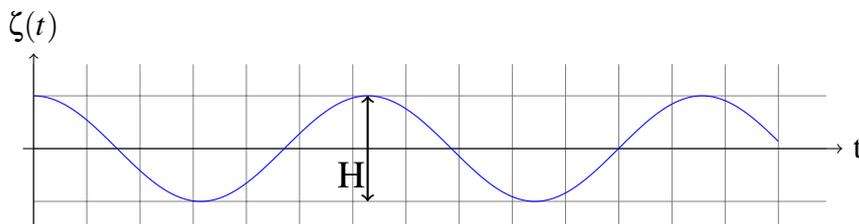


Figure 8: Wave Height - Regular wave

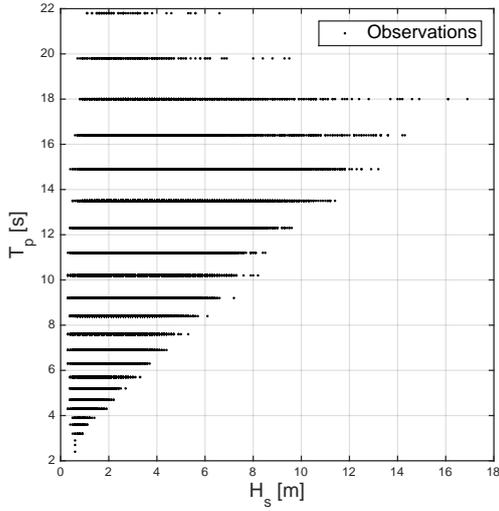


Figure 9:  $T_p$  before modification

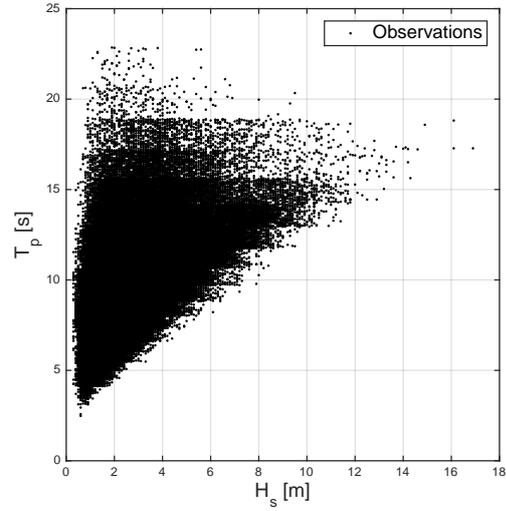


Figure 10:  $T_p$  after modification

Additionally, values of wind speed larger than 15 metres/second were modified by the following equation:

$$w_{corrected} = w + 0.2 \cdot (w - 15) \quad (9)$$

The reason for this modification is due to the experience of *Statoil*, the largest company in Norway in terms of permanent marine offshore structures. They have found the largest values of wind to be slightly small. By using the equation above, the largest values are increased. *MATLAB* scripts used for both procedures are located in a folder named "Modifications of Hindcast data", which is located in the attached file *vedlegg.zip*. The calculations were carried out only once due to their random nature. The modified set of data was then used consistently throughout the rest of the project.

### 2.3.3 Scatter Diagram

In Figure 5, the first value of  $H_s$  is equal to 1.1 metres. Every value of  $H_s$  has a corresponding value of  $T_p$  (spectral peak period). The set of values  $[H_s, T_p] = [1.1, 5.2]$  together with other sets are of interest, and therefore it is practical to present all of the

Table 1: Omnidirectional Scatter Diagram for Haltenbanken

Omni Directional Scatter Diagram Haltenbanken																						
$H_s$	Spectral peak period, $T_p$																				SUM	
	2-3	3-4	4-5	5-6	6-7	7-8	8-9	9-10	10-11	11-12	12-13	13-14	14-15	15-16	16-17	17-18	18-19	19-20	20-21	21-22		22-23
0-1	2	148	1044	1946	3106	3072	2479	1852	898	433	260	109	47	44	25	13	8	4	4	0	0	15494
1-2	0	13	1180	4715	7178	9004	11033	9280	6148	4131	2507	1272	623	382	228	104	75	36	22	14	4	57949
2-3	0	0	7	454	2930	5062	5755	6786	6413	4886	3528	2114	1140	726	361	168	103	29	21	10	7	40500
3-4	0	0	0	4	260	1399	3378	4241	4040	3750	3007	1869	1128	731	383	181	133	21	26	5	3	24559
4-5	0	0	0	0	6	85	928	2024	2599	2494	1892	1326	922	551	254	155	102	13	6	2	0	13359
5-6	0	0	0	0	0	1	95	562	1286	1650	1445	782	495	332	192	90	66	3	6	3	0	7008
6-7	0	0	0	0	0	0	11	61	300	829	1050	612	308	213	121	71	44	4	2	0	1	3627
7-8	0	0	0	0	0	0	1	10	31	223	571	550	244	133	62	51	39	1	0	0	0	1916
8-9	0	0	0	0	0	0	0	0	4	48	147	364	190	107	22	21	24	1	0	0	0	928
9-10	0	0	0	0	0	0	0	0	0	6	27	120	135	83	28	21	11	2	0	0	0	433
10-11	0	0	0	0	0	0	0	0	0	0	4	25	61	41	21	14	10	0	0	0	0	176
11-12	0	0	0	0	0	0	0	0	0	0	0	6	20	19	9	4	5	0	0	0	0	63
12-13	0	0	0	0	0	0	0	0	0	0	0	0	1	10	8	2	1	0	0	0	0	22
13-14	0	0	0	0	0	0	0	0	0	0	0	0	0	4	3	3	0	0	0	0	0	10
14-15	0	0	0	0	0	0	0	0	0	0	0	0	0	1	1	2	2	0	0	0	0	6
15-16	0	0	0	0	0	0	0	0	0	0	0	0	0	0	0	0	0	0	0	0	0	0
16-17	0	0	0	0	0	0	0	0	0	0	0	0	0	0	0	1	2	0	0	0	0	3
SUM	2	161	2231	7119	13480	18623	23680	24816	21719	18450	14438	9149	5314	3377	1718	901	625	114	87	34	15	166053

166053 values in one diagram in order to get a clear overview. This can be conveniently shown in a scatter diagram. In a scatter diagram it is easy to see tendencies. Such a diagram will have  $H_s$  in the vertical direction and  $T_p$  in the horizontal direction. Table 28 shows a scatter diagram for Haltenbanken. It is an omni directional scatter diagram, which means that waves from all directions are considered. The diagram gives the number of entries of a certain class: for example, there are 1044 entries of  $[H_s, T_p] = [0 - 1, 4 - 5]$ . Another insightful way of presenting the data is shown in Figure 10, where  $H_s$  is plotted versus  $T_p$ .

### 2.3.4 Directional Scatter Diagrams

Scatter diagrams for a given direction are also useful. These have been created for 30 degree sectors, as illustrated in Figure 11. Table 30 is a scatter diagram for the northern sector. The distribution among all twelve sectors is presented in Figures 12 and 13. Distributions for both areas (Haltenbanken and Barents Sea) are displayed. It is observed that for Haltenbanken a large portion is found in sectors eight through ten, which represent the western and southwestern directions. On the other hand, only a small portion of the waves are found in sectors three through seven, which represent the

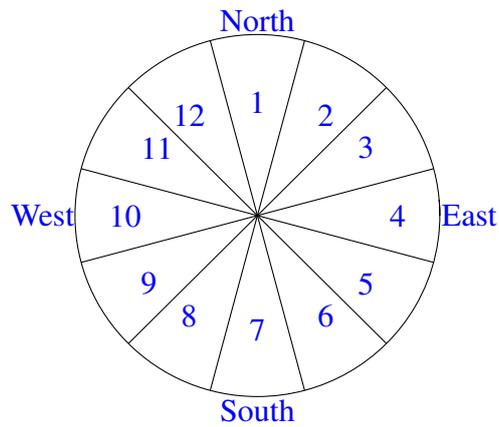


Figure 11: Sectors

eastern and southeastern direction.

The *MATLAB* scripts for the scatter diagrams are given in the folder "Scatter Diagrams". Larger versions of all scatter diagrams are found in appendix F. The sectors for the directional scatter diagrams have been defined as  $(-15^\circ, 15^\circ], (15^\circ, 45^\circ] \dots (315^\circ, 345^\circ]$ . 345 degrees corresponds to  $-15$  degrees.

Table 2: Unidirectional Scatter Diagram, sector 1(north),  $-15^\circ$  to  $15^\circ$ , for Haltenbanken

Scatter Diagram, Haltenbanken, Northern Sector																						
$H_s$	Spectral Peak Period, $T_p$																				SUM	
	2-3	3-4	4-5	5-6	6-7	7-8	8-9	9-10	10-11	11-12	12-13	13-14	14-15	15-16	16-17	17-18	18-19	19-20	20-21	21-22		22-23
0-1	0	19	159	477	836	723	336	145	61	30	12	7	3	0	2	0	0	1	1	0	0	2812
1-2	0	0	95	516	1335	2081	2428	1865	755	259	104	56	32	22	10	1	3	0	0	2	0	9564
2-3	0	0	0	11	140	510	899	1233	1202	793	290	48	35	22	13	6	3	1	0	1	0	5207
3-4	0	0	0	0	1	33	238	489	556	480	324	92	37	10	6	4	2	0	0	0	0	2272
4-5	0	0	0	0	0	0	24	158	261	277	213	83	28	4	6	2	0	0	0	0	0	1056
5-6	0	0	0	0	0	0	0	16	82	121	118	59	16	3	1	0	0	0	0	0	0	416
6-7	0	0	0	0	0	0	0	1	13	49	72	26	4	1	1	0	0	0	0	0	0	167
7-8	0	0	0	0	0	0	0	0	1	9	36	20	5	1	1	0	0	0	0	0	0	73
8-9	0	0	0	0	0	0	0	0	0	1	1	8	8	2	1	0	0	0	0	0	0	21
9-10	0	0	0	0	0	0	0	0	0	1	0	3	2	1	0	0	0	0	0	0	0	7
10-11	0	0	0	0	0	0	0	0	0	0	0	1	2	1	1	0	0	0	0	0	0	5
11-12	0	0	0	0	0	0	0	0	0	0	0	0	3	1	0	0	0	0	0	0	0	4
12-13	0	0	0	0	0	0	0	0	0	0	0	0	0	0	0	0	0	0	0	0	0	0
13-14	0	0	0	0	0	0	0	0	0	0	0	0	0	0	0	0	0	0	0	0	0	0
14-15	0	0	0	0	0	0	0	0	0	0	0	0	0	0	0	0	0	0	0	0	0	0
15-16	0	0	0	0	0	0	0	0	0	0	0	0	0	0	0	0	0	0	0	0	0	0
16-17	0	0	0	0	0	0	0	0	0	0	0	0	0	0	0	0	0	0	0	0	0	0
SUM	0	19	254	1004	2312	3347	3925	3907	2931	2020	1170	403	175	68	42	13	8	2	1	3	0	21604

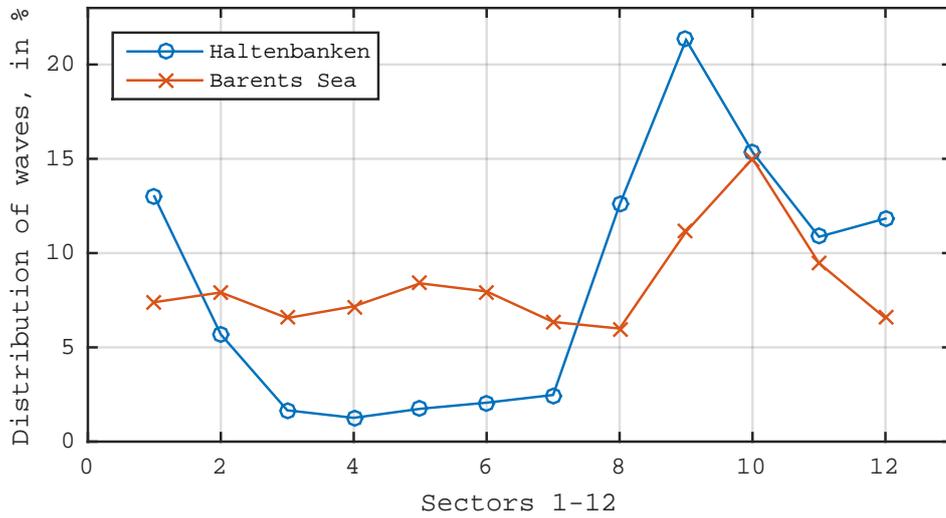


Figure 12: Distribution of waves among sectors

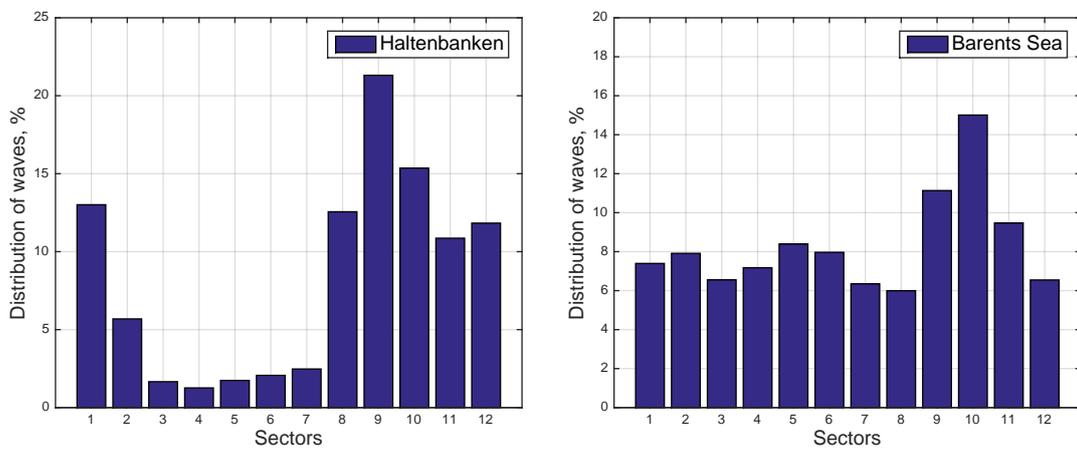


Figure 13: Distribution of waves in sectors for Haltenbanken and Barents Sea

## 2.4 Long Term Joint Distribution of $H_s$ and $T_p$

The description of a sea environment can be separated into two parts, short term and long term. The short term description is a stationary process which is usually defined to last between 20 minutes and 3 hours. An entry in the Hindcast data is a short term description, where the sea state, which is defined to be constant for 3 hours, can be described by its wave spectrum  $S(\omega)$  (by the use of  $H_s$  and  $T_p$ ). Since many analyses study structures which are to operate in a timespan which is significantly longer than that of a short term description, it is of interest to establish a long term description for the Metocean design basis. The long term variation of a sea state can be given as

$$f_{H_s, T_p}(h_s, t_p) = f_{H_s}(h_s) \cdot f_{T_p|H_s}(t_p|h_s) \quad (10)$$

As previously mentioned, it is common to apply mathematical models to the data. What is meant by this is that one attempts to describe some sort of physical quantity, e.g. waves, by a mathematical model. Such a model is often called a distribution function, and the most common distribution function is the so-called normal distribution, which is also called the Gaussian distribution. In this case, where we are considering a model to describe the long term sea state given by  $H_s$  and  $T_p$ , a Weibull distribution is a model which has been successfully used to describe the first part,  $f_{H_s}(h_s)$ , which is often termed the marginal distribution of  $H_s$ . Another proposed model is the hybrid model, termed "LoNoWe", which is an abbreviation for "Lognormal" and "Weibull", i.e. a hybrid model of the Lognormal and Weibull distributions. This hybrid function describes the lower tail of  $f_{H_s}(h_s)$  by the Lognormal distribution and the upper tail by the Weibull distribution. It is defined in Haver [10, p. 128] as

$$f_{H_s}(h_s) = \frac{1}{\sqrt{2\pi} \alpha h_s} \cdot \exp \left[ -\frac{(\ln(h_s) - \theta)^2}{2 \alpha^2} \right] \quad h_s \leq \eta \quad (11)$$

$$f_{H_s}(h_s) = \frac{\beta}{\rho} \left( \frac{h_s}{\rho} \right)^{\beta-1} \cdot \exp \left[ -\left( \frac{h_s}{\rho} \right)^\beta \right] \quad h_s > \eta \quad (12)$$

In this case a 2-parameter Weibull distribution is employed. For the conditional distribution function,  $f_{T_p|H_s}$ , a log-normal distribution, described in Bury [3], is probably the best fit. It is given by

$$f_{T_p|H_s}(t_p|h_s) = \frac{1}{\sqrt{2\pi} \sigma(h_s) t_p} \exp \left[ -\frac{1}{2} \left( \frac{\ln(t_p) - \mu(h_s)}{\sigma(h_s)} \right)^2 \right] \quad (13)$$

Section 2.4.1 presents how parameters are established, while Section 2.4.2 presents monthly distributions.

#### 2.4.1 Establishing parameters

Both  $f_{H_s}(h_s)$  and  $f_{T_p|H_s}(h_s|t_p)$  were produced in the project thesis. The parameters of the marginal distribution of  $H_s$ ,  $f_{H_s}(h_s)$ , were estimated by using a mixture of techniques. The parameters  $\alpha$  and  $\theta$  were estimated by Maximum Likelihood estimators, while  $\eta$ ,  $\rho$  and  $\beta$  were estimated by using a probability plot. The probability plot is a tool which we will look further into later in this report. Figure 14 shows two probability plots, one for the Lognormal part of  $f_{H_s}(h_s)$ , the second for the Weibull part. The complete LoNoWe distribution is seen in Figure 15.

The parameters for the conditional distribution function  $f_{T_p|H_s}(h_s|t_p)$  (Lognormal distribution) were established by using empirical relationships, represented by equations 14 and 15. These equations have been established and used by *Statoil*, and they can be found in [5, p. 23]. In order to use these, the mean and variance given an interval of  $H_s$  were determined (using values of  $H_s$  from the hindcast data file). This was plotted, see Figure 16. Finally, curve fitting by the method of least squares was performed in order to determine parameters of equation 14 and 15.

Established parameters for the complete long term joint probability distribution function (*JPDF*) are given in Table 3, and the distribution is illustrated in Figure 17. The area under investigation is Haltenbanken. A more in-depth description of the methods and work above can be found in the project thesis ([19]).

$$\mu(h_s) = a_1 + a_2 \cdot h_s^{a_3} \quad (14)$$

$$\sigma^2(h_s) = b_1 + b_2 \cdot \exp[-h_s \cdot b_3] \quad (15)$$

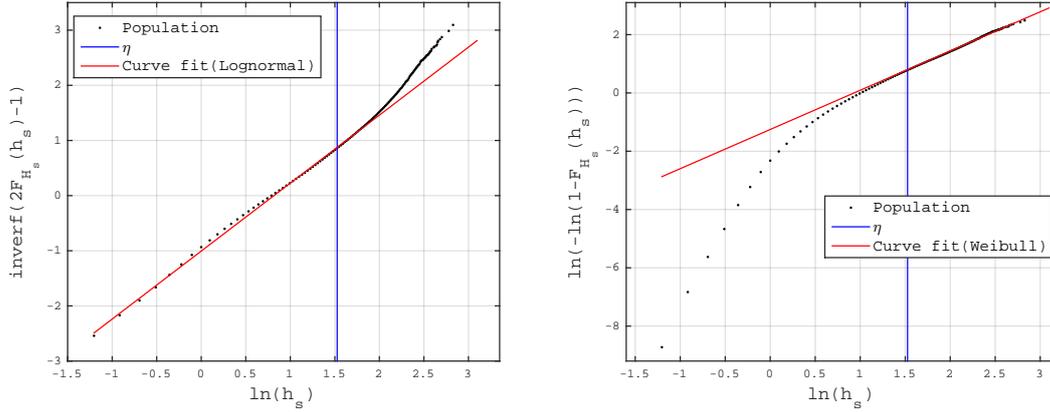


Figure 14: Establishing parameters for LoNoWe distribution

Table 3: Estimated parameters in connection with establishing long term *JPDF* of  $H_s$  and  $T_p$

Estimated parameters for $f_{H_s, T_p}$ , Haltenbanken						
	$\alpha$	$\theta$	$\eta$	$\beta$	$\rho$	
LoNoWe	0.5737	0.8162	4.6	1.3456	2.5382	
	$a_1$	$a_2$	$a_3$	$b_1$	$b_2$	$b_3$
Lognormal	1.5538	0.5476	0.3199	0.00005	0.1056	0.2688

#### 2.4.2 Monthly long term *JPDF*'s

In addition to establishing a distribution for the entire collection of data, it is useful to establish monthly distributions. This implies that one will estimate parameters of monthly distributions. The monthly distributions are useful, and can yield higher accuracy in some situations. This is especially true for marine operations, since these are

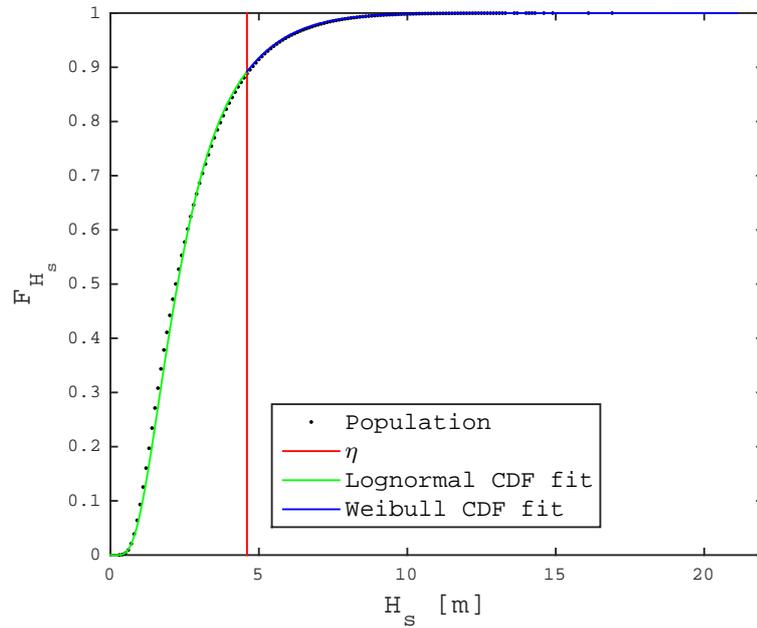


Figure 15: Complete LoNoWe distribution

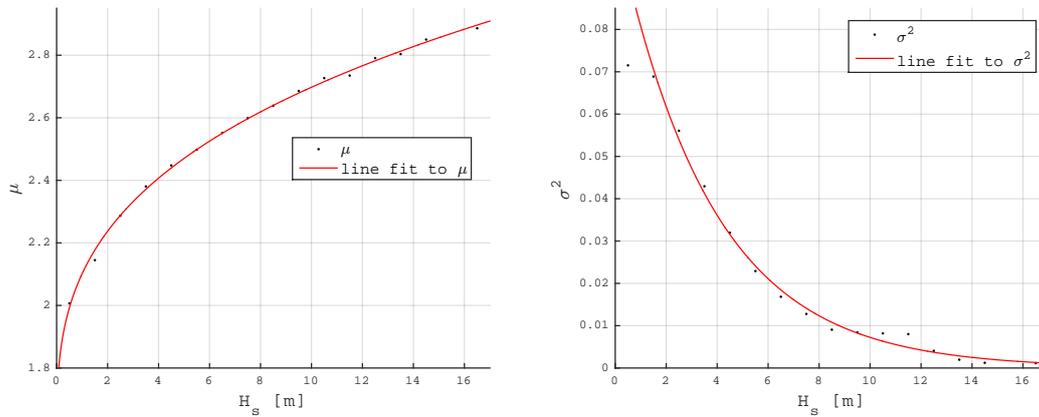


Figure 16: Establishing parameters for Lognormal distribution

planned to happen in a certain time period during one or several of the months of a year, whereas a permanent marine offshore structure is obviously subject to the climate of all months of a year.

The method which was used to estimate these parameters is very similar to the one in

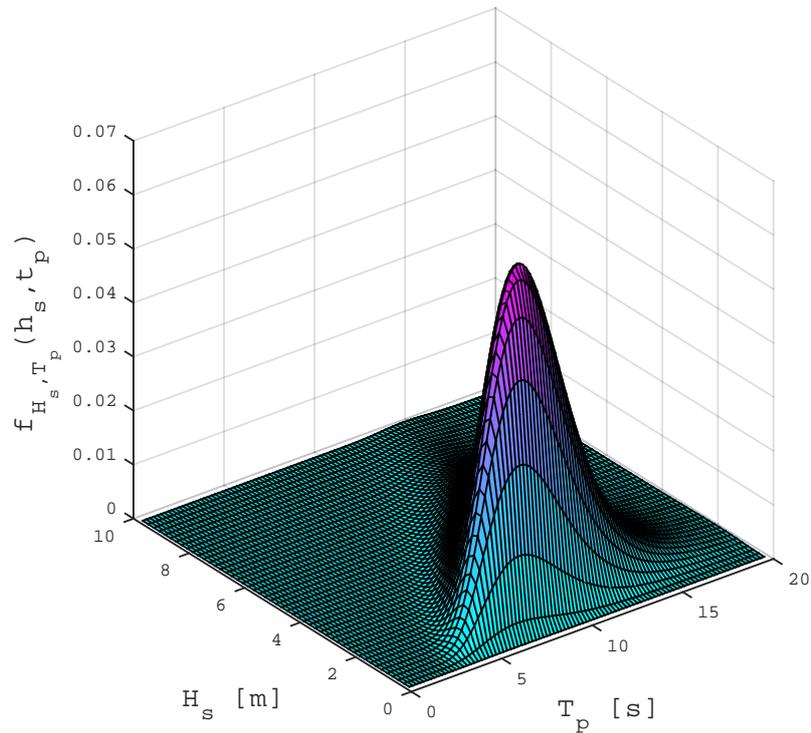


Figure 17: Long Term Joint Probability Distribution of  $H_s$  and  $T_p$

the previous section. The main difference is that one must first sort the data by months, and then apply the same techniques to the twelve data samples. Results can be found in Table 4. In this case both Haltenbanken and the Barents sea has been investigated. The *MATLAB* scripts are located in the folder "Monthly long term distributions".

## 2.5 Monthly marginal distributions of $H_s$

The LoNoWe distribution and the method which was used to estimate parameters, which has been presented in the previous sections, has a few weaknesses. Firstly, the upper part of the distribution, which is the 2-parameter Weibull distribution, does not represent the higher range of  $H_s$  values as well as one would like. Secondly, the method used in order to estimate parameters might not be satisfactory. The LoNoWe parameters were

Table 4: Monthly long term *JPDF*'s

Area	Parameters	Months											
		1	2	3	4	5	6	7	8	9	10	11	12
Haltenbanken	$\hat{\alpha}$	0.4662	0.4794	0.4903	0.4760	0.4694	0.4278	0.4285	0.4480	0.5109	0.4856	0.4679	0.4530
	$\hat{\theta}$	1.2235	1.1738	1.0575	0.7741	0.4792	0.4026	0.3309	0.3759	0.7190	0.9721	1.0825	1.2094
	$\hat{\eta}$	6.5000	5.6000	4.7000	6.1000	5.0000	4.6000	4.3000	4.7000	5.0000	5.4000	7.0000	5.8000
	$\hat{\rho}$	3.6469	3.6065	3.2759	1.9545	1.3605	1.2002	1.1148	1.1604	2.0604	2.8043	2.8954	3.6842
	$\hat{\beta}$	1.5846	1.6545	1.6899	1.2621	1.2093	1.2614	1.2576	1.2074	1.3127	1.4873	1.3952	1.7175
	$\hat{a}_1$	1.9552	1.8249	1.8734	1.9321	1.7589	1.9521	1.9342	1.8460	1.7280	1.9288	2.0661	2.0632
	$\hat{a}_2$	0.2645	0.3754	0.3120	0.2164	0.3181	0.0890	0.0871	0.2014	0.3762	0.2155	0.1339	0.1641
	$\hat{a}_3$	0.4546	0.3649	0.4199	0.5405	0.4543	1.0103	1.0577	0.6068	0.3881	0.5465	0.6675	0.5858
	$\hat{b}_1$	0.0001	0.0001	0.0001	0.0001	0.0001	0.0001	0.0001	0.0001	0.0001	0.0001	0.0003	0.0009
	$\hat{b}_2$	0.1183	0.1213	0.1069	0.1174	0.1208	0.0953	0.0929	0.0807	0.1008	0.0977	0.1188	0.1152
	$\hat{b}_3$	0.2462	0.2397	0.2405	0.3571	0.2434	0.2404	0.1559	0.2757	0.3136	0.2594	0.3150	0.2702
Barents Sea	$\hat{\alpha}$	0.4986	0.5133	0.5107	0.5413	0.5488	0.4933	0.4507	0.4559	0.4707	0.4669	0.4803	0.4843
	$\hat{\theta}$	0.9661	0.9487	0.8305	0.5765	0.3040	0.2488	0.1883	0.2906	0.5665	0.7997	0.8584	0.9433
	$\hat{\eta}$	4.7000	5.8000	4.3000	2.6000	3.0000	2.8000	3.5000	5.5000	4.2000	5.5000	4.5000	4.2000
	$\hat{\rho}$	2.9347	2.6910	2.5452	2.1109	1.4558	1.3325	1.0379	0.8936	1.7283	2.1350	2.5562	2.9127
	$\hat{\beta}$	1.5811	1.3666	1.5149	1.6801	1.3245	1.4196	1.2732	1.0665	1.3869	1.3648	1.5585	1.7025
	$\hat{a}_1$	1.8171	1.7719	1.5598	1.5329	1.6732	1.6174	1.7606	1.7150	1.7888	1.7564	1.5770	1.2496
	$\hat{a}_2$	0.2310	0.2785	0.4318	0.3924	0.2296	0.3146	0.1485	0.2137	0.2026	0.2646	0.4363	0.7552
	$\hat{a}_3$	0.5935	0.5273	0.4318	0.4651	0.6806	0.5034	0.8535	0.6759	0.6839	0.5580	0.3920	0.2730
	$\hat{b}_1$	0.0055	0.0036	0.0087	0.0024	0.0001	0.0033	0.0001	0.0021	0.0001	0.0022	0.0002	0.0001
	$\hat{b}_2$	0.1949	0.2133	0.1950	0.1729	0.1379	0.1579	0.1116	0.1676	0.1101	0.0933	0.1158	0.1624
	$\hat{b}_3$	0.3676	0.4066	0.4546	0.5172	0.4072	0.7087	0.3662	0.7300	0.2851	0.2871	0.2991	0.2724

established partly by applying the probability plot. Since the probability plot is first and foremost meant to indicate whether or not the distribution which is being tested might be a good fit, another method should yield more accurate results. For these two reasons, it was of interest to look at another distribution, namely the 3-parameter Weibull distribution and estimate parameters by the Method of Moments. The 3-parameter Weibull distribution is according to [3] given as

$$f_{H_s}(h_s|\rho, \beta, \lambda) = \frac{\beta}{\rho} \left( \frac{h_s - \lambda}{\rho} \right)^{\beta-1} \exp \left[ - \left( \frac{h_s - \lambda}{\rho} \right)^\beta \right], \quad h_s \geq \lambda \quad (16)$$

**Method of Moments** This is a method which uses the expressions of the moments of the distribution. These moments represent the properties of a distribution, and the moments which are needed to describe the Gaussian distribution are presented in Table 5.

Table 5: Moments of a distribution

Moment no.	Meaning	Mathematical expression
1st	Expected value	$E[X] = \frac{1}{N} \sum_{i=1}^N x_i$
2nd	Variance	$VAR[X] = \frac{1}{N} \sum_{i=1}^N (x_i - E[X])^2$
3rd	Skewness	$\gamma_1 = \frac{\frac{1}{N} \sum_{i=1}^N (x_i - E[X])^3}{(VAR[X])^{3/2}}$
4th	Kurtosis	$\gamma_2 = \frac{\frac{1}{N} \sum_{i=1}^N (x_i - E[X])^4}{(VAR[X])^2}$

The moments of the 3-parameter Weibull distribution are given in Bury [3] as

$$E[H_s] = \lambda + \rho \Gamma \left( 1 + \frac{1}{\beta} \right) \quad (17)$$

$$VAR[H_s] = \rho^2 \left[ \Gamma \left( 1 + \frac{2}{\beta} \right) - \Gamma^2 \left( 1 + \frac{1}{\beta} \right) \right] \quad (18)$$

$$\gamma_1 = \frac{\Gamma \left( 1 + \frac{3}{\beta} \right) - 3\Gamma \left( 1 + \frac{1}{\beta} \right) \Gamma \left( 1 + \frac{2}{\beta} \right) + 2\Gamma^3 \left( 1 + \frac{1}{\beta} \right)}{\left[ \Gamma \left( 1 + \frac{2}{\beta} \right) - \Gamma^2 \left( 1 + \frac{1}{\beta} \right) \right]^{3/2}} \quad (19)$$

where the gamma function is defined as  $\Gamma(u) = \int_0^{\infty} z^{u-1} \exp(-z) dz$ . The 4th moment (kurtosis) is not relevant here, since we are only looking to estimate 3 parameters. The method works in such a way that if one can calculate the mean, variance and skewness from a sample, one can use the expressions above and solve these for the parameters  $\rho$ ,  $\beta$  and  $\lambda$ . In order to acquire a satisfactory accuracy, a rather large sample is needed, which is certainly the case here, considering that the hindcast data consists of 166053 observations, representing a time span from 1957 until 2014.

**Algorithm and results** The parameters were established by a *MATLAB* script which is found in the folder "3 par Wei f\_Hs". The script employs the following algorithm:

1.  $H_s$  is sorted by month. Data is sorted into a table where there are 12 columns, each column containing the entire collection of data corresponding to that particular

month.

2. The mean, variance and skewness of  $H_s$  is determined by using the expressions in Table 5.
3. The skewness is determined by Equation 19, using a range  $\beta$  values. This is then compared to the skewness calculated from the actual data sample, and when a match is found, an estimator of  $\beta$ ,  $\hat{\beta}$  is established. This is illustrated in Figure 18. The 12 vertical lines represent the 12 months. A match corresponds to intersections between vertical lines and red curve.
4. With  $\hat{\beta}$  established,  $\hat{\rho}$  can be established from Equation 18 using the variance found from the data. Finally,  $\hat{\lambda}$  can be established from Equation 17, using the mean calculated from the data.

The estimators are found in Table 6, and the corresponding distributions are found in Figures 19 and 20. It can be seen that the monthly distributions for Haltenbanken include larger values of  $H_s$  than for the Barents Sea, meaning that the wave climate is worse for Haltenbanken. In order to illustrate how the distribution fits the observations, probability plots which correspond to values of July are shown in Figures 21 and 22. Notice that the distribution is only defined for values of  $h_s \geq \lambda$ . In this case,  $\hat{\lambda} = 0.7033$  for Haltenbanken and  $\hat{\lambda} = 0.5827$  for the Barents Sea. It is clear that the 3-parameter Weibull distribution fits the higher part of the observations very well while it deviates quite a bit in the lower part. This is the strength and the weakness of the 3-parameter Weibull distribution in the case of evaluating significant wave heights. Since, for the most part, the largest values of  $H_s$  are the most crucial, the distribution is of practical application. One should of course keep in mind that if one is dealing with a structure or something else which is sensitive to small values of  $H_s$ , a different distribution such as the LoNoWe distribution should be considered.

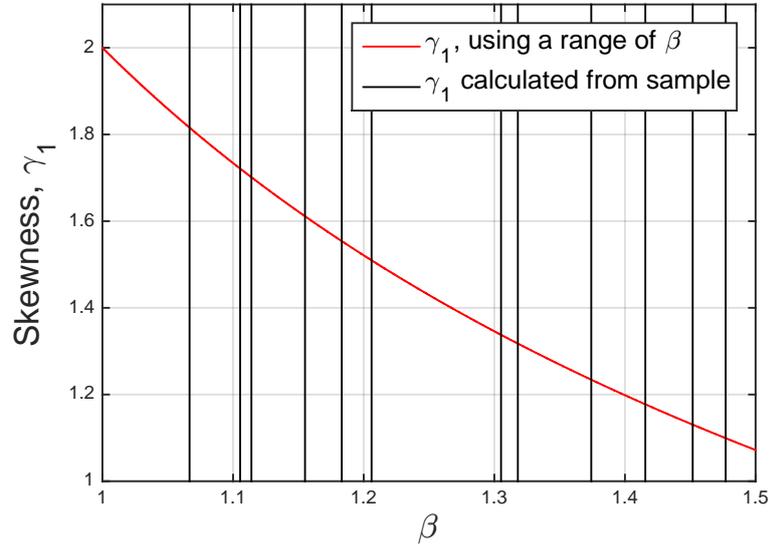


Figure 18: Estimation of  $\beta$  of 3-parameter Weibull distribution, Haltenbanken

Table 6: Estimated parameters for monthly marginal distributions of  $H_s$ .

Months	1	2	3	4	5	6	7	8	9	10	11	12
<b>Haltebanken</b>												
$\hat{\rho}$	2.7087	2.7173	2.5455	1.5703	1.0487	0.8625	0.8701	0.9237	1.5897	2.1052	2.2210	2.7054
$\hat{\beta}$	1.3742	1.4156	1.4771	1.2060	1.1054	1.0667	1.1551	1.1140	1.1832	1.3180	1.3051	1.4519
$\hat{\lambda}$	1.3103	1.1489	0.9323	0.9553	0.7948	0.8046	0.7033	0.7275	0.8391	1.0305	1.2390	1.2566
<b>Barents Sea</b>												
$\hat{\rho}$	2.2825	2.1289	1.9776	1.7671	1.1134	0.9538	0.7970	0.7544	1.2996	1.6361	1.9055	2.2401
$\hat{\beta}$	1.3934	1.2855	1.3732	1.5027	1.1913	1.2041	1.1633	0.9912	1.2474	1.2537	1.3454	1.4645
$\hat{\lambda}$	0.8879	0.9677	0.7945	0.4504	0.5190	0.5502	0.5827	0.7329	0.7582	0.9595	0.8968	0.8518

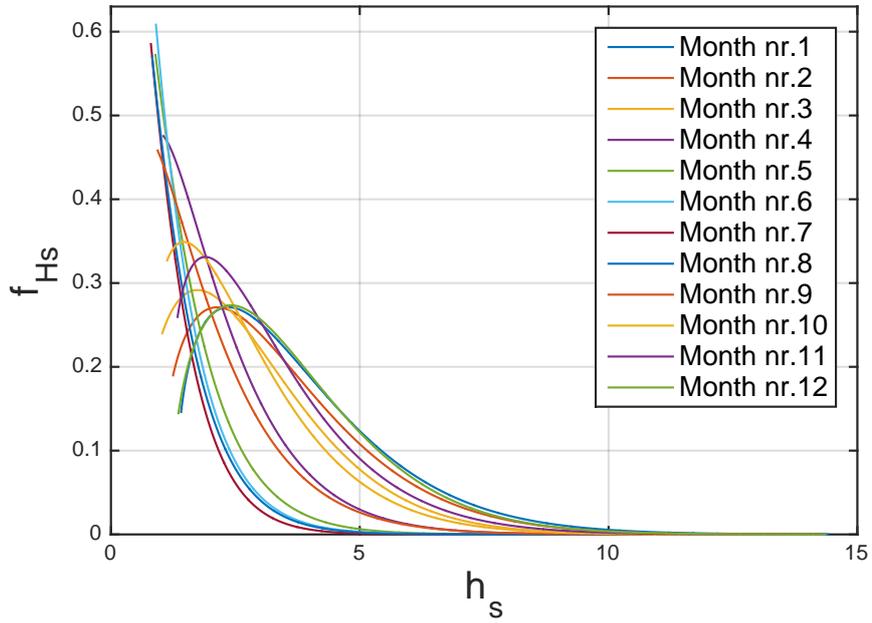


Figure 19: Monthly 3-parameter Weibull distributions of  $H_s$  for Haltenbanken

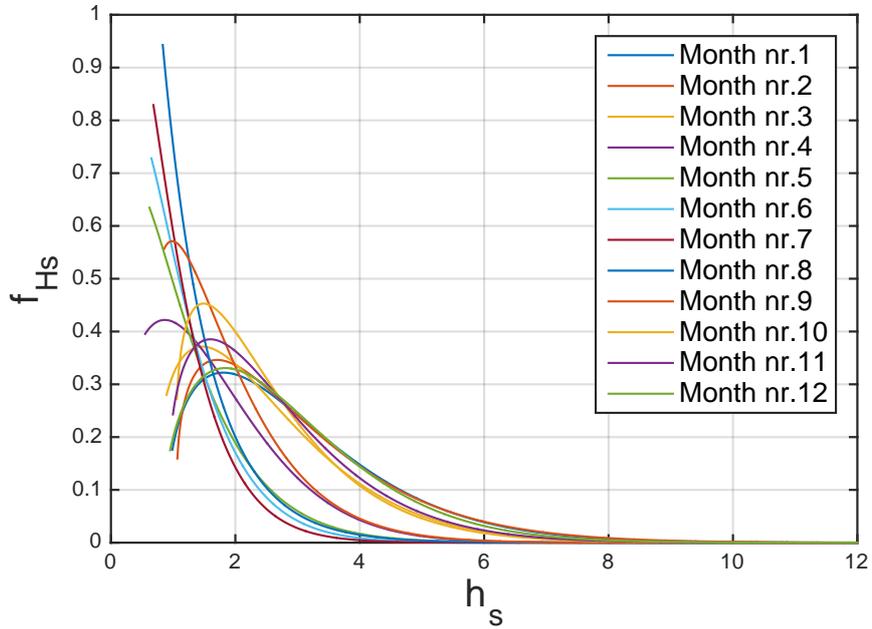


Figure 20: Monthly 3-parameter Weibull distributions of  $H_s$  for Barents Sea

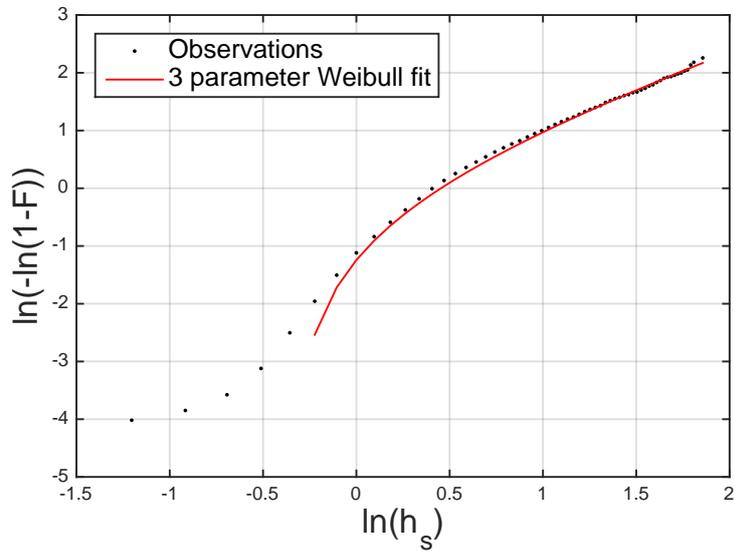


Figure 21: Probability plot, 3-parameter Weibull, July in Haltenbanken

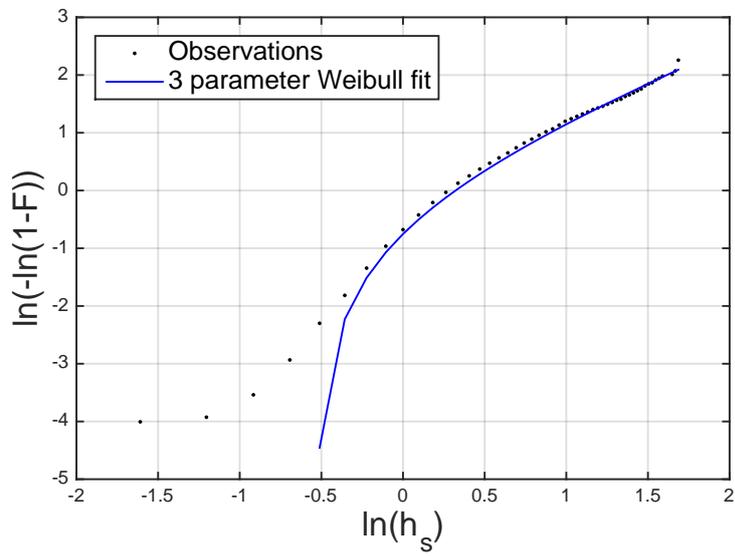


Figure 22: Probability plot, 3-parameter Weibull, July in Barents Sea

## 2.6 Extreme Sea States

Determining extreme values of certain physical quantities is very often of high interest, and such information is often part of a typical Metocean Design Basis. Extreme values of  $H_s$  can be determined according to regulations which are set by the authorities. In this project, the standards of NORSOK [25] have been used. These standards, or criterias, are called *Ultimate Limit State (ULS)* and *Accidental Limit State (ALS)* criterias. These are part of a limit state design, also known as load and resistance factor design. *ULS* and *ALS* correspond to probabilities of 0.01 and 0.0001, respectively. One can of course use any probability for that matter. The probabilities represent return periods of the physical quantity. In the case of significant wave heights, a probability of 0.01 describes a sea state which returns, on average, every 100 years ( $\frac{1}{100} = 0.01$ ).

If the distribution of  $f_{H_s}(h_s)$  has been established, one can determine the extreme sea states by manipulation of the equation. This is in essence the Design Wave Method, a method which seeks to determine a sea state corresponding to a criteria such as the *ULS*. The marine structure which is under consideration is then designed to withstand such a severe sea state as the one corresponding to the *ULS* criteria.

**Method** The procedure which has been used in this project is described in Myrhaug [23, p. 43-44]: The extreme value of  $h_s$  which is exceeded once during  $M$  years (i.e. a sea state which has a return period of  $M$  years),  $h_{s,M}$ , is calculated by

$$P[H_s > h_{s,M}] = 1 - F_{H_s}(h_{s,M}) = \frac{1}{N} \quad (20)$$

where  $N$  = number of sea states during  $M$  years. Equation 20 states that the probability that the wave  $h_{s,M}$  is exceeded once during  $M$  years is equal to  $1/N$ . The Weibull distribution is

$$F_{H_s}(h_s) = 1 - \exp \left[ - \left( \frac{h_s}{\rho} \right)^\beta \right] \quad (21)$$

which inserted in 20 yields

$$\exp \left[ - \left( \frac{h_{s,M}}{\rho} \right)^\beta \right] = \frac{1}{N} \quad (22)$$

$$h_{s,M} = \rho [\ln(N)]^{\frac{1}{\beta}} \quad (23)$$

We have values of  $h_s$  corresponding to every third hour and therefore there are  $N = \frac{365 \cdot 24}{3} = 2920$  values of  $h_s$  (three hour sea states) in one year, and this yields

$$h_{s,M} = \rho \left[ \ln \left( \frac{1}{2920} \right) \right]^{\frac{1}{\beta}} \quad (24)$$

If a 3-parameter Weibull distribution is employed the expression will be slightly different:

$$h_{s,M} = \rho \left[ \ln \left( \frac{1}{2920} \right) \right]^{\frac{1}{\beta}} + \lambda \quad (25)$$

An alternative to the expression above, and which is used in the following, is

$$h_{s,q} = \rho \left[ \ln \left( \frac{q}{2920} \right) \right]^{\frac{1}{\beta}} \quad (26)$$

Here,  $h_{s,q}$  is the significant wave height which is exceeded once during  $q^{-1}$  years. From equation 26 one can calculate the extreme values which are sought for.

**Results** Table 7 displays the extreme values which were produced during the project thesis, found by using the LoNoWe distribution of  $f_{H_s}$ . Corresponding  $T_p$  values are also given in this table. Furthermore, extreme values corresponding to each month, calculated from the monthly distributions presented in Section 2.5 are found in Table 8. As we can see, the tendencies concur with the ones found in Table 7, that is to say the wave climate is worse for Haltenbanken than for the Barents Sea. In addition to this we can see that the values of  $H_s$  are smallest for the summer months and largest for the winter months, which is of course of no surprise. However, it is worth noticing that

for Haltenbanken, the value of  $H_s$  is decreasing as the year goes by from January until July, while on the other hand, this seems to be more random for the Barents Sea. For example, February is worse than January, and August is worse than September for the *ALS* criteria for the Barents Sea. Lastly, it is seen that the largest values of extremes found from the 3-parameter Weibull distribution are larger than the largest found from the LoNoWe distribution. However, it is questionable whether or not it is reasonable to compare the values of these two tables since one of them represents values found from monthly distributions while the other table represents values found from the entire collection of data (the entire year). Therefore, the parameters of a yearly (considering all values of  $H_s$ ) 3-parameter Weibull distribution for  $H_s$  were estimated, and these are shown in Table 9. These were also estimated using the method of moments, employing the same steps taken to produce the monthly distributions. It is seen that the values are as with the monthly distributions slightly larger than the values found by LoNoWe distribution. Based on the fact that it is known that a 3-parameter Weibull distribution can better predict the higher range of  $H_s$  values, and that the method of moments is a more accurate method (especially considering that we have a large sample), it is quite likely that the LoNoWe distribution underpredicts extreme values of  $H_s$ . In other words, the LoNoWe distribution is likely a conservative model.

With the possibility of comparing the monthly distributions with the distribution for the whole year it is interesting to see that there are larger extreme values found from the monthly distributions than for the entire year. It should especially be noticed that the largest monthly value found in the Barents Sea is 19.5 metres (corresponding to the *ALS* criteria), found in the month of February. On the other hand, the largest extreme found from the distribution for the whole year, for the Barents Sea, is 18.2 (corresponding to the *ALS* criteria). By this one can understand that the monthly distributions can reveal valuable information.

The algorithm which calculates the extreme values is found in the same script that calculates the parameters, which is found in the folder "3 par Wei f\_Hs".

Table 7: Extreme Values of  $H_s$  from LoNoWe Distribution

Extreme values of $H_s$ from LoNoWe Distribution				
Area	q	$H_s$ [m]	$T_p$ [s]	90% interval
Haltenbanken	0.01 ( <i>ULS</i> )	16.7	18.2	17.2-19.3
	0.0001 ( <i>ALS</i> )	21	20.2	19.5-20.9
	0.1	14.3	17.1	15.8-18.5
	0.63	12.4	16.1	14.5-17.8
Barents Sea	0.01 ( <i>ULS</i> )	14.2	18.1	16.4-20.0
	0.0001 ( <i>ALS</i> )	18	20.9	19.3-22.7
	0.1	12.2	16.6	14.8-18.8
	0.63	10.5	15.4	13.3-17.7

Table 8: Monthly Extreme Values of  $H_s$  from 3-parameter Weibull distribution

	Months	1	2	3	4	5	6	7	8	9	10	11	12
	q	$H_s$ [m]											
Haltenbanken	0.01 ( <i>ULS</i> )	17.1	16.3	14.1	12.8	10.4	9.27	7.79	8.97	13.5	14.4	15.5	15.5
	0.0001 ( <i>ALS</i> )	21.5	20.3	17.5	16.6	13.7	12.4	10.2	11.9	17.6	18.2	19.6	19.2
	0.1	14.8	14.1	12.3	10.8	8.63	7.67	6.54	7.48	11.4	12.3	13.2	13.5
	0.63	12.8	12.3	10.8	9.21	7.22	6.37	5.52	6.27	9.64	10.6	11.4	11.8
Barents Sea	0.01 ( <i>ULS</i> )	14.1	15.3	12.5	9.53	9.33	7.81	7.03	9.71	9.9	12.3	12.5	12.6
	0.0001 ( <i>ALS</i> )	17.6	19.5	15.7	11.7	12.1	10.1	9.19	13.3	12.7	15.8	15.8	15.6
	0.1	12.2	13	10.8	8.33	7.87	6.61	5.91	7.92	8.42	10.5	10.8	11
	0.63	10.6	11.2	9.35	7.31	6.67	5.61	4.99	6.49	7.19	8.97	9.3	9.61

Table 9: Extreme Values of  $H_s$  from 3-parameter Weibull distribution

	q	$H_s$ [m]	Parameters for 3 p. Weibull	
Haltenbanken	0.01 ( <i>ULS</i> )	17.2	$\hat{\rho}$	1.6694
	0.0001 ( <i>ALS</i> )	22.0	$\hat{\beta}$	1.2074
	0.1	14.7	$\hat{\lambda}$	0.6288
	0.63	12.6		
Barents Sea	0.01 ( <i>ULS</i> )	14.2	$\hat{\rho}$	2.0782
	0.0001 ( <i>ALS</i> )	18.2	$\hat{\beta}$	1.2219
	0.1	12.1	$\hat{\lambda}$	0.7174
	0.63	10.4		

## 2.7 Determining extreme response by a contour plot

When designing a structure such as a permanent offshore rig which is to operate in a certain area, it is necessary to determine the extreme structural response. One can then consider the extreme values which are presented in Section 2.6, but these values might not give the extreme structural response. Therefore, other methods should be considered, taking  $T_p$  into account. The reason why one should consider  $T_p$  as well as  $H_s$  is due to the fact that a certain wave period might cause a greater load on the structure than an extreme wave height. This is known as resonance, a phenomenon that consists of a given system being driven by external forces to oscillate with greater amplitude at some preferential frequencies ([28]). NORSOK [25] recommends producing contour plots which are functions of both  $H_s$  and  $T_p$  (other combinations could also be of relevance, e.g. taking current into consideration). These contour plots, or contour lines, should correspond to the *ULS* and *ALS* criterias, i.e. contour lines which correspond to the 100 and 10 000 year extreme sea states. When such a plot is produced, one should investigate points along the contour, i.e. investigate what kind of response the various sets of  $[H_s, T_p]$  will produce.

One way of creating the contour lines is by using the *Inverse First Order Reliability Method (IFORM)*, as described in Haver [10, p. 85]. The method includes the following steps:

1. The probability of exceeding the value of  $H_s$  corresponding to the *ULS* criteria is established:  $P[H_s > h_{s,ULS}] = 1 - F_{H_s}(h_{s,ULS}) = \frac{1}{N} = \frac{1}{\frac{100 \cdot 365 \cdot 24}{3}} = 3.42 \cdot 10^{-6}$ .
2. The corresponding value of  $x$  in Gaussian space is established:

$$\begin{aligned}
 P[X > x] &= 1 - F(x|\mu, \sigma) = 3.42 \cdot 10^{-6} \\
 P[X \leq x] &= F(x|\mu, \sigma) = 1 - 3.42 \cdot 10^{-6} = 0.9999965 \\
 x &= F^{-1}(p = 0.9999965|\mu, \sigma)
 \end{aligned}$$

3. The absolute value of  $x$  can be considered as the radius  $r$  of a sphere in Gaussian

space. It is found by employing the inverse Gaussian cumulative distribution:

$$\begin{aligned}\mu &= 0, \sigma = 1 \\ \rightarrow x = r &= F^{-1}(p = 0.9999965|0, 1) = 4.5\end{aligned}$$

Figure 23 illustrates the probability under the Gaussian probability distribution function (*PDF*) curve (the Gaussian *PDF* is defined in equation 27, from Walpole [29, p. 173]), which practically covers the entire area, and the value of the radius ( $r = 4.5$ ). The Gaussian contour line, a sphere, is illustrated in Figure 24.

$$f(x|\mu, \sigma) = \frac{1}{\sigma\sqrt{2\pi}} \exp\left[-\frac{(x-\mu)^2}{2\sigma^2}\right] \quad (27)$$

Finally, the points on the Gaussian sphere are transformed into physical space by using the *Rosenblatt*-transformation:

$$F(u_1) = F_{H_s}(h_s) = 1 - \exp\left[-\left(\frac{h_s}{\rho}\right)^\beta\right] \quad (28)$$

$$\rightarrow h_s = \rho \left[-\ln 1 - F(u_1)\right]^{\frac{1}{\beta}} \quad (29)$$

$$F(u_2) = F_{T_p|H_s}(t_p|h_s) = \frac{1}{2} + \frac{1}{2} \operatorname{erf}\left[\frac{\ln(t_p) - \mu(h_s)}{\sqrt{2}\sigma(h_s)}\right] \quad (30)$$

$$\rightarrow t_p = \exp\left[(\sqrt{\sigma} \cdot u_2) + \mu\right] \quad (31)$$

Each value of  $U_1$  and  $U_2$  yield a value of  $H_s$  and  $T_p$ , producing the contour lines which are sought for. Such contour plots for Haltenbanken and the Barents Sea are presented in Figures 25 and 26. With this plot one can investigate the different sets  $[H_s, T_p]$  along the contour line. Each set of  $H_s$  and  $T_p$  yields a structural response, and the structure should according to regulations set by *NORSOK* be able to withstand what is considered the worst of these.

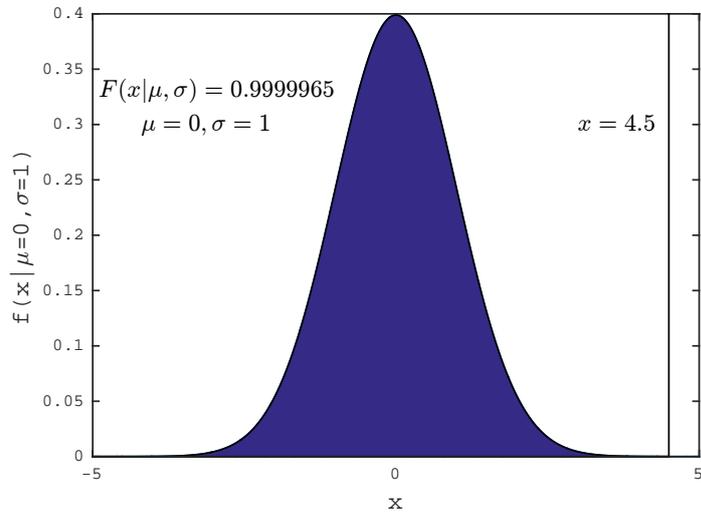


Figure 23: Gaussian pdf

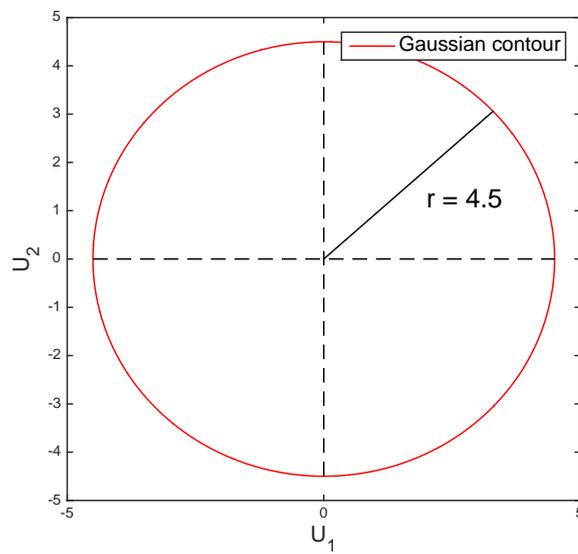


Figure 24: Gaussian space

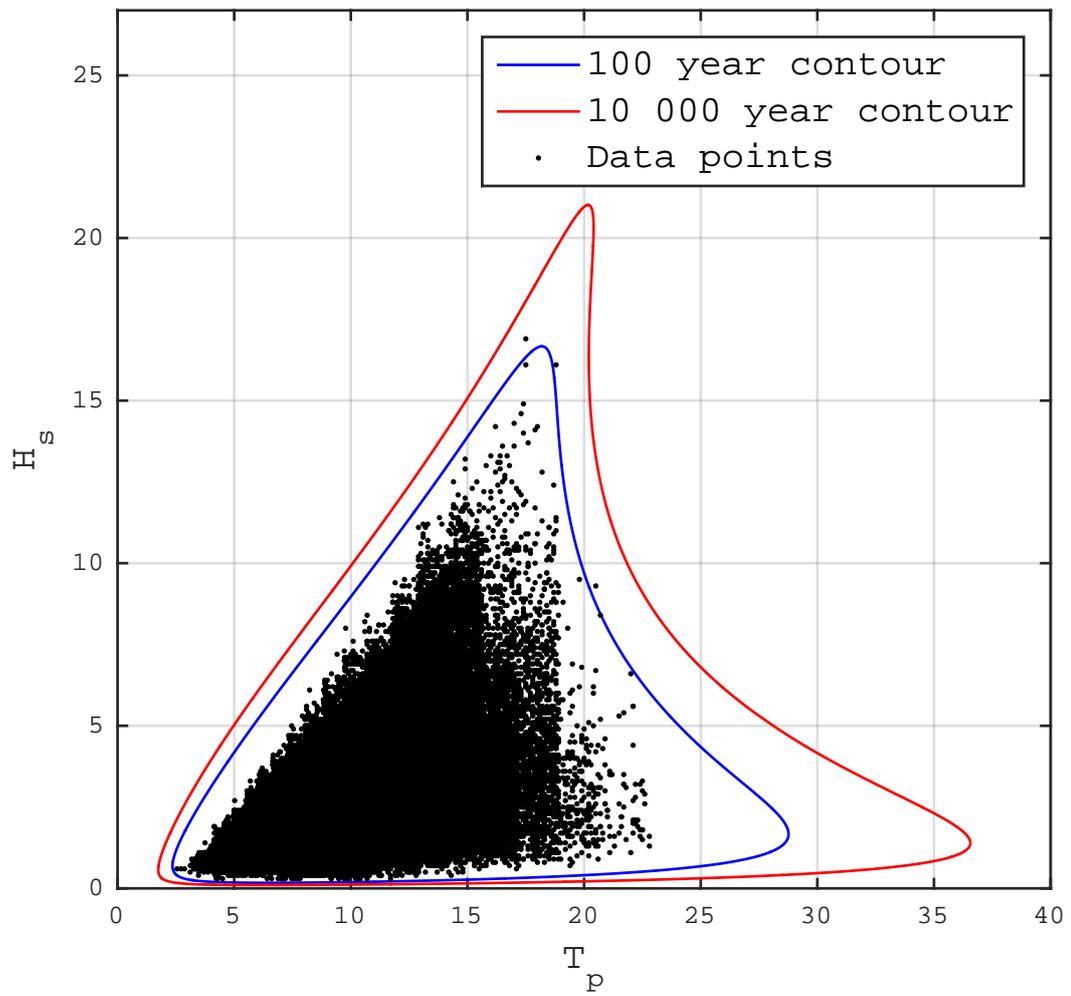


Figure 25: Contour plot, Haltenbanken

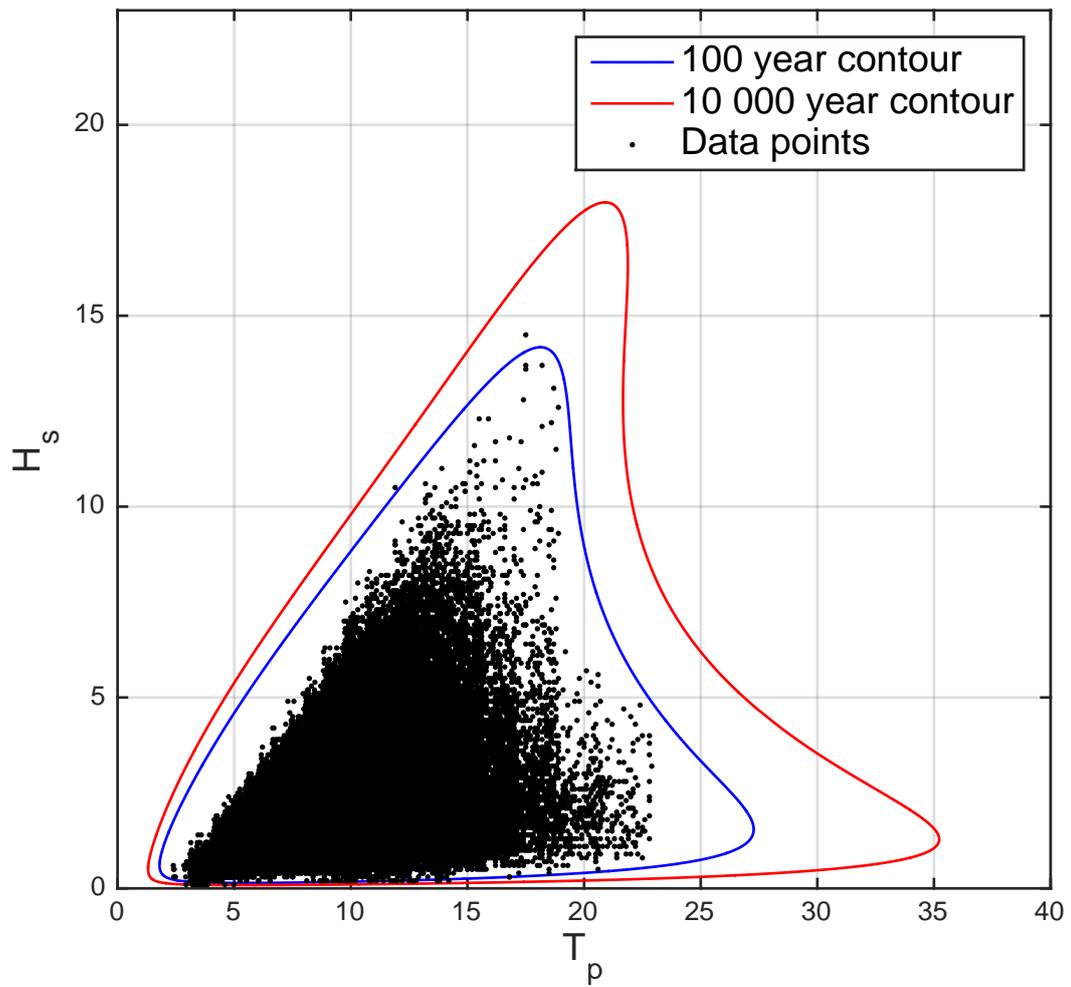


Figure 26: Contour plot, Barents Sea

## 2.8 Duration of good and bad weather windows

In connection to marine operations, it is of high interest to establish information about the duration of good and bad weather windows. Good weather windows are periods of time where there are no occurrences of waves larger than a chosen threshold. If one has information of these weather windows, it is easier to plan when and where a marine operation can happen. In this project, waves have been defined as the phenomenon of interest, but it can be of interest to define weather windows in terms of other phenomena such as wind or current. Figure 27 illustrates the definitions of the duration of good and bad weather windows which are found in Nielsen [24, p. 29]). The terms "calm" and "storm", and "good" and "bad" weather windows, are used throughout the report. The Figure illustrates registered values of  $H_s$ , which are recorded every third hour. Between  $t_1$  and  $t_2$ , all recorded values of  $H_s$  are below the threshold value  $H'_s$  of 2 metres, i.e. this period is a calm period, denoted  $\tau_c$ . On the other hand, between  $t_2$  and  $t_3$ , all recorded values of  $H_s$  are above  $H'_s$ , i.e. it is a stormy period, denoted  $\tau_s$ . The threshold value  $H'_s$ , which will of course play a huge role in determining the weather windows, can vary quite a lot, dependent on what kind of operation one is looking at. Table 10 gives an overview of different marine operations and their operational limits.

The following sections present the average duration of both calms and storms and the distributions for the duration of calms and storms. Both Haltenbanken and the Barents Sea have been investigated, and different techniques have been used in different *MATLAB* scripts, which are located in the folder "Weather Windows".

### 2.8.1 Average Duration of Calms

In connection to planning marine operations, the monthly average duration of a calm, denoted  $\bar{\tau}_c$  is valuable information. The average duration of a calm must be of such length that it seems feasible perform the operation in that particular month

What is the average duration of a calm in July, given a threshold of  $H_s = 2$  metres? What about January? In the following, such an investigation is presented.

Table 10: Table found in Nielsen [24, p. 31]: Approximate operational limits for some marine operations

	<b>Heave double amplitude &lt;(m)</b>	<b>Roll / pitch double amplitude &lt;(deg)</b>	$H_s$ < (m)
<b>Semisubmersible</b>			
Drilling	4	10	
Running casing	2	7	
BOP and riser handling	1.5	2	
Mooring			3
<b>Drill ship (head seas)</b>			
Drilling			5
Running casing			4
BOP and riser handling			3.5
<b>Large crane vessel</b>			
Mooring			3
Piling			4
<b>Pipeline repair, large water depth</b>			
Inspection			
Large monohull			4
Large semisub			7
Install welding habitat			
Large monohull			2
Large semisub			4

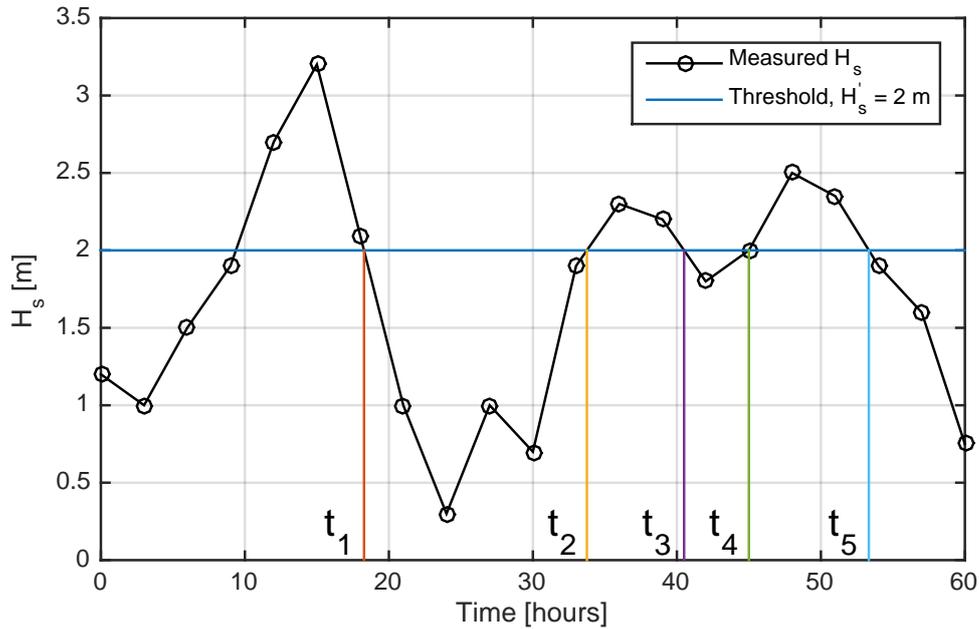


Figure 27: Definition of storms and calms

**Method** A *MATLAB* script called *average\_duration.m* was created in order to solve the task. First, the script uses the function *years.m* to fetch and sort all values of  $H_s$  by month. By doing this, the data is better organized, which in turn makes it easier to design the script. The function *years.m* takes  $H_s$  data and sorts it into one three dimensional array called *years*. This array contains 58 two dimensional arrays, representing 58 years of data. Array number 1 is 1957 while array number 58 is 2014. In each two dimensional array (each year), there are 12 columns which represent the months of the year. Table 11 shows one of these years. The script *years.m* has been used in most scripts for this project.

Secondly, the script inspects every column (month) and determines the number of calms by using a series of logical *if* statements along with variables which are set to "true" or "false" (0 or 1). These variables tell the script whether the last observation was a calm or a storm (if the value was below or above  $H'_s$ ), and in this way contributes in determining the length of the calms. Each observation which is below the threshold value adds another three hours in a calm because there are three hours between every observation. In order to determine the average duration of a calm of e.g. May, every

Table 11: Values of  $H_s$  for 1959, sorted by month

Observation no.	1959											
	Months											
	1	2	3	4	5	6	7	8	9	10	11	12
1	2.5	2.3	8.1	6.1	1.6	1.5	1.2	0.9	1.8	1.9	3.8	4
2	2.3	2.3	7.5	5.5	1.5	1.6	1.1	1	2	1.9	3.9	3.5
3	2.2	2.5	6.8	4.9	1.5	1.6	1	1	2.2	1.8	3.4	3.1
4	2.1	3.2	6	4.2	1.6	1.6	0.9	0.9	2.1	1.7	2.9	2.8
5	2.1	4.2	5.4	3.7	1.9	1.6	0.9	0.9	1.9	1.7	2.6	2.7
6	2.2	4.9	5	3.4	2.3	1.6	0.9	0.8	1.8	1.8	2.5	2.8
7	2.2	5	5	3.1	2.8	1.5	0.8	0.8	1.7	1.8	2.7	3
8	2.2	4.6	5.4	3	2.8	1.4	0.8	0.8	1.5	1.8	3.1	3.1
9	2.2	4.2	6	3.1	2.4	1.3	0.9	0.7	1.4	1.8	3.5	3
10	2.1	3.8	6.3	3.3	2	1.2	0.9	0.7	1.3	1.8	3.8	3.1
11	2	3.5	6.4	3.3	1.8	1.2	1	0.7	1.3	1.8	4.1	3.1
12	2	3.5	6.5	3.2	1.7	1.2	1.1	0.7	1.2	1.9	4.4	3
⋮	⋮	⋮	⋮	⋮	⋮	⋮	⋮	⋮	⋮	⋮	⋮	⋮
237	3.6	0	2.2	2.6	2.1	2	1.1	1.6	1.9	1.2	2.8	4.7
238	3.6	0	2.4	2.2	2.3	1.8	1	1.6	1.9	1.2	3.4	4.9
239	3.7	0	2.7	1.9	2.5	1.5	0.9	1.6	1.9	1.2	4	5
240	4.1	0	2.9	1.7	2.4	1.4	0.8	1.5	1.9	1.2	4.2	5.2
241	4.3	0	3	0	2.3	0	0.8	1.4	0	1.3	0	5.1
242	4.3	0	2.9	0	2.2	0	0.7	1.6	0	1.3	0	5.9
243	4	0	2.8	0	1.9	0	0.7	1.7	0	1.2	0	6.3
244	3.9	0	3.1	0	1.6	0	0.7	1.6	0	1.5	0	5.7
245	3.7	0	3.6	0	1.3	0	0.7	1.7	0	1.9	0	5
246	3.3	0	4.1	0	1.1	0	0.8	1.8	0	2.4	0	5
247	2.9	0	4.7	0	1.1	0	0.8	1.8	0	2.9	0	5.2
248	2.6	0	5.6	0	1.2	0	0.9	1.8	0	3.3	0	5.1

calm corresponding to this month is added together and divided by the total number of calms. Additionally, the worst and best months are determined by evaluating the calms of each year.

**Results** Figure 28 displays the average duration of calms for all months for Haltenbanken and the Barents Sea, given  $H'_s = 2$  metres. The longest average durations of calms are found in the summer months, which is of no surprise. The average duration of a calm in July at Haltenbanken is roughly 110 hours, while it is roughly 135 hours in the Barents Sea, implying that the conditions are more difficult at Haltenbanken. The variation of the length of calms for both areas is displayed in Figure 29, where the worst, mean and best months are plotted. The variation is quite similar for both, with the exception of august in the Barents Sea, which deviates significantly from the same month at Haltenbanken.

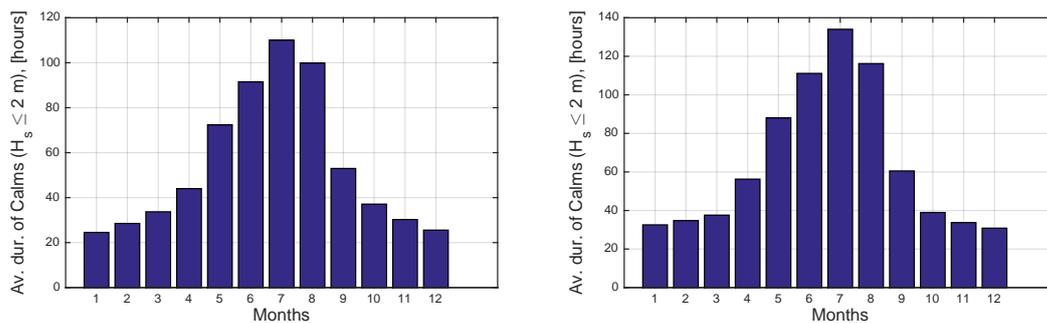


Figure 28: Average duration of calms for Haltenbanken (left) and the Barents Sea (right), using a threshold of  $H_s = 2\text{m}$

Durations of calms were also calculated using a threshold of five metres. Results are shown in Figure 30. The average duration of calms in July is nearly 700 hours, which means that on average, there will be calms with a time span of almost one entire month (30 days · 24 hours = 720 hours). In other words this means that on average you will very rarely see  $H_s$  larger than five metres in July. The variability is illustrated in Figure 31. It is seen that almost all of the best months are of the same value (between 720 and 744 hours). The reason for this is that, with such a large threshold value ( $H_s = 5\text{m}$ ), the best calms, i.e. the best months, will almost always have a calm of nearly the time span of the entire month.

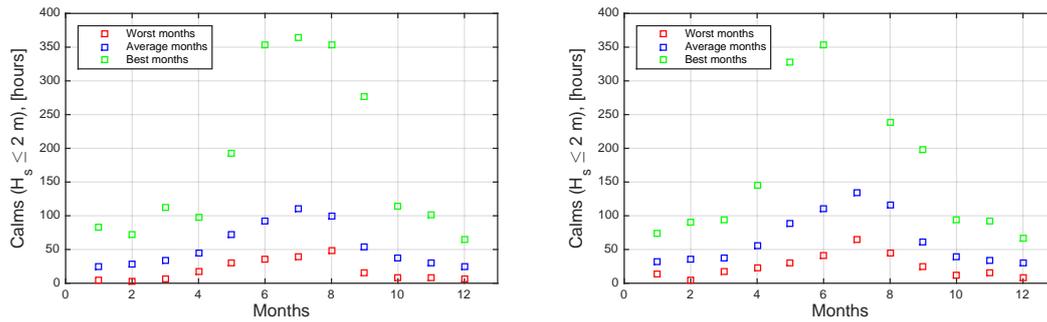


Figure 29: Worst, average and best duration of calms, Haltenbanken (left) and the Barents Sea (right), using a threshold of  $H_s = 2\text{m}$

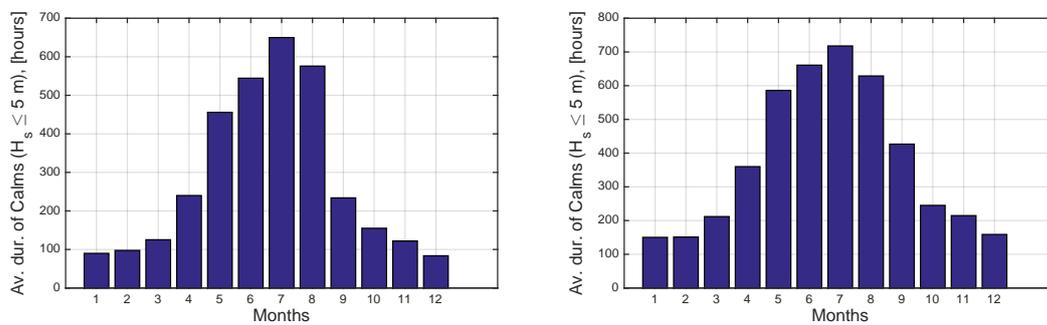


Figure 30: Average duration of calms for Haltenbanken (left) and the Barents Sea (right), using a threshold of  $H_s = 5\text{m}$

Figure 31 shows that the variability of some months is large. The average duration of a calm in December is relatively short, as we can see from Figure 30. But Figure 31 shows that there are some months which have calms which last the entire month of December. In December 2009, there was a calm in the Barents Sea which lasted the entire month (31 days  $\cdot$  24 hours = 744 hours), which is the best month of all months of December. It is easy to verify that this is true, by entering the data. The array `years(:,12,53)` represents December of year number 53 (2009), and the colon sign means that the entire column, i.e. all the data of this month, is looked at. By inspecting the column it goes to show that there are in fact no values of  $H_s$  larger than five metres. This is illustrated in Figure 32.

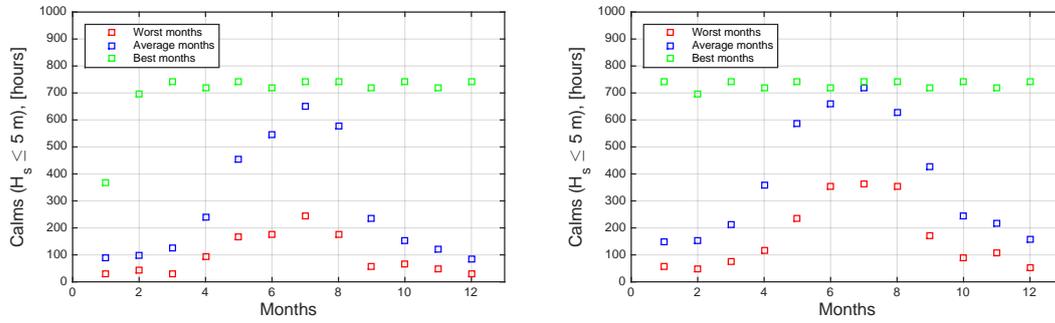


Figure 31: Worst, average and best calms, Haltenbanken (left) and the Barents Sea (right), using a threshold of  $H_s = 5$  m

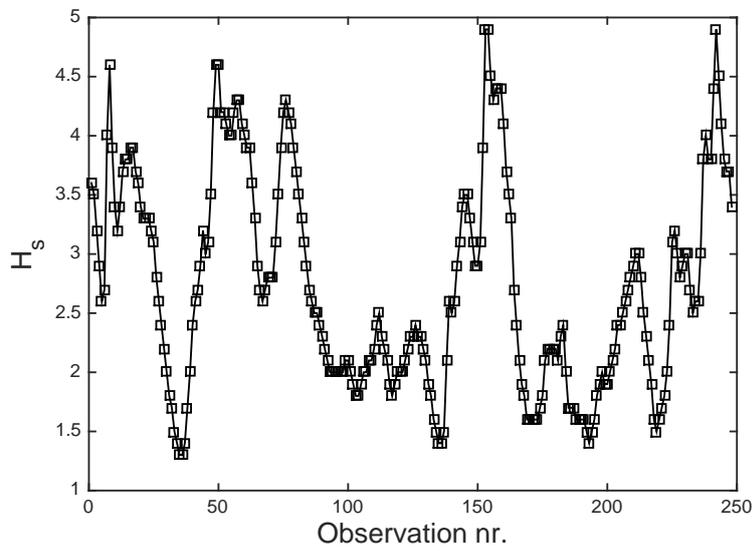


Figure 32: Values of  $H_s$ , December 2009

## 2.8.2 Average Duration of a Storm

Instead of looking at the average duration of a good weather window, how about considering the average duration of a bad weather window? As mentioned above, such a window is defined as a window where registrations are above the threshold value, i.e. above the acceptable value, and such a period of registrations is defined as a storm. It is of interest to know how long on average a storm will last when it first occurs. By having this information one can determine how long one is likely to be forced to sit and wait for the operation to get back on track. Operation costs include numerous expenses, and these are usually of a large scale in terms of marine operations. Hereunder lies crew salary, fuel consumption, rent of equipment, etc. By this one can understand that in terms of economy, information of the duration of stormy periods is useful. It is of course possible to get an indication of the duration of a storm based on the duration of a calm, which was established in Section 2.8.1, but here an accurate investigation has been performed.

**Results** The task was solved by using the script *average\_duration.m*, i.e. the same script as in Section 2.8.1. This script was originally designed to establish both calms and storms. As in Section 2.8.1, figures of the average duration of calms and storms and their corresponding variations are presented, found in Figures 33 through 36. The results show that the conditions are significantly more severe for Haltenbanken than the Barents Sea, in particular for the winter months. When the threshold is increased to five metres, the difference is not as significant. We can observe in Figure 35 that the average duration of a storm is more uniform for the Barents Sea than it is for Haltenbanken. It must be emphasized that in terms of storms, the best are considered to be the ones with the shortest duration, which is the opposite case of the best calms, which are considered to be the longest calms.

## 2.8.3 Describing the duration of calms and storms by a 2-parameter Weibull distribution

The subject of establishing parameters of a long term joint distribution for  $H_s$  and  $T_p$  was briefly discussed in Section 2.4.1. This subject is relevant in this section as well.

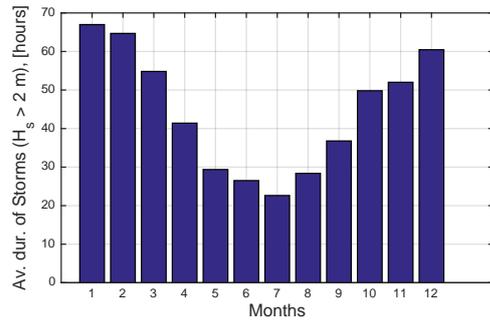
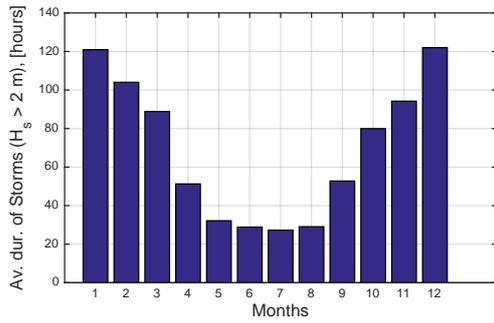


Figure 33: Average duration of storms for Haltenbanken and the Barents Sea, using a threshold of  $H_s = 2\text{m}$

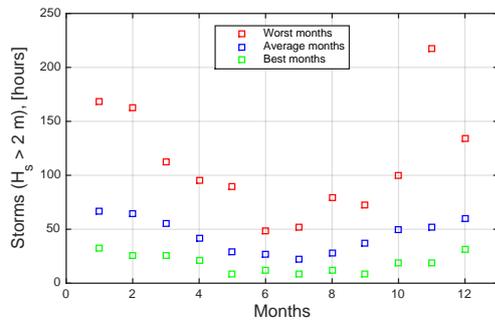
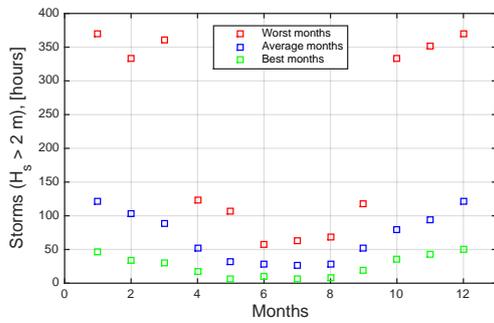


Figure 34: Worst, average and best duration of storms, Haltenbanken and the Barents Sea, using a threshold of  $H_s = 2\text{m}$

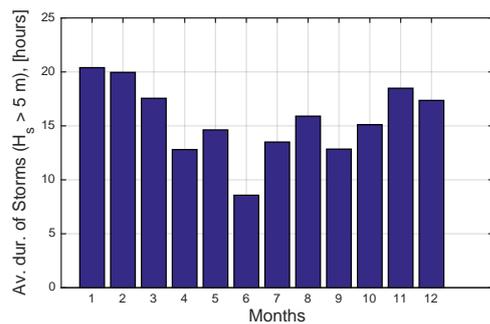
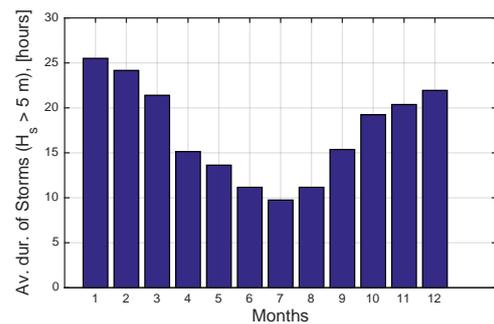


Figure 35: Average duration of storms for Haltenbanken and the Barents Sea, using a threshold of  $H_s = 5\text{m}$

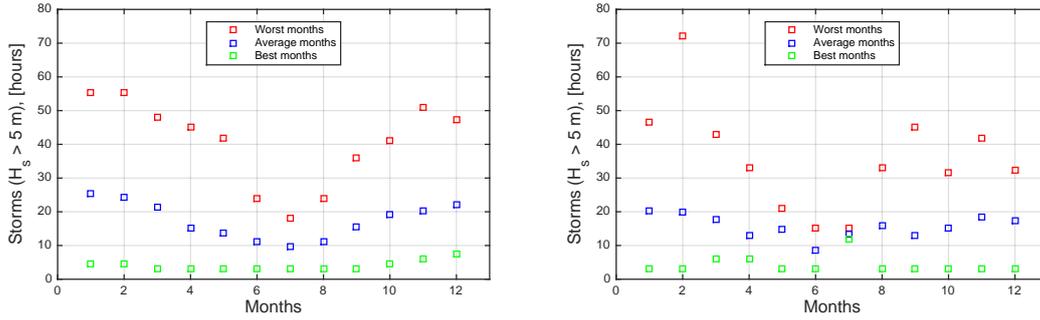


Figure 36: Worst, average and best duration of storms, Haltenbanken and the Barents Sea, using a threshold of  $H_s = 5$  m

With the calms established, is there any distribution which could describe the duration of these? Some theory on the subject is discussed in Nielsen [24, p. 32]: "Based on empirical data it is found that the cumulative probability of the duration of a calm period may be written as a two parameter Weibull distribution":

$$F_{\tau_c}(t) = P[\tau_c \leq t] = 1 - \exp \left[ - \left( \frac{t}{\rho} \right)^\beta \right] \quad x \geq 0 \quad (32)$$

The expression above represents the probability that a calm is below or equal to  $t$ .  $\rho$  is the scale parameter and  $\beta$  is the shape parameter. Here, it should be emphasized that  $\tau_c$  is the duration of a calm and not the average duration of a calm,  $\bar{\tau}_c$ .

The methods and calculations which were performed in order to determine both yearly and monthly 2-parameter Weibull distributions are presented in Section 2.8.3 and Section 2.8.3. The threshold value  $H'_s$  is equal to two metres throughout all calculations.

**Probability plot** In order to see whether or not the Weibull distribution (Equation 32) can be a possibility for describing the calms, a probability plot is a useful tool. As stated in Section 2.4.1, the probability plot is a plot where the y-axis is a linearization of the cumulative distribution and the x-axis is the natural logarithm of the data. The cumulative distribution function (CDF) for the calms is obtained by

$$F_{\tau_c}(t) = P[\tau_c \leq t] = \frac{n_i}{N+1} \quad t \geq 0 \quad (33)$$

$n_i$  is the number of calms lower than or equal to  $t$  and  $N$  is the total number of calms. The *CDF* is displayed in Table 12. As we can see, the intervals, or values of  $t$ , were chosen to be of lengths of 10 hours. Total number of calms is 3891. This table was obtained using the function *prob\_under\_t\_func.m*, which in turn uses the function *durationz.m*. The latter establishes the calms, while the first investigates whether or not the calm is below or equal to  $t$ . In this manner the number of calms below  $t$ ,  $n_i$ , is determined. When the *CDF* had been established, the next step was to use this in the probability plot. As mentioned, this paper has some special axes. Since this was a Weibull probability plot, the y-axis is  $\ln(-\ln(1 - F_{\tau_c}(t)))$  and the x-axis is  $\ln(t)$ . The reason is because the *CDF* is linearized:

$$\begin{aligned}
 F_{\tau_c}(t) &= 1 - \exp \left[ - \left( \frac{t}{\rho} \right)^\beta \right] \\
 -\ln(1 - F_{\tau_c}(t)) &= \left( \frac{t}{\rho} \right)^\beta \\
 \ln(-\ln(1 - F_{\tau_c}(t))) &= \beta \ln(t) - \beta \ln(\rho)
 \end{aligned} \tag{34}$$

The left hand of the last equation can be regarded as "y" and the right hand side as "ax + b" in the linear equation "y = ax + b".

$$\underbrace{\ln(-\ln(1 - F_{\tau_c}(t)))}_{\text{"y"}} = \underbrace{\beta \ln(t)}_{\text{"ax"}} - \underbrace{\beta \ln(\rho)}_{\text{"b"}}$$

We can now see that the term " $N + 1$ " is used to avoid infinite values because  $\ln(-\ln(1 - 1)) = \infty$ . If the probability plot,  $\ln(-\ln(1 - F_{\tau_c}(t)))$  versus  $\ln(t)$ , yields a somewhat straight line, the data might fit a Weibull distribution. Furthermore, one can perform linear regression in order to find estimates of the parameters of the Weibull model.

The probability plot which was established is illustrated in Figure 37, and the data is plotted together with a curve fit. The curve fit was done by using the built-in *MATLAB* function *fit*, which can use a various number of methods. In this case, Method of Least Squares was chosen. Finally, with the parameters  $a$  and  $b$  of the linear curve fit established, the parameters of the distributions,  $\beta$  and  $\rho$ , could be established by the

following relations:

$$\beta = a = 0.7925$$

$$\rho = \exp\left[-\frac{b}{\beta}\right] = \exp\left[-\frac{-3.0993}{0.7925}\right] = 49.9338$$

The *PDF* is plotted in Figure 38, while the *CDF* is plotted in Figure 39. In order to verify that the parameters are reasonable,  $\bar{\tau}_c$  was calculated using the established Weibull distribution and the script *average\_duraton.m* which uses the data directly:

$$\begin{aligned} \text{Weibull estimator: } \bar{\tau}_c = E[\tau_c] &= \rho \Gamma\left(1 + \frac{1}{\beta}\right) \\ &= 49.9338 \cdot \Gamma\left(1 + \frac{1}{0.7925}\right) = 56.96 \text{ hours} \\ \text{data: } \bar{\tau}_c = E[\tau_c] &= 56.26 \text{ hours} \end{aligned}$$

Further comparison was done by calculating some numbers using the Weibull *CDF* (found in Figure 38) and comparing these results to the *CDF* found from the data. This is found in Table 13. One can see that there are discrepancies here. In reality it is difficult to describe a phenomena perfectly, and one might have to accept small discrepancies. The important thing is that the distribution can represent the part which is the most interesting, well enough. If the upper part of the distribution (the largest values) are of interest, then it is important that the chosen distribution can represent the largest values with sufficient accuracy. With that being said, the method of using a probability plot is in most cases only used as a test to see whether or not the phenomena might be described by the proposed model. Therefore, the next chapter will look into estimation of parameters by a different method, assuming that the 2-parameter Weibull distribution is satisfactory.

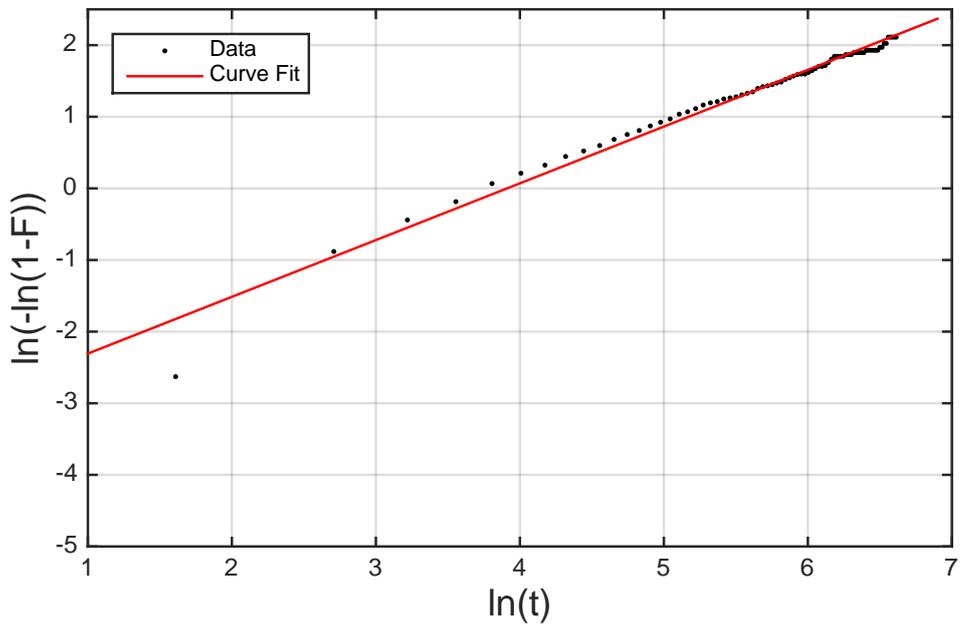


Figure 37: Probability plot and curve fit

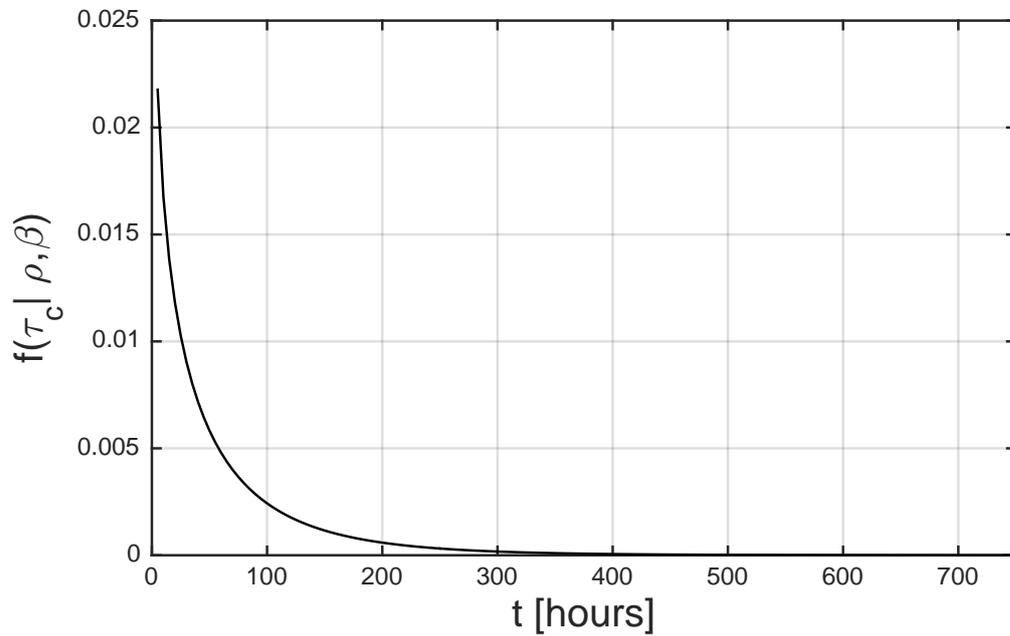


Figure 38: 2-parameter Weibull *PDF* for the duration of calms, Haltenbanken

Table 12: Cumulative Distribution Function of Calms

$t$	$n_i$	$N + 1$	$P[\tau_c \leq t] = \frac{n_i}{N+1}$
5	271	3892	0.0696
15	1320	3892	0.3392
25	1847	3892	0.4746
$\vdots$	$\vdots$	$\vdots$	$\vdots$
395	3864	3892	0.9928
405	3867	3892	0.9936
$\vdots$	$\vdots$	$\vdots$	$\vdots$
745	3891	3892	0.9997

Table 13: Comparing results from data and Weibull, parameters found by probability plot

$t$	$P[\tau_c \leq t], \text{ data}$	$P[\tau_c \leq t], \text{ Weibull}$
5	0.0696	0.1491
25	0.4746	0.4389
55	0.7094	0.6603
105	0.8623	0.8351
455	0.9961	0.9969
705	0.9997	0.9997

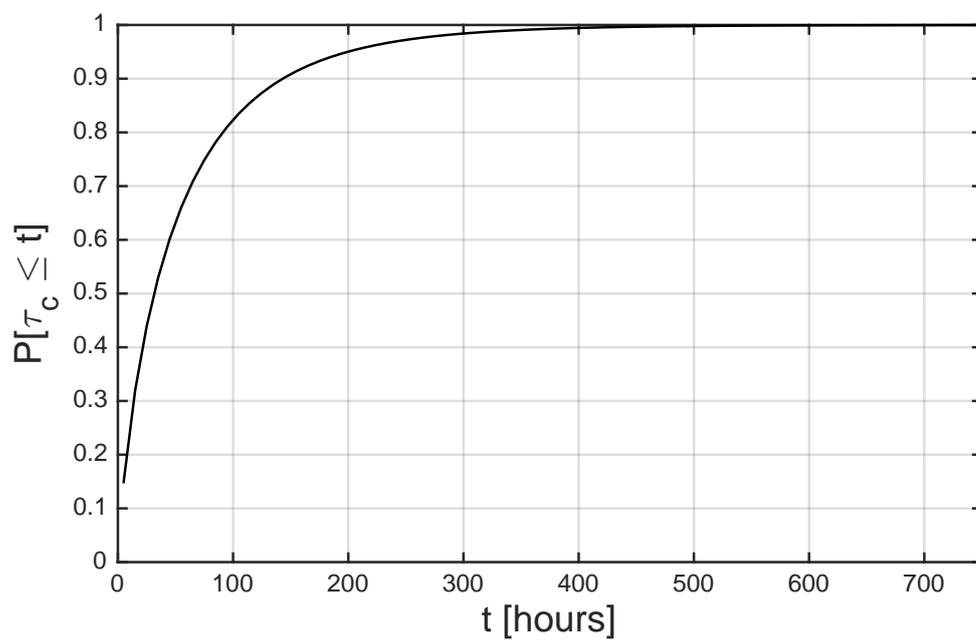


Figure 39: 2-parameter Weibull *CDF* for the duration of calms, Haltenbanken

**Estimating parameters using the Method of Moments** As stated in Section 2.8.3, a probability plot is only used as an indication as to whether or not a phenomena might be described by a certain model. In this case, a 2-parameter Weibull model was proposed to describe the duration of calms. Since the indication was strong, further estimation of parameters using different and more accurate methods was relevant. Method of Moments is a common method, which uses expressions for the mean and variance of a distribution in order to estimate parameters of the distribution. According to [22], the moments of the 2-parameter Weibull distributions are given as

$$E[\tau_c] = \rho \Gamma\left(1 + \frac{1}{\beta}\right) \quad (35)$$

$$VAR[\tau_c] = \rho^2 \left[ \Gamma\left(1 + \frac{1}{\beta}\right) - \Gamma^2\left(1 + \frac{1}{\beta}\right) \right] \quad (36)$$

Since both the mean and variance can be calculated from the hindcast data, the parameters can be calculated by the following method: First, the standard deviation is divided by the mean:

$$\begin{aligned} \frac{STD[\tau_c]}{E[\tau_c]} &= \frac{\sqrt{\rho^2 \left[ \Gamma\left(1 + \frac{1}{\beta}\right) - \Gamma^2\left(1 + \frac{1}{\beta}\right) \right]}}{\rho \Gamma\left(1 + \frac{1}{\beta}\right)} \\ &= \frac{\sqrt{\left[ \Gamma\left(1 + \frac{1}{\beta}\right) - \Gamma^2\left(1 + \frac{1}{\beta}\right) \right]}}{\Gamma\left(1 + \frac{1}{\beta}\right)} \end{aligned} \quad (37)$$

Notice that the parameter  $\rho$  is now out of the equation, leaving only one unknown variable which is  $\beta$ . Secondly, the ratio of the standard deviation and the mean is moved to the right of the equality, giving the following

$$\frac{\sqrt{\left[ \Gamma\left(1 + \frac{1}{\beta}\right) - \Gamma^2\left(1 + \frac{1}{\beta}\right) \right]}}{\Gamma\left(1 + \frac{1}{\beta}\right)} - \frac{STD[\tau_c]}{E[\tau_c]} = 0 \quad (38)$$

With this expression one can find the estimator  $\hat{\beta}$  by iteration. The estimator is established by trying with different values of  $\beta$  in the left term of Equation 38. The  $\beta$  value

Table 14: Comparing results from data and Weibull, parameters found by Method of Moments

$t$	$P[\tau_c \leq t], \text{ data}$	$P[\tau_c \leq t], \text{ Weibull}$
5	0.0696	0.1591
25	0.4746	0.4515
55	0.7094	0.6685
105	0.8623	0.8379
455	0.9961	0.9965
705	0.9997	0.9996

which yields the closest result to zero is chosen as an estimator for  $\beta$ ,  $\hat{\beta}$ . In Section 2.8.3  $\beta$  was established by a probability plot, and it was therefore natural to start with a value close to this. Iteration starting from  $\beta = 0.65$  to  $\beta = 0.9$  was done, producing the graph found in Figure 40. In the graph one can see that the input value of  $\beta$  which gave zero is roughly 0.8 (0.7723), i.e. our estimation of the parameter  $\beta$  is  $\hat{\beta} = 0.7723$ .  $\hat{\rho}$  is then found by

$$\hat{\rho} = \frac{E[\tau_c]}{\Gamma\left(1 + \frac{1}{\hat{\beta}}\right)} = \frac{56.26}{\Gamma\left(1 + \frac{1}{0.7723}\right)} = 48.3731 \quad (39)$$

The parameters are now inspected by evaluating  $E[\tau_c]$ :

$$\text{Weibull estimator: } E[\tau_c] = \rho \Gamma\left(1 + \frac{1}{\hat{\beta}}\right) = 48.373 \cdot \Gamma\left(1 + \frac{1}{0.7723}\right) = 56.26 \text{ hours}$$

$$\text{data: } E[\tau_c] = 56.26 \text{ hours}$$

The two values of  $E[\tau_c]$ , obtained from the Weibull distribution and the data, are now equal. With reference to Table 13, another table comparison was done, now using the new parameters. See Table 14. The values are closer than in Table 13, even though there still are discrepancies. These results suggests that the parameters which have been obtained by the method of moments are more accurate than the ones which were obtained using the probability plot.

By using the data in such a fashion in order to determine the parameters, it is obvious that one is in need of a sufficient amount of data in order to acquire a satisfying accuracy.

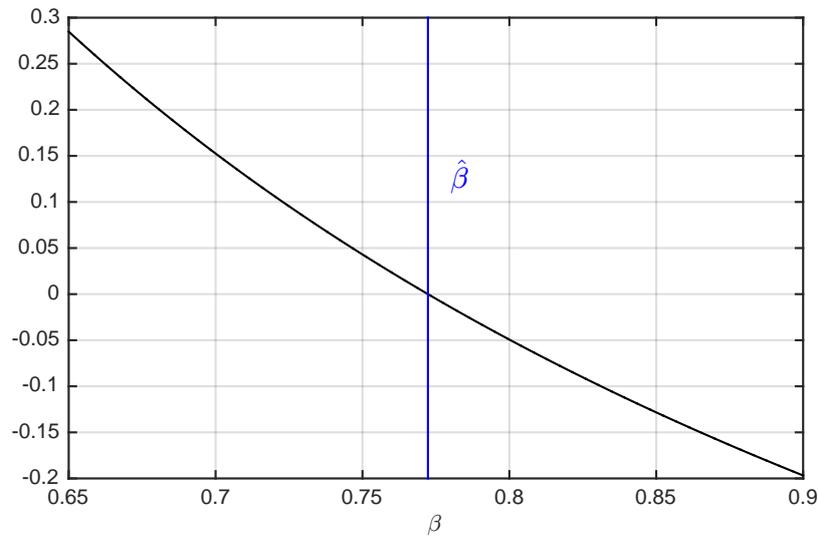


Figure 40: Estimation of  $\beta$  using Method of Moments

The final product can be found in Figure 41 which illustrates the 2-parameter Weibull *PDF* with the estimated parameters. With this, one can now determine how likely it is to experience a calm of a certain length any time of the year. It is also possible to find extreme values by the distribution of the longest calm, which is looked at in Section 3.2.

**Monthly distributions of the duration of calms and storms** As with the monthly distributions of  $H_s$ , presented in Section 2.5, it is of interest to produce monthly distributions of the duration of calms and storms as well. By doing this one can obtain a larger accuracy during relevant analyses or simulations.

Similar to the procedure in Section 2.5, the parameters of the monthly distributions were estimated using the method of moments. First, all values of  $\tau_c$  and  $\tau_s$  were sorted by month. Secondly, the mean, variance and skewness were calculated, and lastly, the parameters were estimated by the expressions for the moments. Estimated parameters for both Haltenbanken and the Barents Sea can be found in Tables 15 and 16. Cumulative distributions of both data and estimated parameters for Haltenbanken can be seen in Figures 42 and 43, while the *PDF*'s can be seen in Figure 44. Figures 42 and 43 show that there are not as many data points for January as there is for July, and this is due to

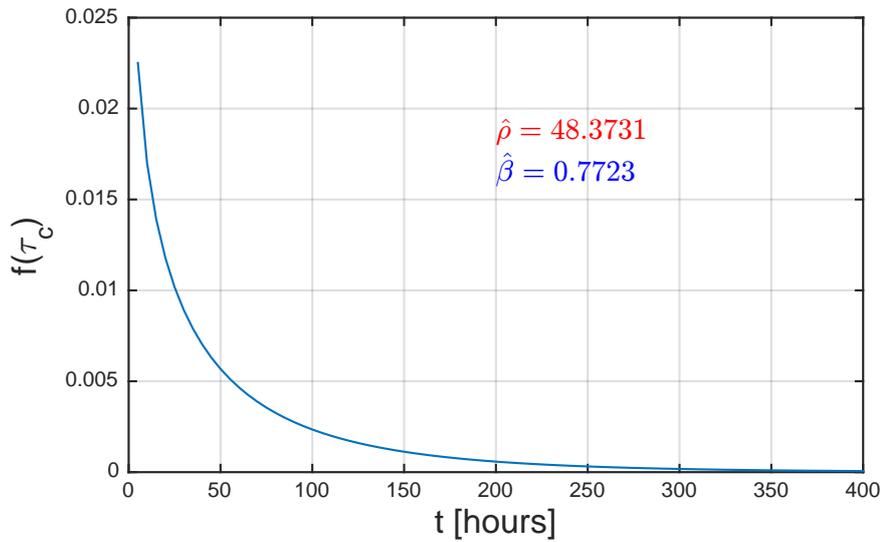


Figure 41: Yearly *PDF* of the duration of calms, parameters estimated by method of moments

Table 15: Estimated parameters for monthly distributions of the duration of a calm,  $\tau_c$ .

Months	1	2	3	4	5	6	7	8	9	10	11	12
<b>Haltenbanken</b>												
$\hat{\rho}$	23.296	26.698	31.958	41.273	63.527	80.04	94.621	84.525	43.813	34.119	26.535	24.468
$\hat{\beta}$	1.0519	0.9523	0.9689	0.9702	0.9363	1.0188	0.8785	0.8871	0.8417	0.9888	0.9054	1.0992
<b>Barents Sea</b>												
$\hat{\rho}$	30.661	31.545	35.177	51.747	81.243	95.29	114.77	103.68	51.108	36.354	32.232	27.4
$\hat{\beta}$	0.9825	1.0768	0.9968	0.9582	0.9643	0.9216	0.9205	0.9859	0.8661	0.9256	0.9788	0.9720

the fact that sea state is more severe in January than in July. Since the sea states are more severe, there are less calms, hence there is less data available to estimate parameters by. This is probably why the *CDF* curve seem to fit better in July than in January. With that being said, the distribution for January is useful, even though the parameters might not be as accurate as one would have liked. In January, there is a 50 % chance that the duration of a calm is below or equal to roughly 20 hours, while in July, there is a 50 % chance that the duration of a calm is below or equal to roughly 60 hours.

Table 16: Estimated parameters for monthly distributions of the duration of a storm,  $\tau_s$

Months	1	2	3	4	5	6	7	8	9	10	11	12
<b>Haltenbanken</b>												
$\hat{\rho}$	131.426	117.056	92.951	54.931	33.744	30.752	31.296	30.835	52.756	81.681	101.913	139.821
$\hat{\beta}$	0.8929	0.8601	0.7968	0.9477	0.9657	1.0958	1.1607	1.0089	0.9085	0.9027	0.9552	0.9323
<b>Barents Sea</b>												
$\hat{\rho}$	69.469	59.859	59.095	45.503	33.914	29.602	26.157	31.994	41.592	56.203	58.946	65.768
$\hat{\beta}$	0.9113	0.8263	0.9842	1.1180	1.2233	1.2902	1.2605	1.2497	1.1427	1.0080	0.9924	1.0094

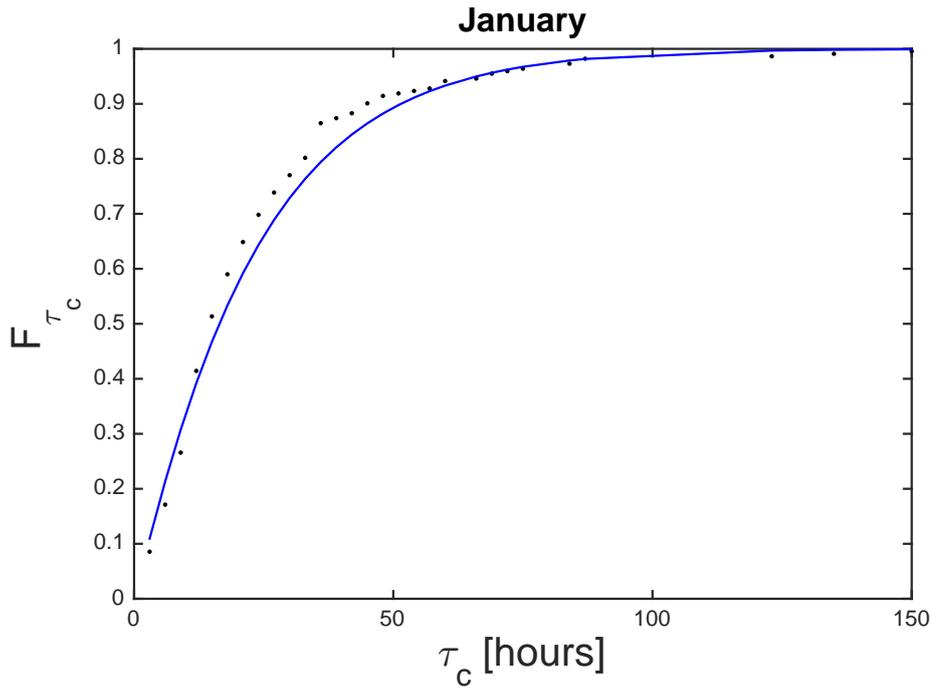


Figure 42: Weibull *CDF* for the duration of calms, January, Haltenbanken

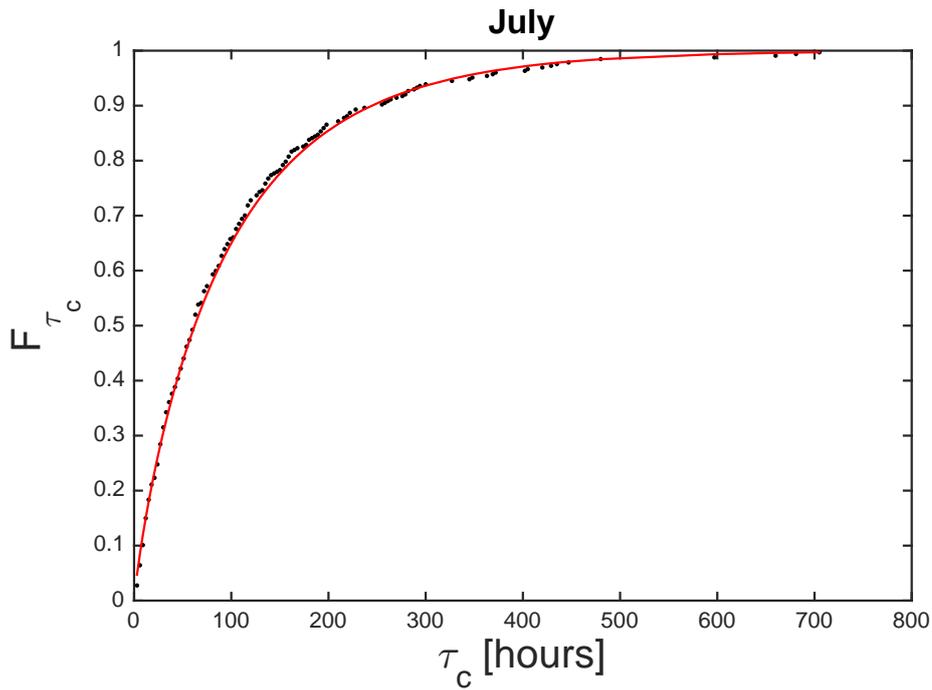


Figure 43: Weibull *CDF* for the duration of calms, July, Haltenbanken

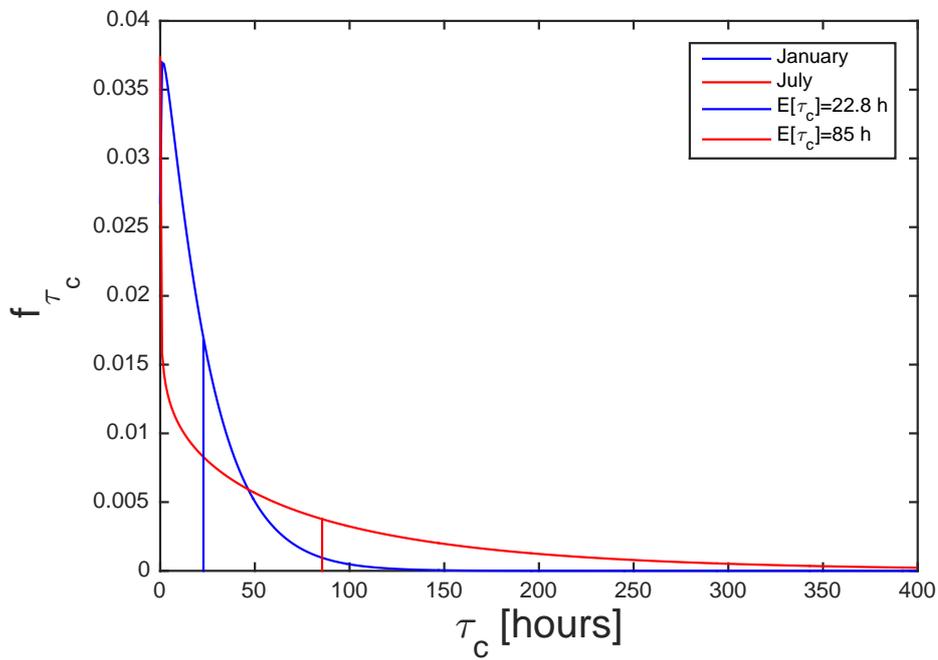


Figure 44: Weibull *PDF* for the duration of calms, January and July, Haltenbanken

## 3 Marine Operations

This part presents evaluations of marine operations. These have been conducted both with and without using the Metocean Design Basis which is presented in Section 2.

### 3.1 Establishing a limiting pair of $H_s$ and $T_p$ from a critical heave motion

Section 3.1.1 presents the background for this part of the project, while Section 3.1.2 presents relevant theory for the analysis which is presented in Section 3.1.3 and Section 3.1.4.

#### 3.1.1 Background

In connection to planning and conducting marine operations, establishing a feasible weather window is of high importance, particularly in terms of avoiding critical loads on the structure performing the operation, installation equipment or the structure which is operated on. An example of this could be a ship lowering a structure to the bottom of the ocean by a winch. In such an operation the load on the wire and the motion of the ship would be of utmost importance to keep under control. In this part of the report a general approach to how one can find limiting pairs of  $H_s$  and  $T_p$  corresponding to a critical heave amplitude is presented. The outline of the master thesis reads:

*”Discuss a particular operation where the critical variable is heave at midship, and indicate how one can establish a limiting pair of  $H_s$  and  $T_p$  from the critical heave motion.”*

The following presents an analysis where limiting values of  $H_s$  and  $T_p$  are determined by using a critical heave amplitude, response characteristics of a vessel and the hindcast data.

### 3.1.2 Theory

This section aims to establish some of the relevant theory which was used to perform the analysis which is presented in the next section.

Evaluation has been simplified by considering a point exactly at midship ( $x = 0, y = 0, z = 0$ ), see Figure 47). If one considers a point in the negative or positive x-direction of the vessel, one must also take the pitch motion  $\eta_5$  into consideration. If one considers a point in the negative or positive y-direction, the roll motion  $\eta_4$  must be considered. This is understood by the equation of motion of any point on the body, defined in Faltinsen [7, p. 41]:

$$s = (\eta_1 + z \eta_5 - y \eta_6)i + (\eta_2 - z \eta_4 + x \eta_6)j + (\eta_3 + y \eta_4 - x \eta_5)k \quad (40)$$

$\eta_3 + y \eta_4 - x \eta_5$  represents the vertical motion, and we can see that both roll  $\eta_4$  and pitch  $\eta_5$  influences the total vertical motion. Therefore, it must be emphasized that results which are presented in the following will most certainly change if one considers a different point on the vessel.

Since  $x = y = 0$ , Equation 40 reduces to  $s = \eta_3$  (considering only the vertical displacement). We can then start by defining the heave process  $\eta_3(t)$  of the structure on hand. The definition is based on the one which is used in Pettersen [27, p. 3.5]. Figure 45 illustrates a structure with zero velocity ahead, bobbing in waves coming in straight ahead of the structure. In this case, the motion in focus is the heave motion  $\eta_3$ . This motion is also illustrated in Figure 47. The waves are moving in negative x-direction, and the waves and the heave response can be written as

$$\zeta(t) = \zeta_A \cos(\omega t + kx) \quad \text{Waves} \quad (41)$$

$$\zeta(t) = \zeta_A \cos(\omega t) \quad \text{Waves at midship}(x = 0)$$

$$\eta_3(t) = \eta_{3A} \cos(\omega t + \varepsilon) \quad \text{Heave response} \quad (42)$$

The system is a linear response system, which implies that the heave process  $\eta_3(t)$  is linearly dependent on the wave process  $\zeta(t)$ , illustrated in Figure 46. This is commonly accepted for some quantities such as heave and pitch. The difference between the wave

process and the heave process is the phase shift  $\epsilon$ . In Figure 46 one can observe that the heave response comes after the waves. The wave process and therefore also the response process is a short term process dependant on one particular sea state.

**Describing the heave process by the Rayleigh distribution** If the right assumptions are made, the heave process can be described by a probability distribution function. The following theory is found in Myrhaug [23], and the assumptions are:

1. The heave process is stationary, i.e. the mean heave response  $\mu$  and variance  $\sigma^2$  is constant for our sea state.
2. Gaussian: the heave process is normal distributed with mean heave response  $\mu$  equal to zero and constant variance  $\sigma^2$ .
3. The heave process is narrow banded, i.e. all frequencies are close to  $\omega = 2\pi/T$ .

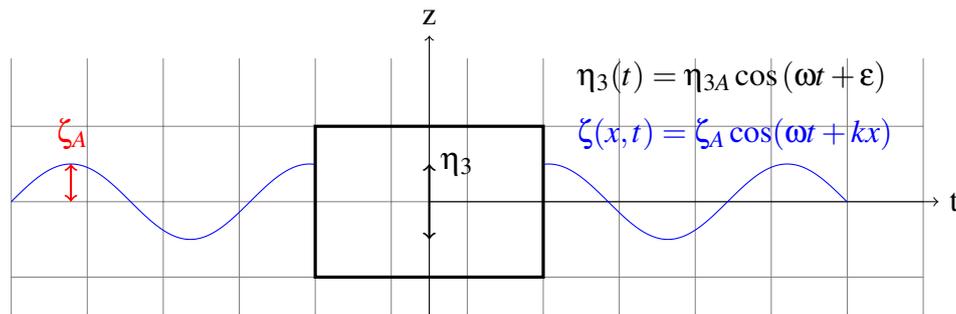


Figure 45: Structure in Waves

Based on these assumptions the heave process can be described by a Gaussian probability distribution function with expected heave response equal to zero. This is plotted in Figure 48 by the blue curve. The Gaussian distribution is written as

$$f_{\eta_3}(\eta_3) = \frac{1}{m_0\sqrt{2\pi}} \exp \left[ -\frac{(\eta_3 - \mu)^2}{2m_0^2} \right] \quad (43)$$

Furthermore, the heave response amplitudes  $\eta_{3a}$  (the maximum values in the heave process  $\eta_3(t)$ ) can be described by a Rayleigh distribution. The Rayleigh PDF is given

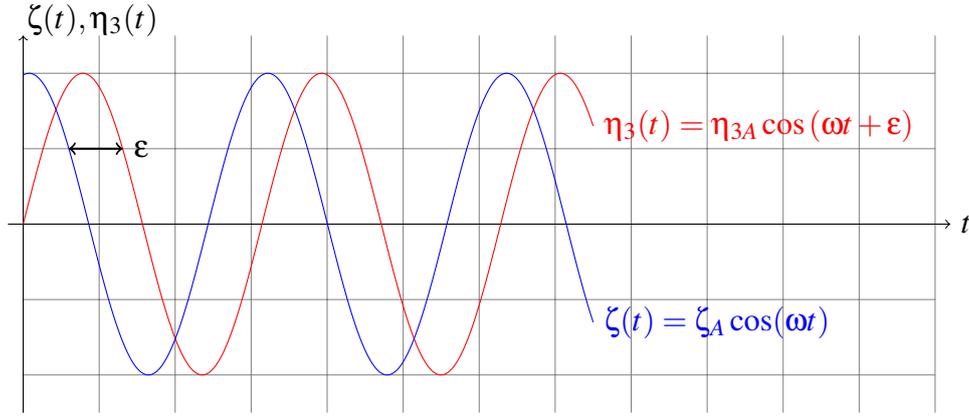


Figure 46: Wave Process and Response Process

as

$$f_{\eta_{3A}}(\eta_{3a}) = \frac{\eta_{3a}}{\sigma_{\eta_3}^2} \exp \left[ -\frac{1}{2} \left( \frac{\eta_{3a}}{\sigma_{\eta_3}} \right)^2 \right] \quad (44)$$

This is plotted in Figure 48 by the red curve. The cumulative distribution function can be written as

$$F_{\eta_{3A}}(\eta_{3a}) = 1 - \exp \left[ -\frac{1}{2} \left( \frac{\eta_{3a}}{\sigma_{\eta_3}} \right)^2 \right] \quad (45)$$

The standard deviation of the heave process,  $\sigma_{\eta_3}$ , is defined as

$$\sigma_{\eta_3} = \sqrt{\int_0^{\infty} S_{\eta_3}(\omega) d\omega} \quad (46)$$

$S_{\eta_3}(\omega)$  is the heave response spectrum, and is given by

$$S_{\eta_3}(\omega) = |RAO(\omega)|^2 \cdot S(\omega) \quad (47)$$

$RAO$  is a response amplitude operator and  $S(\omega)$  is a wave spectrum. The  $RAO$  is a transfer function which describes the motion characteristics of the structure, while the

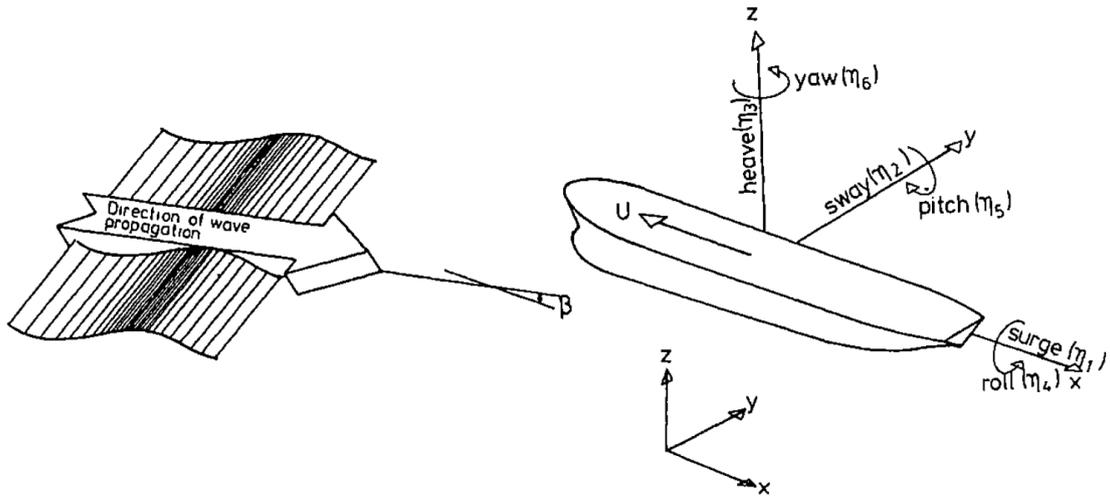


Figure 47: Figure found in Faltinsen [7, p. 41]: Rigid-body motions modes and wave propagation

wave spectrum  $S(\omega)$  represents the sea state at hand. The *RAO* will be evaluated more thoroughly in Section 3.1.3.

According to Haver [13, p. 22], Equation 47 is deduced by first considering the expression  $S_{\eta_3}(\omega_n) = \frac{\eta_{3a,n}^2}{2\Delta\omega}$ , which is analogous to  $S(\omega) = \frac{\zeta_{A,n}^2}{2\Delta\omega}$ . Assuming a linear relationship between waves and response,  $RAO(\omega_n) = \frac{\eta_{3a,n}}{\zeta_{A,n}}$ , we get

$$S_{\eta_3}(\omega_n) = \frac{|RAO(\omega_n)|^2 \zeta_{A,n}^2}{2\Delta\omega} = \frac{|RAO(\omega_n)|^2}{2\Delta\omega} S(\omega_n) 2\Delta\omega = |RAO(\omega_n)|^2 S(\omega_n) \quad (48)$$

**Critical Heave Amplitude** Let us say that the critical heave response amplitude of heave at midship is  $\eta_{3a_c}$ . In order to evaluate whether or not this value is exceeded, the largest heave response has to be inspected. This value can be found by manipulation of the cumulative distribution function of heave response amplitudes  $\eta_{3a}$ , Equation 45. If we have  $\eta_{3a_1}, \eta_{3a_2}, \dots, \eta_{3a_N}$  during a three hour sea state, then  $\eta_{3a_{max}}$  is the largest heave response amplitude among these  $N$  values.  $N$ , which is the number of zero up-crossing

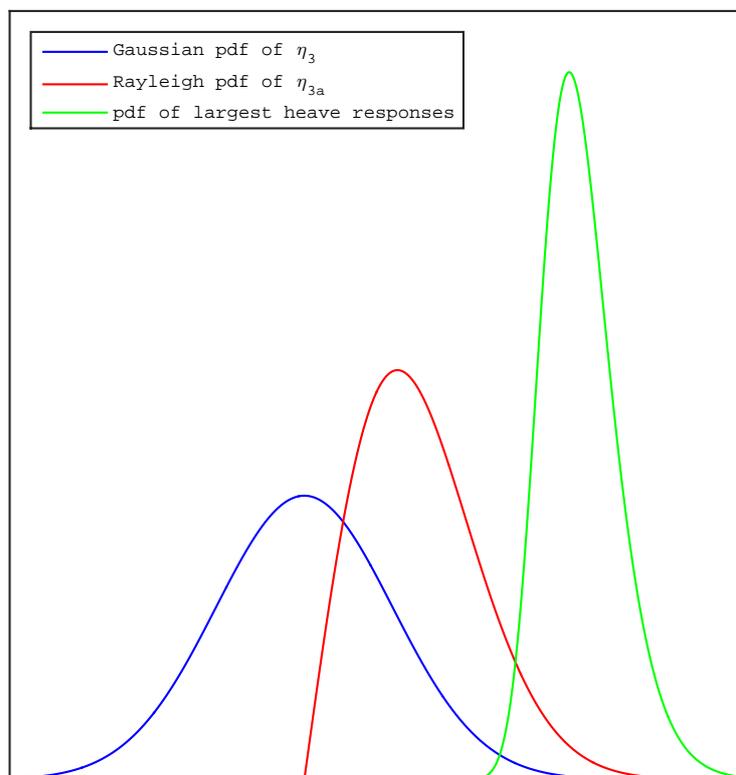


Figure 48: Probability distribution functions

response cycles during these three hours, is found by

$$m_n = \int_0^{\infty} \omega^n S_{\eta_3}(\omega) d\omega \quad n = 0, 1, 2, \dots \quad (49)$$

$$T_{m02} = 2\pi \sqrt{\frac{m_0}{m_2}} \quad (50)$$

$$N = \frac{3 \text{ hours}}{T_{m02}} = \frac{10800 \text{ s}}{T_{m02}} \quad (51)$$

Furthermore, if we assume that

1. all heave response amplitudes are identically Rayleigh distributed

2. all heave response amplitudes are statistically independent

we can define the cumulative distribution of the largest heave response amplitude as given in Myrhaug [23, p. 32]:

$$\begin{aligned}
P[\eta_{3a_{max}} \leq \eta_{3a}] &= P[(\eta_{3a_1} \leq \eta_{3a}) \cap \dots \cap (\eta_{3a_N} \leq \eta_{3a})] \\
&= P(\eta_{3a_1} \leq \eta_{3a}) \cdot P(\eta_{3a_2} \leq \eta_{3a}) \cdot \dots \cdot P(\eta_{3a_N} \leq \eta_{3a}) \\
&= [P(\eta_{3a_i} \leq \eta_{3a})]^N = [F_{\eta_{3A}}(\eta_{3a})]^N \\
&= \left[ 1 - \exp \left[ -\frac{1}{2} \left( \frac{\eta_{3a}}{\sigma_{\eta_3}(H_s, T_p)} \right)^2 \right] \right]^N = F_{\eta_{3a_{max}}} \quad (52)
\end{aligned}$$

By that,  $F_{\eta_{3a_{max}}}$  is the cumulative distribution function for the largest heave response amplitude. In Figure 48, the *PDF* is plotted by the green curve.

With this it is possible to determine a limiting value of  $H_s$  and  $T_p$  by following the formulation in Haver [13, p. 24]. If we now consider the probability of exceeding  $\eta_{3a_c}$ , we write

$$P[\eta_{3a_{max}} > \eta_{3a_c}] = 1 - \left[ 1 - \exp \left[ -\frac{1}{2} \left( \frac{\eta_{3a_c}}{\sigma_{\eta_3}(H_s, T_p)} \right)^2 \right] \right]^N \quad (53)$$

$$(54)$$

The accept criteria is  $P[\eta_{3a_{max}} > \eta_{3a_c}] \leq q$ , i.e.:

$$1 - \left[ 1 - \exp \left[ -\frac{1}{2} \left( \frac{\eta_{3a_c}}{\sigma_{\eta_3}(H_s, T_p)} \right)^2 \right] \right]^N \leq q \quad (55)$$

The free variable is the heave standard deviation. Solving with respect to heave standard deviation,  $\sigma_{\eta_3}(H_s, T_p)$ , we establish the following operational criteria:

$$\sigma_{\eta_3}(H_s, T_p) \leq \frac{\eta_{3a_c}}{\sqrt{-2 \ln [1 - (1 - q)^{1/N}]}} \quad (56)$$

The equation above states that as long as the standard deviation of the heave process is smaller or equal to the term to the right in the equation, the sea state is acceptable.

Keeping in mind that the objective of the task on hand is to show how one can establish a limiting pair of  $H_s$  and  $T_p$ , we can find these values by evaluating  $\sigma_{\eta_3}$ . If the value of  $\sigma_{\eta_3}$  fulfills the criteria above, one can say that the  $H_s$  and  $T_p$  values which produced  $\sigma_{\eta_3}$  are acceptable.

The value of  $q$  has been set to 0.1 in the following analysis. This means that we define  $\eta_{3a}$  to be below  $\eta_{3a_c}$  90 % of the time, which implies that there is a 10 % chance that  $\eta_{3a}$  exceeds  $\eta_{3a_c}$ . The reasoning behind the set value is nothing else than common sense. Which value to choose is something which is not studied in this project.  $\eta_{3a_c}$  has been set to 4 metres. Table 10 has been used as reference here. Values of both  $q$  and  $\eta_{3a_c}$  are of course easily changed.

### 3.1.3 Case

A case with a drill ship which is to perform a marine operation at Haltenbanken was chosen in order to discuss the subject in more detail. The theory presented in the previous section has been used to determine the response of the vessel. The critical responses and their corresponding sea states have been compared to relevant sea states represented by contour plots. Total sea has been used as input.

**Wave Spectrum** A wave spectrum was needed in order to carry out the analysis, and Section 2.3.1 spoke briefly about wave spectrums. There exists several standardized spectrums today, and for this case the JONSWAP spectrum was chosen: "Numerous models for the wave frequency spectrum have been proposed over the years. At present the most common model is the JONSWAP spectrum" (p. 117, Haver, 2013). The JONSWAP spectrum is more peaked than the Pierson Moskowitz spectrum, and this is based on research which was carried out in the North Sea. The JONSWAP spectrum for grow-

ing wind sea is given as (Haver [10, p. 150])

$$S(\omega) = \frac{1}{2\pi} H_s^2 T_p \left( \frac{\omega}{\omega_p} \right)^{-5} \exp \left[ -1.25 \left( \frac{\omega}{\omega_p} \right)^{-4} \right] (1 - 0.287 \ln \gamma) \gamma^{\exp \left[ -0.5 \left( \frac{\omega - \omega_p}{\omega_p \sigma} \right)^2 \right]} \quad (57)$$

where

$$\gamma = 42.2 \left( \frac{2\pi H_s}{g T_p^2} \right)^{\frac{6}{7}} \quad (58)$$

and

$$0.07, \omega \leq \omega_p \quad (59)$$

$$\sigma =$$

$$0.09, \omega > \omega_p$$

Figure 49 shows a wave spectrum with  $H_s = 1$  metres and  $T_p = 5$  seconds.

Verification of the *MATLAB* script and wave spectrum was done by the following considerations:

1. Verifying that the input value of  $T_p$  corresponded with the  $T_p$  of the wave spectrum which was produced: The spectral peak frequency,  $\omega_p$ , is found from  $\omega_p = \frac{2\pi}{T_p}$ . The input value of  $\omega_p$  was then compared to the peak value of the graph in Figure 49, by using a function in *MATLAB* which calculates the frequency corresponding to the peak of the graph. An almost perfect match of  $\omega_p = 1.27$  seconds was found.
2. Verifying that the input value of  $H_s$  corresponded with the  $H_s$  of the wave spec-

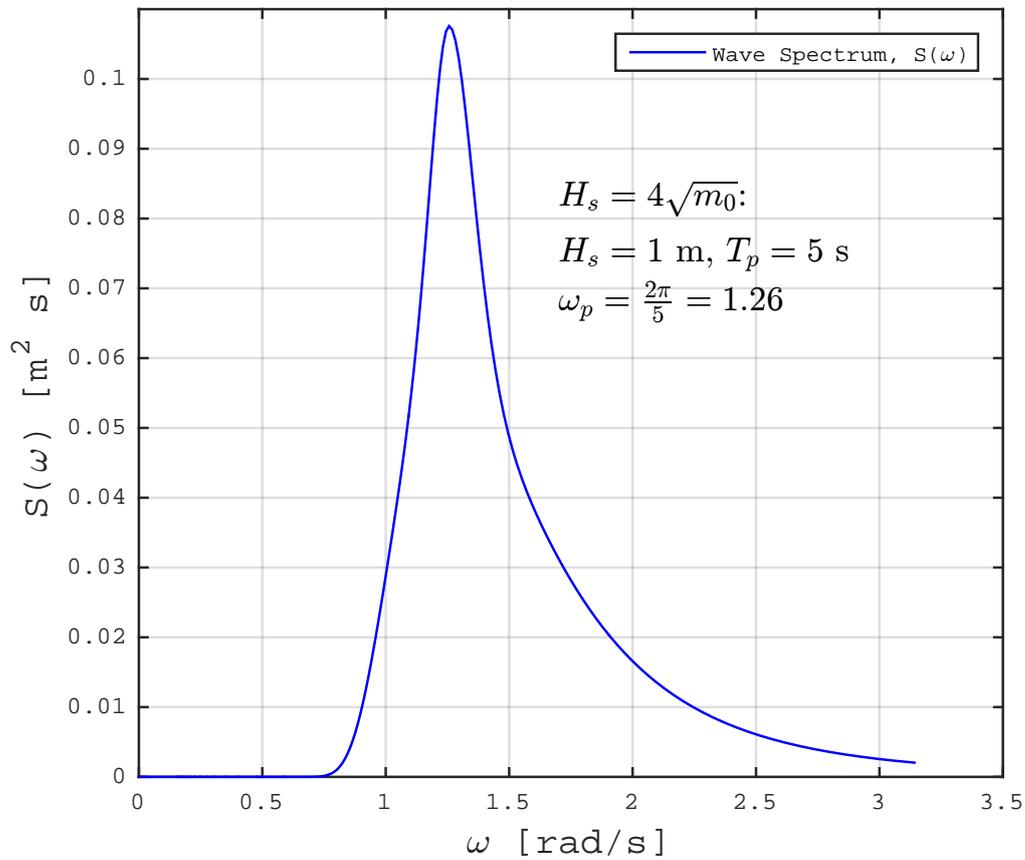


Figure 49: Wave Spectrum,  $H_s = 1\text{ m}$  and  $T_p = 5\text{ s}$

trum which was produced: This was done by calculating  $m_0$  of the wave spectrum:

$$\begin{aligned}
 m_n &= \int_0^{\infty} \omega^n S(\omega) d\omega, n = 0, 1, 2, \dots \\
 m_0 &= \int_0^{\infty} \omega^0 S(\omega) d\omega \\
 &= \int_0^{\infty} S(\omega) d\omega
 \end{aligned} \tag{60}$$

As we can see  $m_0$  is the area under the graph, and this area was calculated by using the trapezoidal integration function *trapz* in *MATLAB*.  $H_s$  was then calculated by  $H_s = 4\sqrt{m_0}$ . A  $H_s$  value equal to 9.855 metres was found (the input was 1 me-

tres). This is considered acceptable, since the trapezoidal method is a numerical method.

**Response Amplitude Operator** As mentioned in the previous section, an *RAO* for the structure is needed in order to determine the response spectrum  $S_{\eta_3}(\omega)$  and its corresponding standard deviation  $\sigma_{\eta_3}(\omega)$ . An *RAO* is a function which represents a certain motion characteristic of some structure. It is the ratio of the response amplitude to the wave amplitude,  $\eta_{3A}/\zeta_A$ . In this problem the heave motion is under consideration:

Table 17: Definition of Response Amplitude Operator

Wave process: $\zeta(t) = \zeta_A \cos(\omega t)$
Heave process: $\eta_3(t) = \eta_{3A} \cos(\omega t + \epsilon)$
<i>RAO</i> : $\frac{\eta_{3A}}{\zeta_A}$

For this task we chose to use an *RAO* for a drill ship, illustrated in Figure 50. The curve for head seas is used, meaning that we are considering waves which are headed straight towards the bow of ship. Head seas and beam seas (beam seas are waves which are headed towards the side of the ship,  $90^\circ$ ) have a different impact on the heave response  $\eta_3$ , which can also be seen in the figure. According to Faltinsen [6, p. 83], the larger response from beam seas can be understood by considering

$$|\eta_3|_{head\ sea} = |\eta_3|_{beam\ sea} \cdot \frac{2}{kL} \left| \sin\left(\frac{kL}{2}\right) \right| \quad (61)$$

The relation above shows that the length of the vessel  $L$  and the wave number  $k$  determines the size of  $|\eta_3|_{head\ sea}$ .  $L$  is relatively large, meaning that  $\frac{2}{kL}$  is small, giving a small value of  $|\eta_3|_{head\ sea}$ . As the wave period  $T$  increases,  $k$  decreases, increasing the fraction  $\frac{2}{kL}$ . Therefore,  $|\eta_3|_{head\ sea}$  and  $|\eta_3|_{beam\ sea}$  approach each other as the wave period increases. For relevant wave periods,  $|\eta_3|_{beam\ sea}$  is always larger than  $|\eta_3|_{head\ sea}$  (see Figure 50). A larger version of this figure is found in appendix B.

Points on the curve in Figure 50 were visually interpreted and stored in an array in the *MATLAB* script, and the results are shown in Figure 51. Next, the points were transformed to be dependant of frequency  $\omega[rad/s]$  instead of wave period, by  $\omega = \frac{2\pi}{T}$ . This is illustrated in Figure 52. In order to make the data more complete and the curve

smoother, it was interpolated using an interpolation function in *MATLAB*. The results are shown in Figure 53.

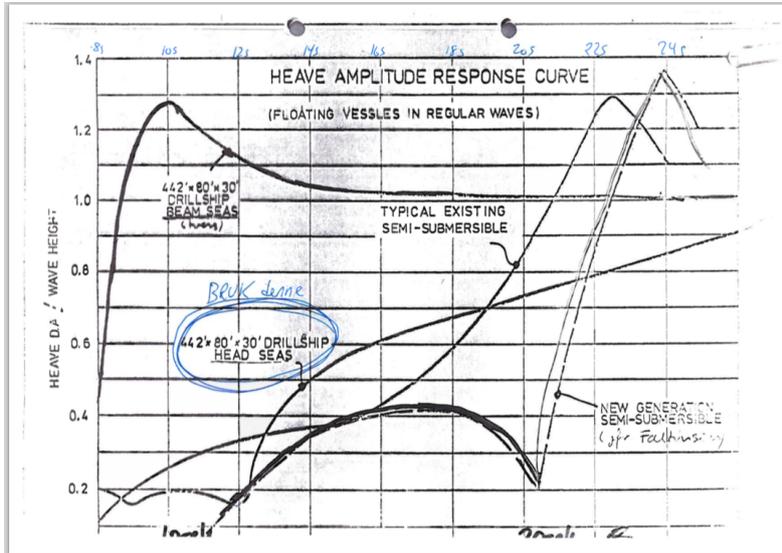


Figure 50: RAO for Drill Ship

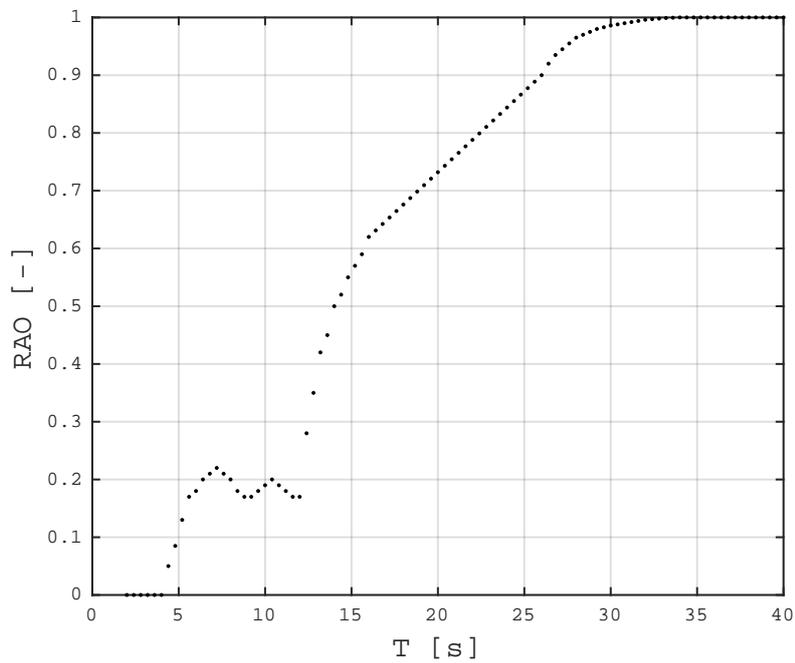


Figure 51: RAO for Drill Ship

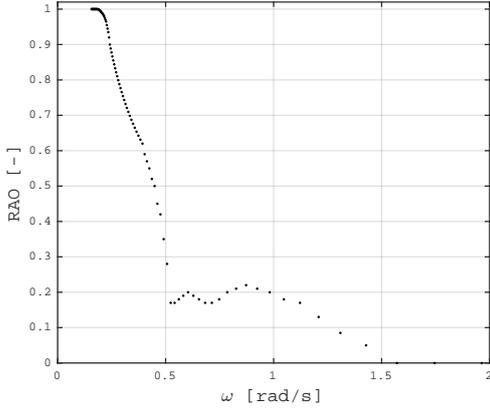


Figure 52:  $RAO(\omega)$  versus  $\omega$

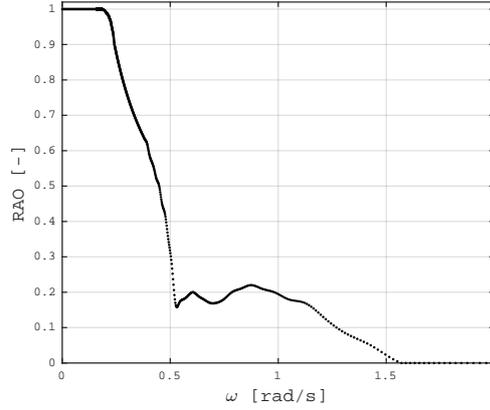


Figure 53:  $RAO(\omega)$  versus  $\omega$ , interpolated

**Determining acceptable pairs of  $H_s$  and  $T_p$**  As stated in Section 3.1.2 we can determine a limiting pair of  $H_s$  and  $T_p$  by

$$\sigma_{\eta_3}(H_s, T_p) \leq \frac{\eta_{3ac}}{\sqrt{-2 \ln [1 - (1 - q)^{1/N}]}} \quad (62)$$

An iteration process was performed, producing unique wave spectrums  $S(\omega)$  from different pairs of  $(H_s, T_p)$  and calculating  $\sigma_{\eta_3}(H_s, T_p)$  for every iteration. The iteration loop which was used in *MATLAB* looks like this:

1.  $H_s$  and  $T_p$  are first set to an arbitrary value, e.g.  $H_s = 1$  metre and  $T_p = 5$  seconds. We then have a wave spectrum,  $S(\omega)$
2.  $S_{\eta_3}(\omega)$  is determined by  $S_{\eta_3}(\omega) = |RAO(\omega)|^2 \cdot S(\omega)$
3.  $N$  is determined by  $m_0, m_2$
4.  $\sigma_{\eta_3}$  is determined by  $\sqrt{\int_0^\infty S_{\eta_3}(\omega) d\omega}$ . If this value is smaller than the right side of Equation 62, the set of  $H_s$  and  $T_p$  is acceptable and stored in an array.

This is an iteration process which calculates  $\sigma_{\eta_3}(H_s, T_p)$  for many different wave spectrums. This implies that each iteration starts with a value of  $H_s$  and  $T_p$ . In the total picture, each value of  $H_s$  is combined with a series of  $T_p$  values, and it looks like this:

1. A value of  $H_s, H_{s_1}$ , is combined with a series of different  $T_p$ -values ( $T_{p_1}, T_{p_2}, \dots, T_{p_n}$ )
2. Taking the next fixed value of  $H_s, H_{s_2}$ , and combining this with the same series of different  $T_p$ -values
3. Continuing doing this until our last value of  $H_{s_m}$

In this fashion a large number of different sets of  $(H_s, T_p)$  are tested.

#### 3.1.4 Results and Discussion

The iteration process took a series of values of both  $H_s$  and  $T_p$  and combined these to produce several wave spectrums. The standard deviation of each response spectrum was evaluated. If the criteria in Equation 62 was fulfilled, the corresponding values of  $H_s$  and  $T_p$  were acceptable and stored. A range of  $H_s$  values from 1 to 25 metres with increments of 0.5 metres, and a range of  $T_p$  values from 5 seconds to 30 seconds with increments of 0.5 seconds was chosen. The combinations of these values which were found acceptable are plotted in Figure 54. In other words, the figure illustrates the sea states which are acceptable (blue dots), while the white space corresponds to the area of critical sea states.

As the figure illustrates, any set of  $H_s$  and  $T_p$  is acceptable for  $T_p \leq 12$  seconds. From an intuitive point of view this can be explained by evaluating what kind of effect waves with small periods will have on the ship. If there is a rapid frequency of wave crests (a large frequency  $\omega$ ) hitting the hull of the ship, the hull might experience rapid but small movements (vibrations), but these waves will not have the ability to give a large heave displacement of the ship. Such a large frequency corresponds to small wave periods  $T$ ,  $\omega = \frac{2\pi}{T}$ , i.e. roughly corresponding to  $T_p \leq 12$  seconds. On the other hand, waves with large periods will have the ability to give large heave displacements. Figure 55 seeks to illustrate how waves with large wave periods can give large vertical displacements. Such a wave, with a period of e.g.  $T = 15$  seconds, has a length,  $\lambda$ , of approximately

351 metres if we assume the deep water relation:

$$\begin{aligned}
 \omega^2 &= kg \\
 \omega &= \frac{2\pi}{T}, \quad k = \frac{2\pi}{\lambda} \\
 \rightarrow \lambda &= \frac{T^2}{2\pi} g = \frac{15^2}{2\pi} 9.81 = 351.3 \text{ m}
 \end{aligned}
 \tag{63}$$

The *RAO* and two frequency domains are illustrated in Figure 56. The blue domain corresponds to waves with frequencies that have no effect on the ship at all. This naturally corresponds to the domain where the *RAO* is zero (where the response is zero), i.e.  $0 \text{ s} < T < 4 \text{ s}$ . There is also plotted another cut off at  $T = 12$  seconds which signifies where the region of some unacceptable values of  $T_p$  begins.

Another way of explaining the results is to look at the equations. Now, the value of  $\sigma_{\eta_3}$  is the value which decides if the sea state is acceptable or not. So one is therefore interested in evaluating this particular value, from the equation

$$\sigma_{\eta_3}(H_s, T_p) = \sqrt{\int_0^{\infty} S_{\eta_3}(\omega) d\omega}
 \tag{64}$$

As we can see the value is dependent on the value of  $S_{\eta_3}(\omega)$ , which in turn is dependent of the *RAO* multiplied with the wave spectrum:

$$S_{\eta_3}(\omega) = |RAO(\omega)|^2 \cdot S(\omega)
 \tag{65}$$

It is now of interest to look at a wave spectrum with a small value of  $T_p$  ( $T_p \leq 12$  seconds), since these are acceptable for any value of  $H_s$ . Figure 57 shows such a wave spectrum  $S(\omega)$  and its corresponding response spectrum  $S_{\eta_3}(\omega)$ .  $H_s = 3.5$  metres and  $T_p = 10$  seconds. Because the peak of  $S(\omega)$  is sufficiently far to the right,  $S(\omega)$  does not coincide sufficiently enough with the *RAO* to produce a significant response spectrum  $S_{\eta_3}(\omega)$ , i.e. yielding a small standard deviation  $\sigma_{\eta_3}$ . This is possible to observe in the figure if one pays careful attention to the red curve which represent a small response spectrum  $S_{\eta_3}(\omega)$ . The area under the curve is small, which in turn, yields a small

standard deviation  $\sigma_{\eta_3}$ , resulting in a fulfillment of the criteria in Equation 62.

Going back to Figure 54: In order to make it more helpful, a ten year contour plot of Haltenbanken was plotted in the same figure. By doing this, one can see which severe sea states (during a ten year period at Haltenbanken) coincides with the sea states which the drill ship can not operate in. The result is an empty pocket in the top part of the contour plot, which defines which relevant severe sea states that the drill ship can not operate in. This pocket is in other words an area which defines critical sets of  $H_s$  and  $T_p$ . For example, it is seen from the figure that the sea state  $[H_s, T_p] = [8m, 19s]$  is not an acceptable sea state to perform the operation in, nor is  $[H_s, T_p] = [12m, 14s]$ .

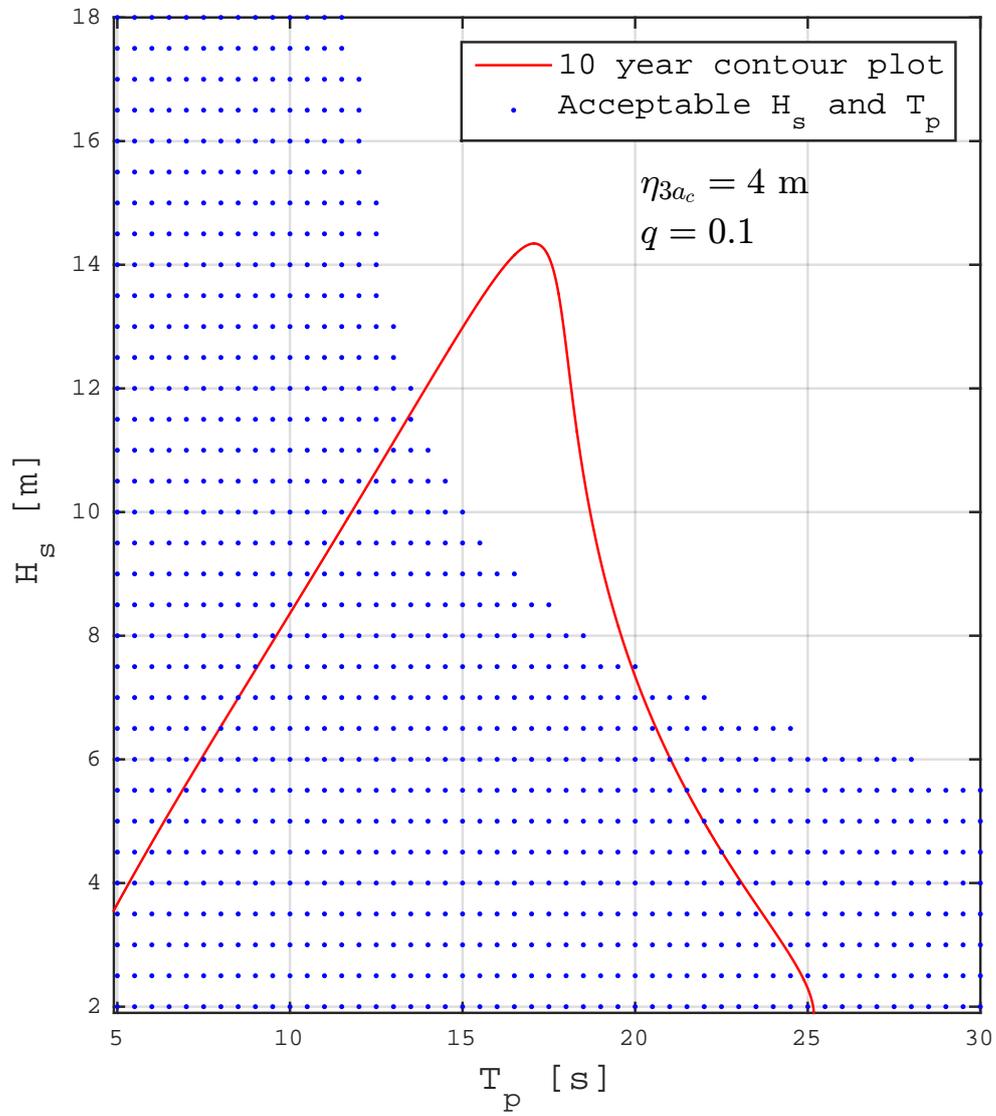


Figure 54: Acceptable pairs of  $H_s$  and  $T_p$  together with severe sea states (10 year contour plot)

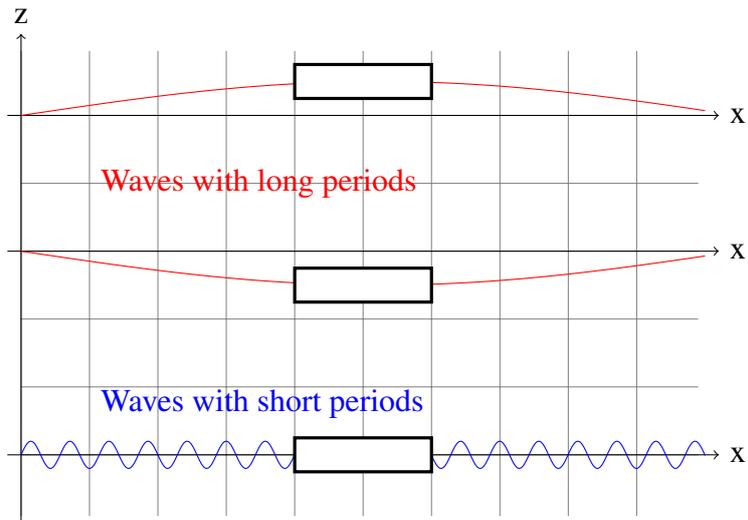


Figure 55: Wave frequencies. Large and small heave displacements.

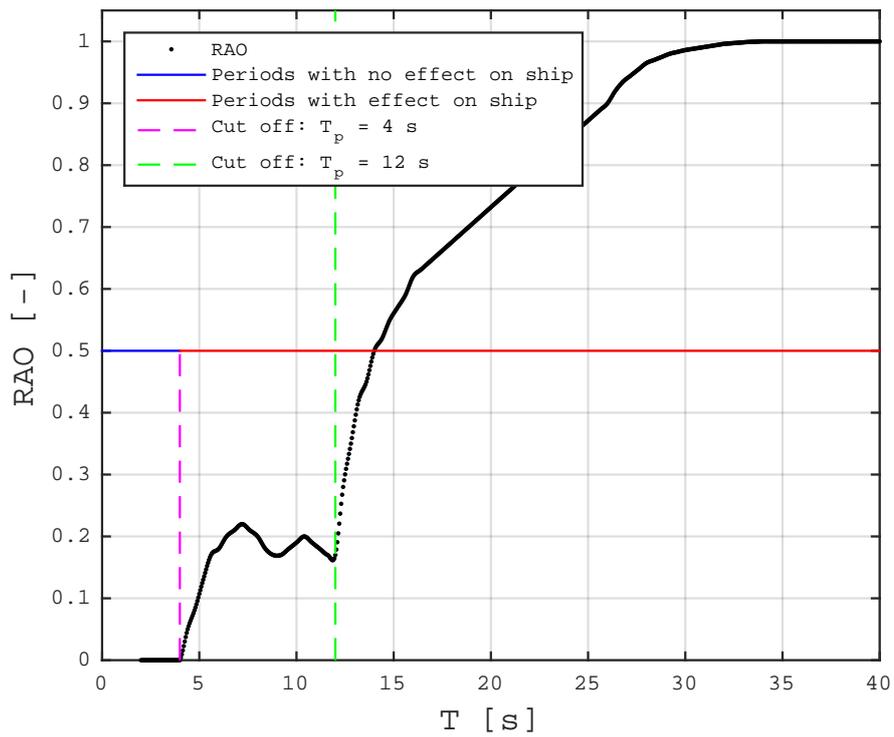


Figure 56: Frequency domains

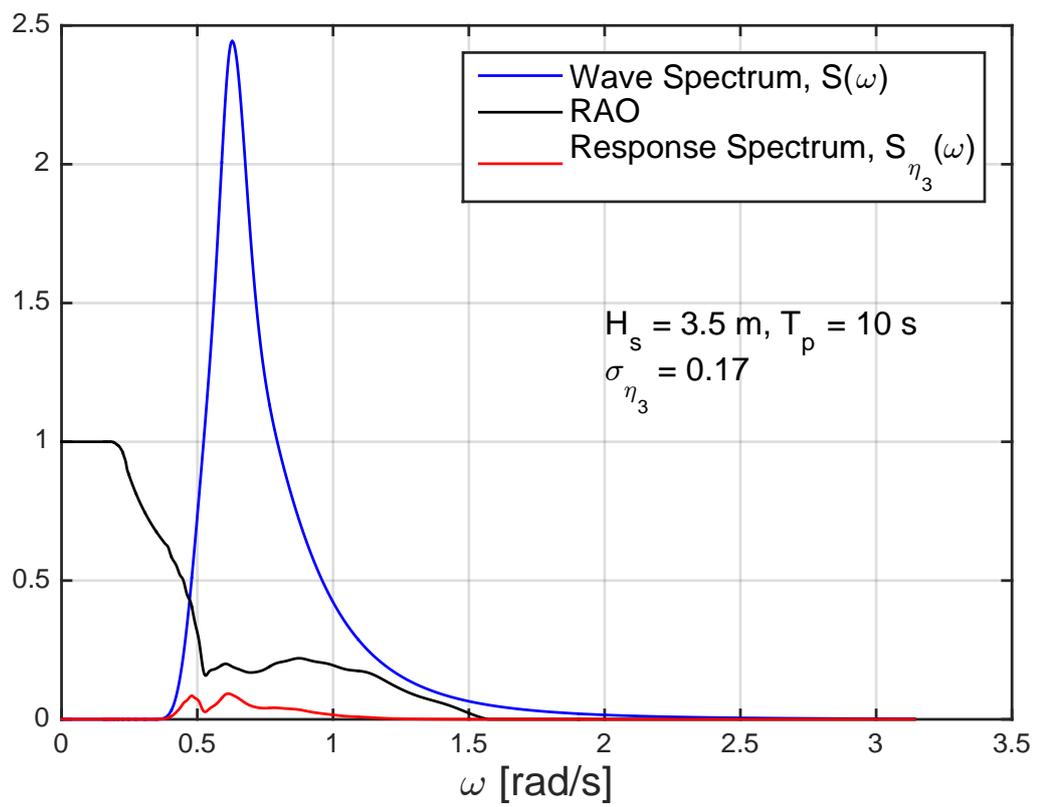


Figure 57: Small Response Spectrums

## 3.2 Assessing the feasibility of a marine operation by using the distribution of the longest calm

As mentioned in previous sections, one is in many cases interested in estimating extreme values. By doing this, one can for example design structures to withstand extreme waves. Such waves, extreme values of  $H_s$ , and the procedure behind calculating these were presented in Section 2.6. Extreme values are relevant in this section as well. What is the longest expected calm for a certain month? Such information is valuable in connection to planning marine operations.

If one is planning an operation which is to be performed in one continuous time span, one can estimate the feasibility of performing the operation in a certain month by evaluating the distribution of the longest calm. A premise for performing the operation is that the duration of the longest calm is at least as long as the duration of the operation. If this is not the case, then it is not reasonable to perform the operation in this particular time period and area. With such information one can avoid unwanted situations, where one might have to wait for an unwanted period of time before the operation can be performed. By avoiding this one will of course also avoid extra costs. The following evaluation is only carried out for the area of Haltenbanken, in order to avoid excess work, tables and figures.

### 3.2.1 Theory and examples

**Theory** In order to determine the distribution of the longest calm one can apply the techniques used in Section 2.6. As an example, let us consider how we can establish the distribution of the longest calms in July. The calms are defined by the threshold value  $H'_s = 2\text{m}$ , and we can start by making the following assumptions:

1. we have  $\tau_{c1}, \tau_{c2}, \dots, \tau_{cN}$ , where  $\tau_{c_{max}}$  is the largest among these. All observations are found in months of July.
2. we have the distribution of calms for July (found in Section 2.8.3).
3. we can assume that all calms are equally distributed.

4. we can assume that all calms are independent.

The last assumption is debatable, and it will probably lead to conservative results (Myrhaug [23, p. 31]). With the assumptions above, the distribution of the longest calms can then be determined in the following manner:

$$\begin{aligned}
P[\tau_{c_{max}} \leq \tau_c] &= P[(\tau_{c1} \leq \tau_c) \cap \dots \cap (\tau_{cN} \leq \tau_c)] \\
&= P(\tau_{c1} \leq \tau_c) \cdot (\tau_{c2} \leq \tau_c) \cdot \dots \cdot (\tau_{cN} \leq \tau_c) \\
&= [P(\tau_{ci} \leq \tau_c)]^N = [F_{\tau_c}(\tau_c)]^N \\
&= \left[ 1 - \exp \left[ - \left( \frac{\tau_c}{\rho} \right)^\beta \right] \right]^N = F_{\tau_{c_{max}}}(\tau_c) \tag{66}
\end{aligned}$$

The value of  $N$ , which is the number of calms, is found from previous work presented in Section 2.8.1 and 2.5. Firstly, the average duration of a calm in July is determined from Figure 28 to be roughly 120 hours. Secondly, the total number of hours below 2 metres is determined from the monthly cumulative distribution of  $H_s$  which was established in Section 2.5. Since we are considering a small value of  $H_s$ , the Lognormal part of the LoNoWe distribution is used:

$$\begin{aligned}
P[H_s \leq h_s] &= \frac{1}{2} + \frac{1}{2} \operatorname{erf} \left[ \frac{\ln(h_s) - \theta}{\sqrt{2}\alpha} \right] \tag{67} \\
P[H_s \leq 2m] &= \frac{1}{2} + \frac{1}{2} \operatorname{erf} \left[ \frac{\ln(2) - 0.3309}{\sqrt{2} \cdot 0.4285} \right] = 0.80
\end{aligned}$$

Which means that, since there are a total of  $31 \cdot 24 = 744$  hours in July, there will be  $0.80 \cdot 744 \approx 596$  hours which are below 2 metres. Finally, in order to calculate  $N$ , this is divided by the average duration of a calm

$$N = \frac{596 \text{ hours}}{121.4 \frac{\text{hours}}{\text{calm}}} = 4.9 \text{ calms} \tag{68}$$

In other words, there are on average roughly 5 calms in each month of July. The *CDF* of the longest calm for July is then determined by applying the *CDF* of the duration of calms for July, parameters  $\rho = 94.621$  and  $\beta = 0.8785$  (found in Table 15), together

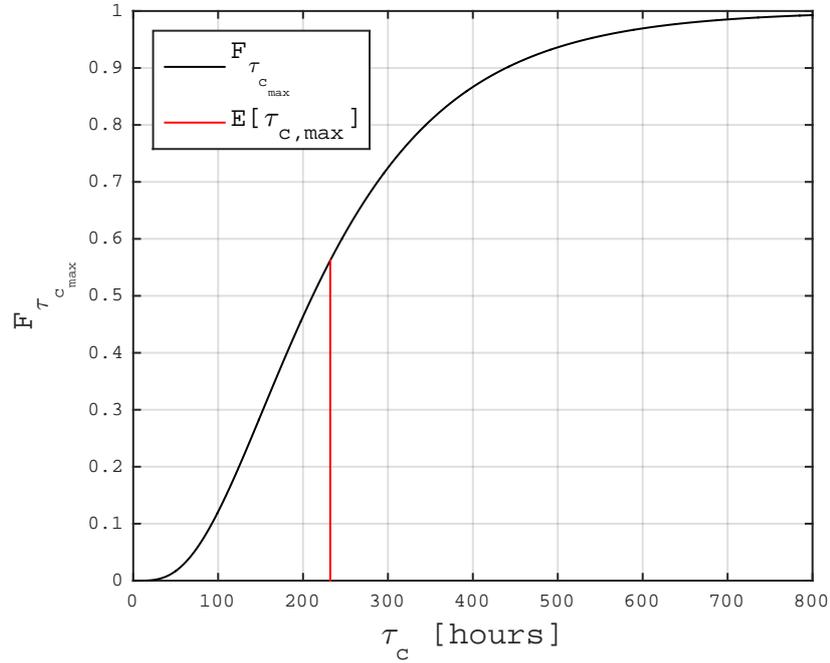


Figure 58: *CDF* of longest calm in July

with  $N = 4.9$ :

$$F_{\tau_{c_{max}}}(\tau_c) = \left[ 1 - \exp \left[ - \left( \frac{\tau_c}{94.621} \right)^{0.8785} \right] \right]^{4.9} \quad (69)$$

This is the cumulative distribution function for the longest calm in July. The expected longest calm is calculated by

$$E[\tau_{c_{max}}] = \int_0^{\infty} \tau_c f_{\tau_{c_{max}}} d\tau_c \approx 232 \text{ h} \quad (70)$$

This is plotted together with the *CDF* and *PDF* in Figures 58 and 59.

**Examples** As an example, let us consider an operation with duration of 24 hours, which is to be performed in July. We should then investigate the probability that the

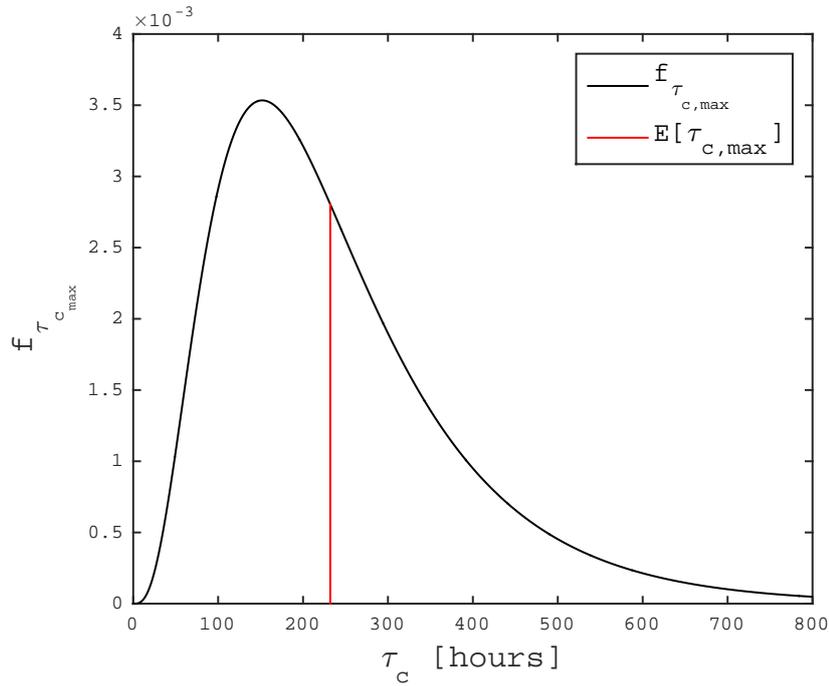


Figure 59: *PDF* of longest calm in July

longest calm in July is below or equal to 24 hours:

$$P[\tau_{c_{max}} \leq 24] = \left[ 1 - \exp \left[ - \left( \frac{24}{94.621} \right)^{0.8785} \right] \right]^{4.9} = 0.0013$$

There is only a 0.13 % chance that the longest calm is below or equal to 24 hours, i.e. there is a  $(1 - 0.0013) = 0.9987$ , 99.87 % chance that the longest calm is larger than 24 hours. By this one can understand that it would be safe to say that it is reasonable to perform the operation. On the other hand, if the operation is going to take place in January, with a duration of 24 hours, and a limiting value  $H'_s = 1\text{m}$ , the calculation will be

$$N = \frac{3.23 \text{ hours}}{6.75 \frac{\text{hours}}{\text{calm}}} = 0.48 \text{ calms}$$

$$P[\tau_{c_{max}} \leq 24] = \left[ 1 - \exp \left[ - \left( \frac{24}{23.296} \right)^{1.0519} \right] \right]^{0.48} = 1.0$$

In other words, there is a 100 % chance that the longest calm is below or equal to 24 hours, yielding a 0 % chance that the longest calm will be larger than 24 hours. It is therefore not feasible to perform this operation.

### 3.2.2 $P[\tau_{c_{max}} > t]$ for various values of $H'_s$ and $t$

In the same manner as above, one can calculate the probability that the longest calm is larger than  $t$  for a range of values of  $t$  and threshold values  $H'_s$ . Table 18 displays  $P[\tau_{c_{max}} > t]$  for  $t = 12 - 84$  hours and a fixed threshold value  $H'_s = 1$  m, while Table 22 displays the same range of  $t$  but  $H'_s = 3$  m. Tables 18 through 22 show two things: Firstly, as the value of  $t$  increases, the value of  $P[\tau_{c_{max}} > t]$  decreases. In other words, the longer the operation, represented by  $t$ , the more difficult it will be to perform the operation. Secondly, as the value of  $H'_s$  increases,  $P[\tau_{c_{max}} > t]$  increases as well. This means that the likelihood of performing the operation increases, which is expected, since as the threshold value increases, one has a larger margin to operate under.

The *MATLAB* scripts which performs the analysis is located in the folder "Feasibility of Op Longest Calm". The main script is an accumulation of almost all of the work up until now in the report. The script uses several functions, and these functions are built on earlier work. A flowchart for the algorithm is found in appendix D.1. The algorithm can be described by the following steps:

1. Number of calms,  $N$ , in each month is determined by
  - (a) Calculating the average duration of a calm for each month,  $\bar{\tau}_c$ , by calling function *avg\_dur\_func.m*.
  - (b) Calculating the expected hours below threshold  $H'_s$  by employing the Log-normal part of the LoNoWe distribution  $F_{H_s}(h_s)$ . Monthly parameters are fetched by the function *monthly\_lon\_func.m*.
  - (c)  $N$  is then equal to the expected number of hours below  $H'_s$  divided by  $\bar{\tau}_c$ .
2. Fetching parameters for monthly distribution of calms by using function *monthly\_calms\_func.m*.

Table 18:  $P[\tau_{c_{max}} > t]$ , threshold value  $H'_s = 1\text{m}$

$H'_s = 1\text{ m}$	$t$	Months											
		1	2	3	4	5	6	7	8	9	10	11	12
$P[\tau_{c_{max}} > t]$	12	0.04	0.27	0.51	0.85	0.98	1.00	1.00	1.00	0.92	0.56	0.26	0.13
	24	0.00	0.05	0.21	0.49	0.87	0.92	0.95	0.94	0.68	0.27	0.05	0.01
	36	0.00	0.01	0.07	0.21	0.71	0.70	0.83	0.80	0.44	0.12	0.01	0.00
	48	0.00	0.00	0.02	0.08	0.54	0.44	0.64	0.62	0.26	0.05	0.00	0.00
	60	0.00	0.00	0.00	0.02	0.39	0.24	0.46	0.44	0.14	0.02	0.00	0.00
	72	0.00	0.00	0.00	0.01	0.28	0.12	0.31	0.30	0.07	0.01	0.00	0.00
	84	0.00	0.00	0.00	0.00	0.20	0.06	0.20	0.20	0.04	0.00	0.00	0.00

Table 19:  $P[\tau_{c_{max}} > t]$ , threshold value  $H'_s = 1.5\text{m}$

$H'_s = 1.5\text{ m}$	$t$	Months											
		1	2	3	4	5	6	7	8	9	10	11	12
$P[\tau_{c_{max}} > t]$	12	0.80	0.74	0.92	1.00	1.00	1.00	1.00	1.00	1.00	0.98	0.92	0.71
	24	0.44	0.48	0.72	0.96	1.00	1.00	1.00	1.00	0.97	0.84	0.68	0.36
	36	0.20	0.31	0.51	0.85	0.98	0.99	0.99	0.99	0.90	0.61	0.42	0.15
	48	0.08	0.19	0.34	0.68	0.93	0.96	0.98	0.96	0.78	0.38	0.24	0.06
	60	0.03	0.12	0.22	0.49	0.86	0.91	0.95	0.91	0.65	0.22	0.13	0.02
	72	0.01	0.08	0.14	0.34	0.76	0.83	0.90	0.85	0.52	0.12	0.06	0.01
	84	0.00	0.05	0.09	0.22	0.65	0.74	0.83	0.77	0.41	0.06	0.03	0.00

3. Calculating  $P[\tau_{c_{max}} > t] = \left[ 1 - \exp \left[ - \left( \frac{t}{\rho} \right)^\beta \right] \right]^N$  for a range of values of  $t$  and  $H'_s$ .

Table 20:  $P[\tau_{c_{max}} > t]$ , threshold value  $H'_s = 2\text{m}$

$H'_s = 2\text{ m}$	$t$	Months											
		1	2	3	4	5	6	7	8	9	10	11	12
$P[\tau_{c_{max}} > t]$	12	0.98	0.98	1.00	1.00	1.00	1.00	1.00	1.00	1.00	1.00	0.99	0.99
	24	0.85	0.88	0.97	1.00	1.00	1.00	1.00	1.00	0.99	0.98	0.93	0.87
	36	0.63	0.72	0.88	0.98	1.00	1.00	0.99	1.00	0.97	0.92	0.80	0.65
	48	0.42	0.55	0.76	0.94	0.99	0.99	0.99	0.99	0.93	0.82	0.64	0.43
	60	0.26	0.40	0.61	0.86	0.96	0.98	0.97	0.98	0.87	0.68	0.49	0.26
	72	0.15	0.28	0.48	0.77	0.93	0.96	0.95	0.95	0.80	0.55	0.36	0.15
	84	0.09	0.20	0.36	0.66	0.88	0.93	0.92	0.93	0.72	0.42	0.26	0.09

Table 21:  $P[\tau_{c_{max}} > t]$ , threshold value  $H'_s = 2.5\text{m}$

$H'_s = 2.5\text{ m}$	$t$	Months											
		1	2	3	4	5	6	7	8	9	10	11	12
$P[\tau_{c_{max}} > t]$	12	1.00	1.00	1.00	1.00	1.00	1.00	1.00	1.00	1.00	1.00	1.00	1.00
	24	0.98	0.98	0.99	1.00	1.00	1.00	1.00	1.00	1.00	0.99	0.99	0.98
	36	0.90	0.92	0.96	0.99	1.00	0.99	0.99	0.99	0.99	0.97	0.95	0.91
	48	0.77	0.82	0.91	0.97	0.99	0.98	0.98	0.98	0.97	0.93	0.87	0.78
	60	0.62	0.70	0.83	0.94	0.98	0.96	0.96	0.97	0.93	0.87	0.76	0.63
	72	0.48	0.57	0.74	0.90	0.96	0.94	0.95	0.96	0.89	0.79	0.63	0.48
	84	0.35	0.45	0.65	0.84	0.93	0.92	0.92	0.94	0.84	0.70	0.52	0.36

Table 22:  $P[\tau_{c_{max}} > t]$ , threshold value  $H'_s = 3\text{m}$

$H'_s = 3\text{ m}$	$t$	Months											
		1	2	3	4	5	6	7	8	9	10	11	12
$P[\tau_{c_{max}} > t]$	12	1.00	1.00	1.00	1.00	1.00	1.00	1.00	1.00	1.00	1.00	1.00	1.00
	24	1.00	0.99	1.00	1.00	1.00	0.99	0.99	1.00	0.99	1.00	1.00	1.00
	36	0.97	0.96	0.98	0.98	0.99	0.98	0.99	0.99	0.98	0.99	0.98	0.97
	48	0.92	0.90	0.95	0.96	0.99	0.97	0.98	0.98	0.96	0.96	0.93	0.91
	60	0.84	0.82	0.90	0.93	0.98	0.96	0.97	0.97	0.93	0.93	0.87	0.82
	72	0.74	0.73	0.84	0.90	0.97	0.94	0.95	0.96	0.90	0.87	0.79	0.72
	84	0.63	0.64	0.77	0.85	0.95	0.92	0.93	0.95	0.86	0.81	0.70	0.61

### 3.3 Assessing the feasibility of a generic marine operation by simulation

The outline of the thesis suggests investigating simplified methods which can assess the feasibility of a marine operation. The procedure of one of the methods is specified while the other is open. In this context a marine operation is chosen by the author to consist of a custom number of intervals, breaks and limiting weather thresholds. The limiting weather is chosen to be the significant wave height, i.e. spectral peak period is not considered. Haltenbanken is the only area which has been considered in this part. The following analyses are performed by *MATLAB* scripts located in the folder "Generic Marine Op". It should be emphasized that the operations in the following have been specified, hence "generic" might seem strange. The point is that any type of operation, consisting of  $n$  number of intervals and different thresholds  $H'_s$ , can be simulated. The goal of the following analyses is to investigate whether such methods are reasonable and if they can potentially be used as a quick tool at an early stage when planning a marine operation.

Section 3.3.1 presents a method where simulations are carried out by employing the distributions of the duration of calms and storms combined with Monte Carlo simulation. Section 3.3.2 presents a method where simulations are carried out using the Hindcast data directly.

#### 3.3.1 Utilizing the distributions of the duration of calms and storms and Monte Carlo simulation

The company *DeepOcean*, which collaborated on the project, suggests establishing a simple tool for considering the feasibility of a generic marine operation based on a monthly scatter diagram for  $H_s$  and  $T_p$ . A proposed method is to employ the distribution for the duration of calms and storms in a simulation employing the technique of Monte Carlo simulation. These monthly distributions are presented in Section 2.8.3, and they were established using the monthly scatter diagrams (the hindcast data).

**Method** At first it was considered to define a marine operation with different required thresholds  $H'_s$ . An operation consisting of two intervals with two different thresholds was chosen. Item 1 in Figure 62 illustrates this. The method assumes that the first period is a calm ( $\tau_{c_1}$ ), i.e. it is assumed that vessel and crew will wait until the weather is good enough to start the operation, e.g. utilizing a weather forecast. Furthermore it is assumed that the following period is a storm ( $\tau_{s_1}$ ). This is a natural assumption, otherwise the definition of a calm would be unclear. The simulation can unfold in several different ways, but a problem arises with a calm of such a duration that it covers the whole operation. For example, if the first calm  $\tau_{c_1}$  (given  $H'_s = 3$  metres) is determined to be 40 hours, it is long enough to cover both intervals. The issue is that the calm is determined given  $H'_s = 3$  metres, which means that the second interval of the operation is not suitable for this calm, since this interval requires  $H'_s = 1.5$  metres. A calm can not be estimated for two different thresholds  $H'_s$ .

It was therefore decided to simplify the definition of the operation by reducing  $H'_s$  from two to only one, i.e. requiring the same threshold for the entire operation. It is thereby possible that one sufficiently long calm is enough to finish the operation in only one time span. It was also decided to increase the number of intervals from two to three and adding two breaks in between these. This is illustrated by item 3 in Figure 62. It is assumed that a calm of any length is used to operate. Let us say that the first calm lasts only 3 hours. This calm is then used to complete the 3 first hours of the first interval. Duration of calms and storms are determined by the 2-parameter Weibull distributions:

$$\tau_c = \rho_c [-\ln(1 - U)]^{\frac{1}{\beta_c}} \quad \tau_s = \rho_s [-\ln(1 - U)]^{\frac{1}{\beta_s}} \quad (71)$$

$U$  is a random generated number between 0 and 1. This is in essence the Monte Carlo simulation. Each value of  $U$  is independent of each other. This is a sensible assumption considering that the start of each calm or storm is separated by a fairly long time span. Parameters of the distributions are dependent upon what month we are evaluating. These are displayed in Tables 15 and 16. It is assumed that the operation is a failure if it is not possible to carry it out in one month. The script which performs the simulation is named "mar\_op\_weibull.m", and a flowchart is found in appendix D.2.

Table 23: Simulations of generic operation, constant threshold  $H'_s$ , 10 000 simulations

3 Intervals x 24 hours $H'_s = 2$ m	Months											
	1	2	3	4	5	6	7	8	9	10	11	12
Average duration of operation [hours]	373.5	308.5	267.0	181.7	120.7	106.3	104.0	108.2	175.8	257.3	312.5	373.0
No. of impossible months	2470	2011	975	19	0	0	0	0	19	314	1082	2432
Probability of not performing operation	0.25	0.20	0.1	0.00	0	0	0	0	0.00	0.03	0.11	0.24

**Results** Results are displayed in Table 23. If the operation is finished in only one time span, including breaks, the total duration of the operation is  $3 \cdot 24 + 2 \cdot 3 = 78$  hours. Due to the fact that July has arguably the best conditions, a large portion of the simulations (42%) in this month yield results where the operation is finished in one calm. This is why there is a horizontal fat line in the bottom of Figure 60. This figure displays all of the 10 000 simulations and their corresponding operational durations. Furthermore, it is seen from Figure 61 that the simulations are significantly more spread for January than for July, illustrating the increased uncertainty in January. This is confirmed by considering the standard deviation,  $\sigma = 37.1$  hours for July and  $\sigma = 188.4$  hours for January. Note that the x-axis for January ends at roughly 7500 simulations because 25 % of the simulations yields zero, meaning that it was impossible to perform an operation in these simulations.

### 3.3.2 Utilizing the Hindcast data directly

**Method** A different idea is to use the Hindcast data directly, i.e. simulating operations using the data for each month and each year. Let us say that we have a marine operation consisting of only one interval, with a given limiting threshold  $H'_s$ , which will take place in the month of May. We can then go into the first entry corresponding to May in the Hindcast data and evaluate whether or not  $H_s$  is below  $H'_s$ . Every entry in the relevant month is inspected, for all years (1958-2014). In this manner it is possible to perform simulations for different marine operations.

Let us say that we have an operation which consists of two intervals where the first interval lasts 24 hours and requires  $H'_s = 3$  metres, while the second lasts 12 hours and requires  $H'_s = 1.5$  metres. There are no breaks. The simulation can unfold in different

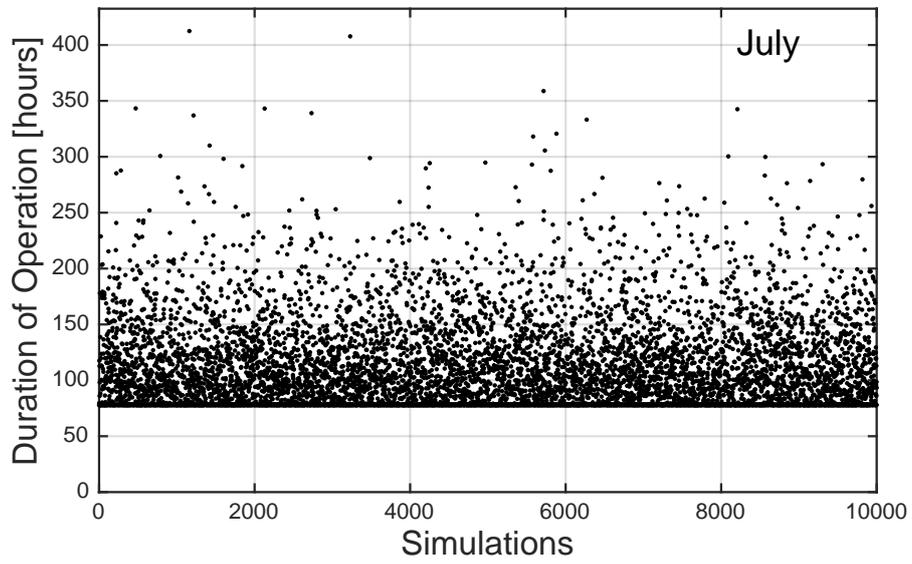


Figure 60: Simulations of a generic operation, July

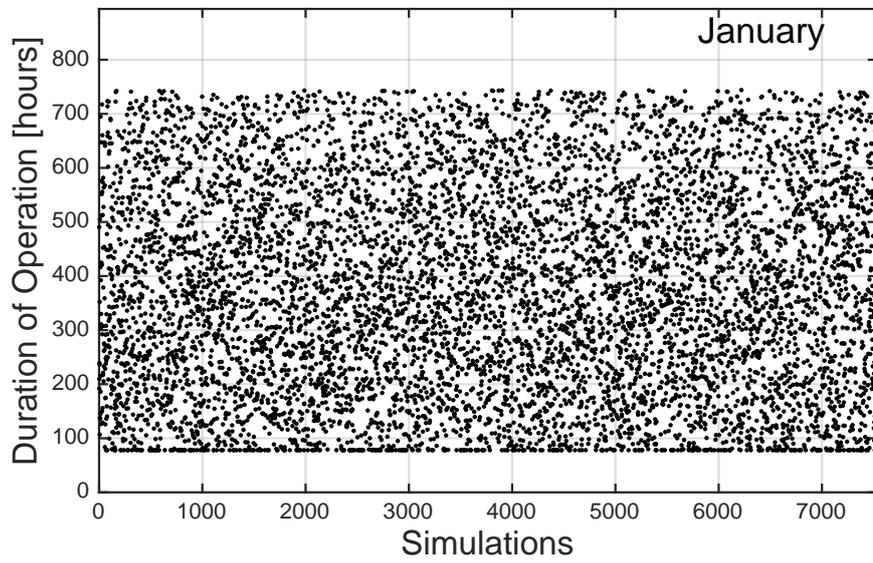


Figure 61: Simulations of a generic operation, January

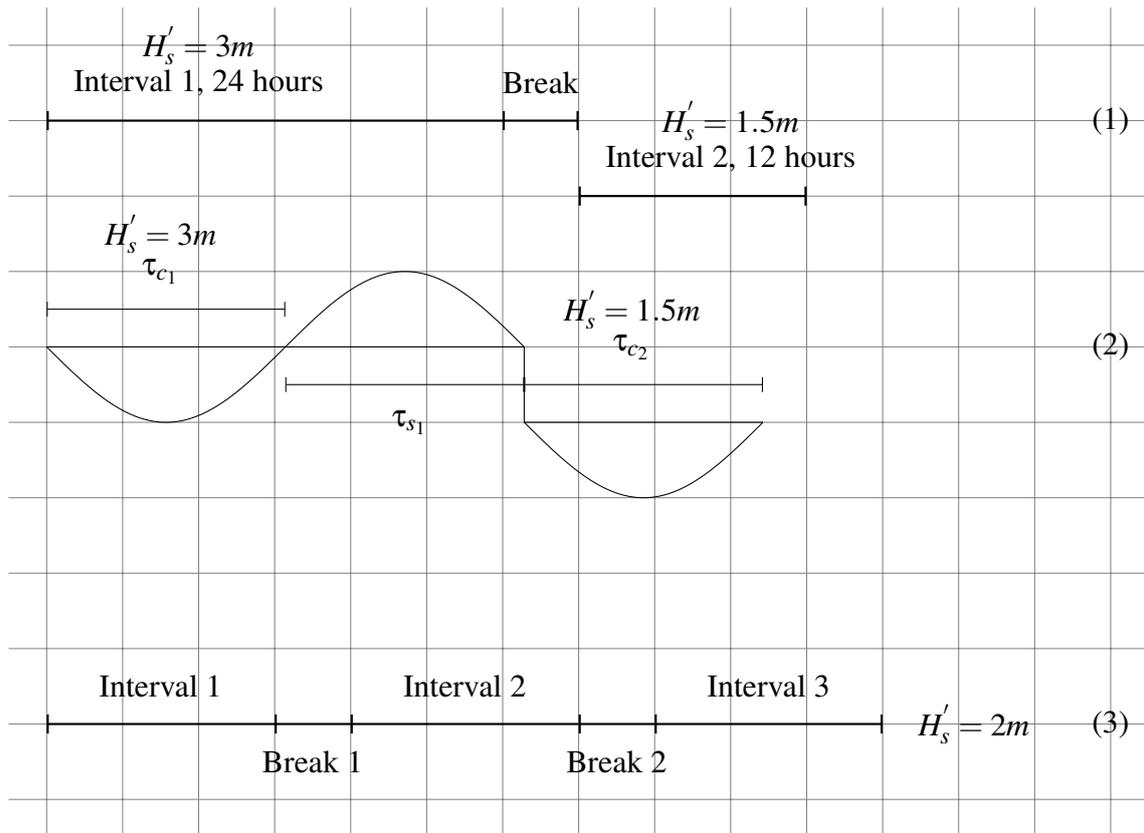


Figure 62: Generic Marine Operations

ways, and the following shows a couple of examples in order to illustrate a simulation.

1. The first 14 observations of  $H_s$  are below 1.5 metres, yielding a time span of 42 hours (there is an observation every third hour,  $14 \cdot 3 = 42$  hours). In other words, one would have been able to carry out the entire operation at the first attempt, and the total duration would have been  $24 + 12 = 36$  hours, which is the minimum possible time.
2. The first 3 observations are below 3 metres, yielding a time span of 9 hours, which is not enough to perform the first interval. Two observations larger than then required  $H'_s = 3$  metres occur after this, yielding 6 hours (there is in other words a storm). The next 8 observations are below 3 metres, yielding 24 hours, finishing the first interval. There are then 5 observations larger than 3 metres, yielding a storm which lasts 15 hours. Finally there are 4 observations below 1.5 metres, yielding 12 hours and finishing the last interval. Total duration of the operation is then:  $9 + 6 + 24 + 15 + 12 = 66$  hours.

In this manner one can consider the total duration of the marine operation. Each year yields a unique operation time for a particular month, and the average operational time for e.g. May is found by adding all operation times for May and dividing it by the total number of years, which is 58. It is also here assumed that the operation is considered a failure if it is not possible to finish it in one month.

**Results** Results are displayed in 24 and 25. These tables correspond to two different operations. The latter consists of three intervals and a constant  $H'_s$ , such as the one in the previous section. This was done in order to compare the methods. The previous method yielded an average operational time for July equal to 104.0 hours, while in this simulation it was determined to be 108.3 hours. The result is a bit surprising, since it was expected that the method which employs the Weibull distributions would not be particularly accurate. Although this by no means validates either method, it is a good indication that it could be studied in more detail and improved. Furthermore, results from both methods, for all months, are displayed in Figure 63. The figure shows a significant discrepancy for the months during spring, in particular March.

Table 24: Simulation of generic operation, two intervals, two thresholds

Interval 1: 24 hours, $H'_s = 3m$ Interval 2: 12 hours, $H'_s = 1.5m$	Months											
	1	2	3	4	5	6	7	8	9	10	11	12
Average duration of operation [hours]	326.9	286.6	310.5	200.0	102.6	64.2	54.4	55.0	110.7	220.9	258.8	344.0
No. of impossible months	29	24	17	1	1	1	2	2	2	8	14	25
Probability of not performing operation, %	51	42	30	2	2	2	4	4	4	14	25	44

Table 25: Simulation of generic operation, constant threshold  $H'_s$

3 Intervals x 24 hours $H'_s = 2m$	Months											
	1	2	3	4	5	6	7	8	9	10	11	12
Average duration of operation [hours]	370.8	351.7	372.2	255.6	144.9	112.4	108.3	98.79	168.8	264.8	357.1	433.7
No. of impossible months	32	32	18	1	1	1	2	2	1	10	19	30
Probability of not performing operation	0.55	0.55	0.31	0.02	0.02	0.02	0.03	0.03	0.02	0.2	0.33	0.52

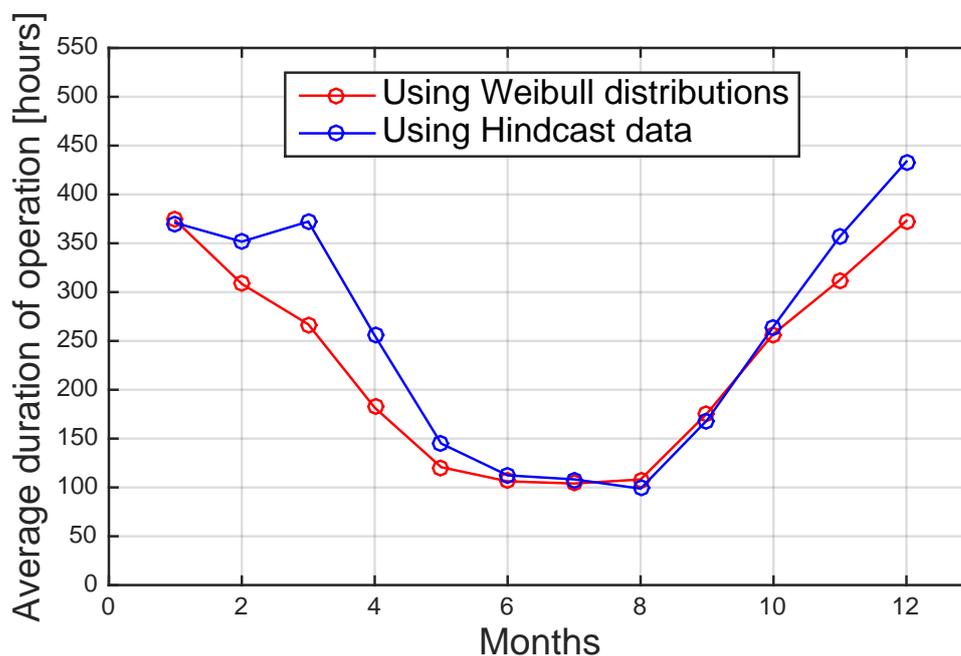


Figure 63: Monthly duration of operation, both methods

### 3.3.3 Comments

There are weak and strong points to both methods. When the first method estimates calms by the Weibull distribution of such length that they can cover several intervals, but not several intervals of different thresholds, it limits the method significantly. Another concern is the quality of the Weibull distributions. The discrepancies for the winter months (Figure 63) suggests that the simulated durations of calms in these winter months are too large. Its strength is its ability to run thousands of simulations. The second method which uses the Hindcast directly employs 58 samples of the month it evaluates, while the Monte Carlo technique can simulate thousands of months. As the methods stand, the one which uses the hindcast data directly is the most reliable because it uses real data, and is also the most flexible since it can manage several thresholds. This method can be considered as a reasonable and good alternative when investigating the feasibility of a marine operation at an early stage. On the other hand, it would be very interesting to work more on the one which uses Monte Carlo simulation, since one can simulate such a large number. If one is able to overcome the challenge of using different thresholds, while at the same time employing the distributions of durations of calms and storms in a sensible way, this could possibly be a better method.

## 3.4 Rolling, a challenge in marine operations

Section 3.4.1 presents the motivation behind this chapter. Section 3.4.2 briefly presents theory on roll damping and equipment used in order to decrease the roll motion. Furthermore, a specific case with a Platform Supply Vessel (*PSV*) is presented in Section 3.4.3, with the intention of investigating the effect that the swell sea has on the operational potential of the vessel. First, the roll motion due to swell sea is evaluated, and secondly, the effect that this roll motion has on the usability of a good weather window is investigated.

### 3.4.1 Background

During marine operations, the roll motion is typically the most problematic motion. It is common that a marine structure, especially a ship, will have large roll amplitudes (resonance effects in roll), which is due to little damping. Roll amplitudes of 30 and 40 degrees have occurred. During marine operations, it is common to turn the bow of the vessel against the wind sea so that the motions of the vessel are minimized. In particular, sway, roll and yaw are reduced by doing this (see Figure 47). Swell sea, on the other hand, does not necessarily have the same direction as the wind sea, which means that the swell sea can cause a problem, e.g. in terms of significant roll amplitudes.

Typically, a ship and its crew will wait until the value of  $H_s$  is suitable to perform the operation. This limiting value of  $H_s$ ,  $H'_s$ , has to be determined beforehand by analysis of the operation which is to be performed. Such an analysis can be performed by computer simulation software. Experience has shown that these analyses might not be able to predict the response well enough, in particular the response due to swell sea. Operations which have been started during seemingly perfect conditions have been delayed for long periods of time due to a problematic swell sea. The swell sea can cause large roll amplitudes which prevent the operation from being carried out. There were problems during the installation of the deck at Kvitebjorn [26]. Even though the conditions seemed more than suitable, there were problems which delayed the operation significantly. According to S. Haver (personal communications, 15th of February 2015) the vessel which were to lift the deck of the barge, experienced large roll motions due to the swell sea. These

were of such magnitude that the operation had to be stopped.

Therefore, the outline of this master thesis suggests investigating the impact of swell sea on the usability of the good weather windows.

### 3.4.2 Roll damping and roll stabilization equipment

Damping in a system is understood to be mechanisms which drain the system for energy, i.e. damping the system and reducing its oscillations. In this case, the roll motion and roll damping is under consideration. The roll motion is illustrated in Figure 47. The uncoupled roll equation can be defined in Faltinsen [6, p. 53] as

$$(I_{44} + A_{44})\ddot{\eta}_4 + B_{44}\dot{\eta}_4 + C_{44}\eta_4 = F_4 \quad (72)$$

$I_{44}$  is the moment of inertia,  $A_{44}$  is added mass moment in roll,  $B_{44}$  is damping in roll while  $C_{44}$  is the restoring coefficient (stiffness coefficient). Damping in roll can be divided into four categories (Faltinsen [6, p. 54]):

1. Wave generating
2. Effects due to lift
3. Viscous effects
4. Roll stability systems

Damping due to wave generating is understood by considering the energy that is needed to generate waves. Because of the roll motion of the ship, waves are generated, and these are in essence using energy from the roll motion, i.e. damping the roll motion. Roll damping is dependant of the structure's speed relative to the frequency of waves coming head on, while it is independent of the structure's speed relative to waves coming straight in from the side. Wave roll damping is typically small for common ship sections, while it is significantly larger if the ratio of the width and the depth of a section is either small or large. Because of the lack of moment generated by pressure forces, sections which are in the vicinity to quadratic shapes will have little roll damping (Faltinsen [6]).

Linearized roll damping can be written as in Faltinsen [6, p. 56]:

$$B_{44} = \int b_{44} d\xi + U \alpha_{44}^A + B_{44}^* \quad (73)$$

The first term is the roll wave damping while the third term is the damping due to viscous effects and roll stabilizing systems. The second term is roll damping due to lift effects.  $U$  is the forward speed of the structure, while  $\alpha_{44}^A$  is the two dimensional added moment in roll. "The lift effects are expected to be more significant for fine ship hulls than for blunt hulls"(Faltinsen [6, p. 56]).

Viscous damping is in general due to two effects: Effects due to the friction of the skin of the structure, and effects due to vortex shedding.

Stability systems can be categorised as passive and active systems. Passive systems are for example bilge keels, passive anti-roll tanks or fixed fins, whereas active systems are for example active anti-roll tanks or active fins. One of the most used systems is the bilge keel, because it is effective while at the same time a cheap option. Passive anti-roll tanks are also quite popular, but these are more costly and have little effect in severe seas due to large roll motions which in turn will make the fluid inside the tanks slam against the ceiling of these. A simple sketch of bilge keels and a passive anti-roll tank is illustrated in Figure 64. Another system is the Voith Schneider propeller, a type of propulsion system which can reduce roll motion. In the case of marine operations, where the vessel often lies still, or almost still, with the bow against the wind, systems such as fixed and active fins or Voith Schneider propellers become almost insignificant due to very little or no forward speed. This leaves us with anti-roll tanks and bilge keels as the most relevant systems for the *PSV* which is evaluated in the following.

**Passive anti-roll tanks** A passive anti-roll tank, such as the one which is seen in Figure 64, counters the roll motion because the liquid is sloshing inside the tank, hence it functions as a roll damping device. The *RAO* which is seen in Figure 69 represents a *PSV* with a passive anti-roll tank. The *RAO* in Figure 52 displays the same vessel but without a tank, thereby illustrating the difference.

In order to obtain the best roll damping, the lowest natural frequency of the liquid should

be set equal to the natural roll frequency of the vessel. The sloshing frequency can be altered by changing the water depth inside the tank. Vessels which operates with a number of different metacentric heights  $\overline{GM}_T$  will operate with different natural roll frequencies, which makes the passive anti-roll tank practical.

One of the challenges with the passive anti-roll tank is saturation which occurs at large roll amplitudes. As the roll motion increases, so does the sloshing, and if the roll motion is sufficiently large the liquid might slam against the ceiling of the tank, reducing its function severely.

According to Faltinsen [8, p. 83], the effect of the anti-roll tank can be found by considering the moment which the sloshing of the liquid inside the tank creates. If we assume regular waves inside the tank and describe the forced roll oscillations as  $\eta_4 = \eta_{4a} \sin(\omega t)$ , the moment due to the anti-roll tank can be written as given in Faltinsen [8, p. 85]:

$$\begin{aligned} F_4^t &= K_{ta} \sin(\omega t + \varepsilon_t) \\ &= K_{ta} \sin(\omega t) \cos(\varepsilon_t) + K_{ta} \cos(\omega t) \sin(\varepsilon_t) \\ &= \frac{K_{ta}}{\eta_{4a}} \cos(\varepsilon_t) \eta_4 + \frac{K_{ta}}{\omega \eta_{4a}} \sin(\varepsilon_t) \dot{\eta}_4 \end{aligned} \quad (74)$$

$K_{ta}$  and  $\varepsilon_t$  can be established experimentally through tests of the tank. The effect of the anti-roll tank comes into Equation 85 through  $F_4^t$  (given in Faltinsen [8, p.85]):

$$\begin{aligned} (I_{44} + A_{44})\ddot{\eta}_4 + B_{44}\dot{\eta}_4 + C_{44}\eta_4 &= F_4 + F_4^t \\ (I_{44} + A_{44})\ddot{\eta}_4 + \left( B_{44} - \frac{K_{ta}}{\omega \eta_{4a}} \sin(\varepsilon_t) \right) \dot{\eta}_4 + \left( C_{44} - \frac{K_{ta}}{\eta_{4a}} \cos(\varepsilon_t) \right) \eta_4 &= F_4 \end{aligned} \quad (75)$$

”The term  $-K_{ta} \sin(\varepsilon_t)$  is large if we choose the natural period for the flow inside the tank to coincide with the natural roll period” (Faltinsen [8, p.85]). As we can see, the restoring coefficient  $C_{44}$  has been changed, but this not of significance since the term  $\frac{K_{ta}}{\eta_{4a}} \cos(\varepsilon_t)$  is small when the the sloshing frequency is close to its natural frequency. It should be noted that for sufficiently accurate estimates the coupling between the motions sway, roll and yaw should be considered.

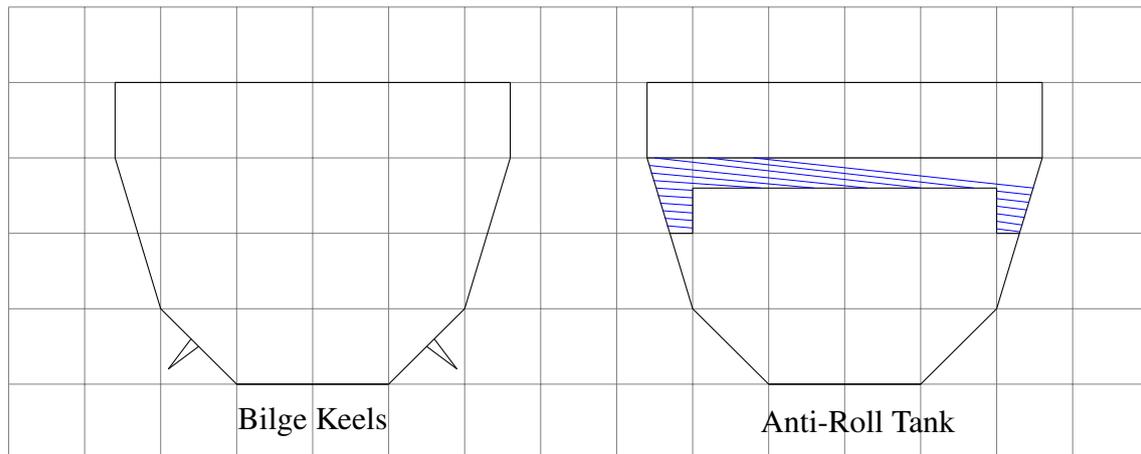


Figure 64: Anti-rolling devices

**Bilge keels** As mentioned above, the bilge keel is often used because it is very cheap while at the same time effective, even in severe seas. There are several positive sides to such a system and very few negative. There are only two negative aspects worth mentioning: it marginally increases the resistance of the vessel, and it can promote bio-fouling growth around the keel (Baniela [2, p. 676]). On the other hand, the bilge keel is very effective and can constitute more than 50 % of the total roll damping (Faltinsen [6, p. 68]). It is a cheap option, it has a light weight and it can be added to the ship after it is built.

Ikeda [17] and Himeno [14] have carried out model tests in order to predict the roll damping effect due to bilge keels. Some of the theory is briefly presented in the following.

Bilge keel damping components are defined in Himeno [14, p. 19] as

$$B_{BK} = B_N + B_S + B_W \quad (76)$$

$B_N$  is the normal force damping of the bilge keels,  $B_S$  is the hull surface pressure damping to due bilge keels and  $B_W$  is the wave damping of the bilge keels. "Although these components are seemingly linear, their values may vary with roll amplitude and frequency" (Himeno [14, p. 19]).

Forced roll tests have been carried out in order to compare experimental results with

empirical formulas. Ikeda [17, p. 5] has found a prediction formula for  $B_N$  at zero forward speed:

$$B_N = \frac{8}{3\pi} \rho r l \omega \left( 22.5 \frac{b_{BK}^2 r}{\pi} + 2.40 b_{BK} r^2 \phi_A \right) \quad (77)$$

$\rho$  is the density of water,  $r$  is the mean distance from  $G$  (centre of gravity) to bilge keel,  $l$  is the moment lever,  $b_{BK}$  is the breadth of the bilge keel,  $\omega$  is the frequency of the roll motion and  $\phi_A$  is there roll amplitude. Figure 65 shows how the formula matches experimental results.

$B_S$  is suggested by Ikeda [17] to be predicted by

$$B_S = \frac{4}{3\pi} \rho r^2 d^2 \omega \phi_A f^2 I \quad (78)$$

where  $I = \frac{1}{d^2} \int C_P l_0 ds$

$f$  is the modification factor of the flow velocity at the bilge keel, while  $d$  is the draft.  $I$  is integrated along the complete girder of the hull.  $C_P$  is the distribution of the pressure difference coefficient, which is multiplied by the moment lever  $l_0$ . The pressure around the hull is changed because of the bilge keels. Pressure  $p$  on an infinitesimal surface of the hull  $ds$  creates a force, which creates a moment around the axis of rotation.  $l_0$  is the arm of this moment. The positive pressure coefficient  $C_P^+$  on the front of the bilge keel and the negative pressure coefficient  $C_P^-$  on the back of the bilge keel are given as:

$$C_P^+ = 1.2 \quad (79)$$

$$C_P^- = -\frac{22.5 b_{BK}}{\pi r f \phi_A} - 1.2 \quad (80)$$

This is illustrated in Figure 66.

$B_W$  can according to Himeno [14, p. 42] be neglected: "[..] it can be noted that for bilge keels with ordinary breadth [...] we can safely neglect the wave effect of bilge keels. [...] it can be concluded that the total damping increment due to bilge keels can be predicted as the sum of two bilge-keel dampings,  $B_N$  and  $B_S$ ". Predicted values of  $B_{BK}$  together with experimental results are illustrated in Figure 67.

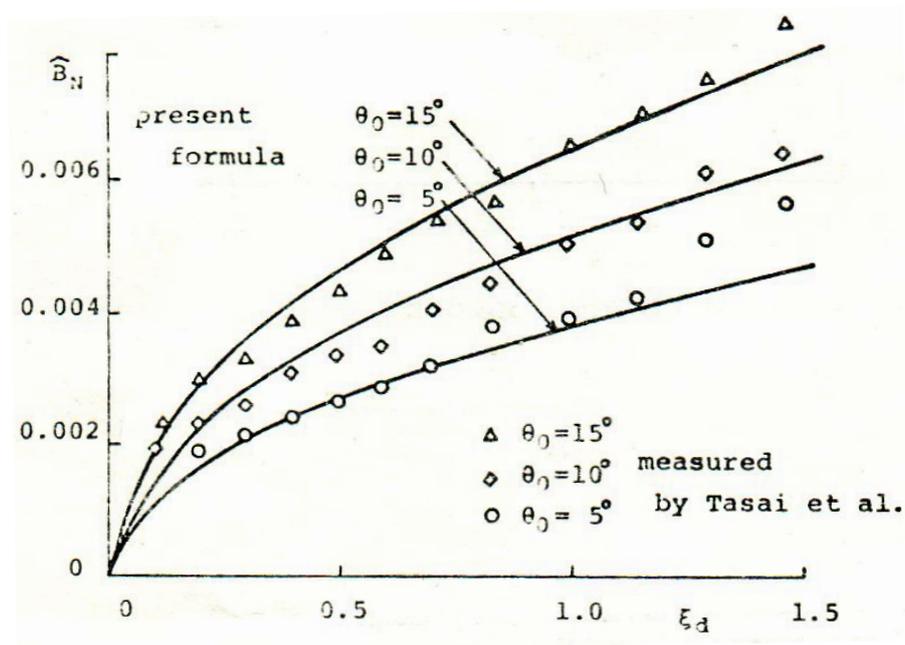


Figure 65: Figure found in Ikeda [16, p. 10]. Damping coefficient  $B_N$  due to the normal force of bilge keels

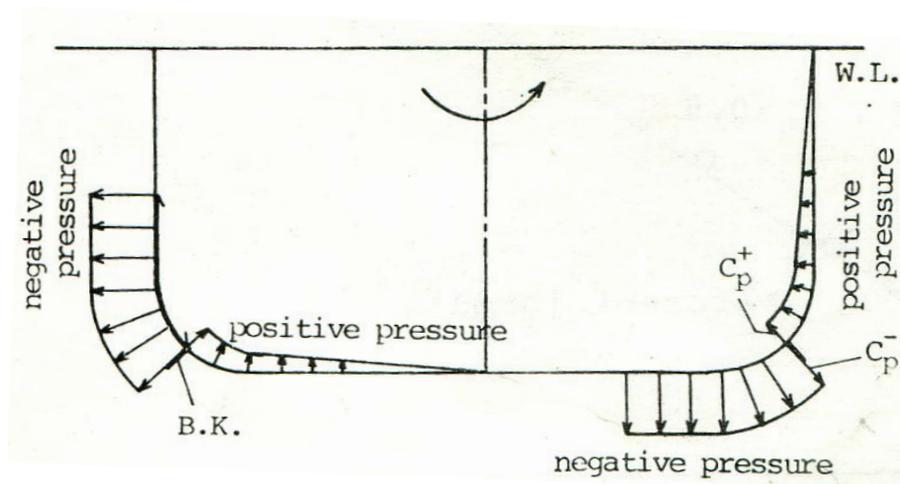


Figure 66: Figure found in Ikeda [17, p. 9]. Change in hull pressure due to bilge keels

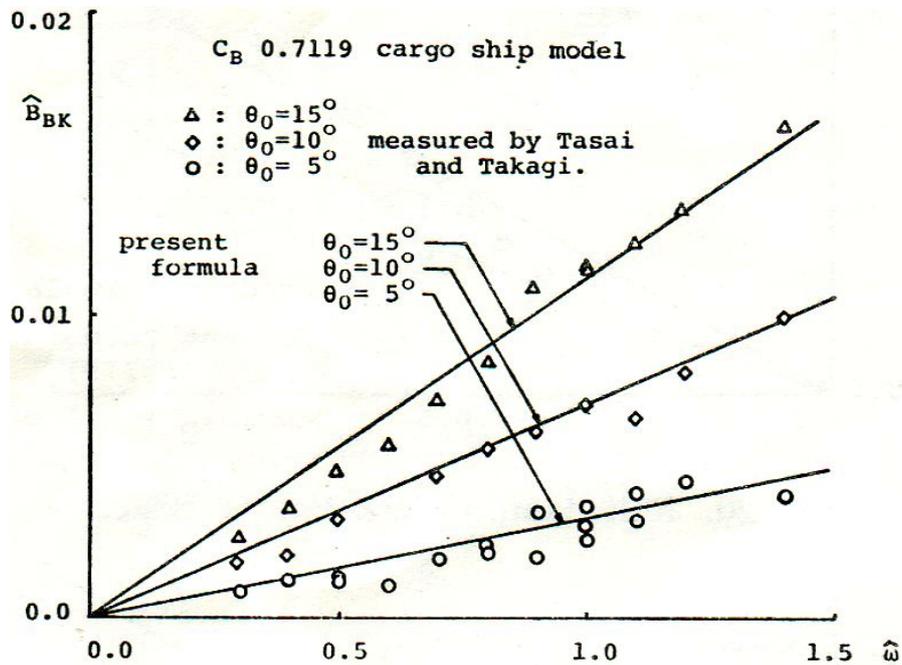


Figure 67: Figure found in Ikeda [17, p. 10]. Roll damping coefficient  $B_{BK}$  due to bilge keels

### 3.4.3 Case

The following case is presented with the intention of investigating the effect that the swell sea has on the operational potential of vessel, and in this case a *PSV* with length 90 metres, breadth 21 metres and draught 6 metres has been employed.

The roll response is investigated by using *DSM*. A *RAO* with and without an anti-roll tank for the *PSV* is shown Figures 68 and 69, respectively. These *RAO*'s have been handed to the author by professor Sverre Steen of the Department of Marine Technology. These have been generated by the software *ShipX*, a software which performs hydrodynamic analysis. An anti-roll tank has been added to the ship in the second *RAO* (Figure 69). The curve shows that the roll response is smaller with an anti-roll tank than without. Furthermore, one can observe that some of the directions coincide in the same curve due to symmetry around the y-axis of the vessel (see Figure 47 for reference). For example, the blue curve in Figure 68, which corresponds to waves coming in at a  $30^\circ$  angle, lies behind the curve which corresponds to waves coming in at an angle of

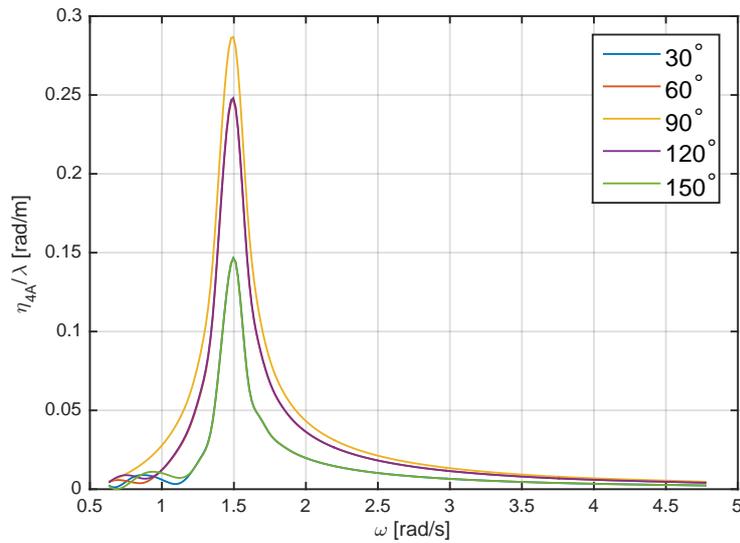


Figure 68: RAO without anti-roll tank

150°. Finally, because the vessel is symmetric around the x-axis, waves coming in at starboard and port will produce the same roll response. Therefore, roll response on only one side is studied (0 to 180°).

Wave spectrums due to swell sea are established by using the Hindcast. Wind sea and swell sea is represented by each their values of  $H_s$ , and corresponding directions. This implies that it is possible to determine the angle of attack of the swell sea if we assume that the bow of the ship is turned straight against the wind sea.

The following text presents the roll response which is caused by the swell sea alone, and what effect this roll response has on the operational potential of the vessel.

**Roll motion due to swell sea** The following assumptions were made in order to investigate roll response due to swell sea:

1. Wind sea is assumed to have no effect on roll, because the bow of the ship is always pointed straight towards the direction of the wind sea. In reality this is not correct. Since the wind sea is short crested, there will be waves from wind sea which do not come in straight at the bow, hence some of the waves from the wind

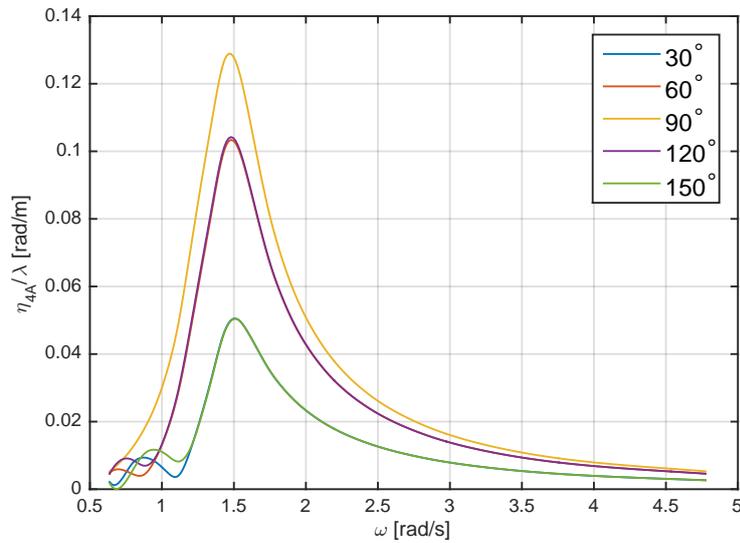


Figure 69: RAO with anti-roll tank

sea will contribute to roll.

2. *RAO's* for the vessel are not continuous. Because of this, the side of the ship has been discretized into sectors, and therefore there will be discretization errors.

Even though the assumptions above can lead to incorrect results, the results should be good enough in order to investigate any tendencies due to swell sea.

The calculations were carried out using a *MATLAB* script, and the script is found in the folder "Rolling due to swell sea". The algorithm can be described by the following steps:

1. *RAO's* are fetched from a *.mpl* file produced by *ShipX*. First, all points on the curves are multiplied by the wave number  $k$  in order to obtain the unit which is sought for. Secondly, due to very few points on the graph, it is interpolated, giving the graphs in Figure 68 and 69.
2. The angle between swell and wind sea is determined. This angle is assumed to produce roll. These values are fetched from the Hindcast data.

3. Swell angles are investigated in order to determine which *RAO* is used in order to calculate response. *RAO*'s are discretized into sectors.
4. For each swell angle the corresponding value of  $H_s$  (i.e.  $H_s$  found for swell sea) is used to produce a wave spectrum,  $S(\omega)$ .
5. The response spectrum for each swell angle and its corresponding value of  $H_s$  is then calculated by  $S_{\eta_4}(\omega) = |RAO(\omega)|^2 \cdot S(\omega)$ .
6. Finally, the standard deviation of the response spectrum is obtained:  $\sigma_{\eta_4} = \sqrt{\int_0^{\infty} S_{\eta_4}(\omega) d\omega}$ . Since there are 166053 observations in the hindcast data, 166053 values of  $\sigma_{\eta_4}$  are produced.

As stated in 3, the *RAO*'s are discretized into sectors (each *RAO* covers a sector):

$$\begin{aligned}
(15, 45], \quad RAO &= 30^\circ \\
(45, 75], \quad RAO &= 60^\circ \\
(75, 105], \quad RAO &= 90^\circ \\
(105, 135], \quad RAO &= 120^\circ \\
(135, 165], \quad RAO &= 150^\circ
\end{aligned}$$

The *RAO* which is chosen in order to determine  $S_{\eta_4}(\omega)$ , is dependant on which sector the swell angle (relative to the wind sea angle) lies in.

In 1, the *RAO*'s are multiplied by the wave number  $k$ . The original unit of the *RAO*'s,  $\frac{\eta_{4A}}{\lambda k}$  [rad], leads to values with an undesired unit. Since the variance of the roll process is given as  $\sigma_{\eta_4}^2 = \int_0^{\infty} S_{\eta_4}(\omega) d\omega$ , we know that the unit of  $S_{\eta_4}(\omega)$  should be  $rad \cdot s$  because

$$\begin{aligned}
\sigma_{\eta_4}^2 &= \int_0^{\infty} S_{\eta_4}(\omega) d\omega = rad \cdot s \frac{rad}{s} = rad^2, \\
\rightarrow \sigma_{\eta_4} &= rad
\end{aligned} \tag{81}$$

Radians is the desired unit of the standard deviation. We also know that the wave spectrum  $S(\omega)$  has the unit  $\frac{m^2 s}{rad}$ , i.e. the desired unit of  $RAO$  is decided by considering

$$S_{\eta_4}(\omega) = RAO(\omega)^2 S(\omega)$$

$$rad\ s = RAO(\omega)^2 \frac{m^2\ s}{rad}$$

$$\rightarrow RAO(\omega) = \frac{rad}{m} \quad (82)$$

$$(83)$$

The original  $RAO$  is found in appendix B.

Figure 70 show how  $\sigma_{\eta_4}$  varies with the adjusted swell sea direction. There are 166053 values in the figure, meaning that the observations stack on top of each other. The figure shows that  $\sigma_{\eta_4}$  increases with increasing angle up until approximately somewhere between 75 and 105 degrees, while it decreases after this. This is as expected: swell waves which come towards the ship close to 90 degrees will produce larger roll amplitudes than waves which come in close to the bow or stern. This is understood by considering the  $RAO$ 's. The response is also dependant on  $H_s$  and  $T_p$  which is used to create the wave spectrum. This is elaborated in the next section.

Figures 71 and 72 show the distribution of adjusted swell sea direction and  $\sigma_{\eta_4}$ . Figures 73 and 74 show the distribution of swell sea  $H_s$  and  $T_p$ . There is an inconsistency in Figure 73, and this is probably due to the problems regarding polarized values of  $T_p$ . It seems as if the modifications have not been able fix the problem sufficiently. At last, some results are given in Table 26.

Table 26: Average values of standard deviation of roll due to swell sea.  $\eta_{4ac} = 4^\circ$

Angle	Average $\sigma_{\eta_4}$ [deg]	Extreme values of $\sigma_{\eta_4}$ [deg]
All	1.12	13.83
30°	0.53	4.47
60°	1.25	8.02
90°	1.67	13.75

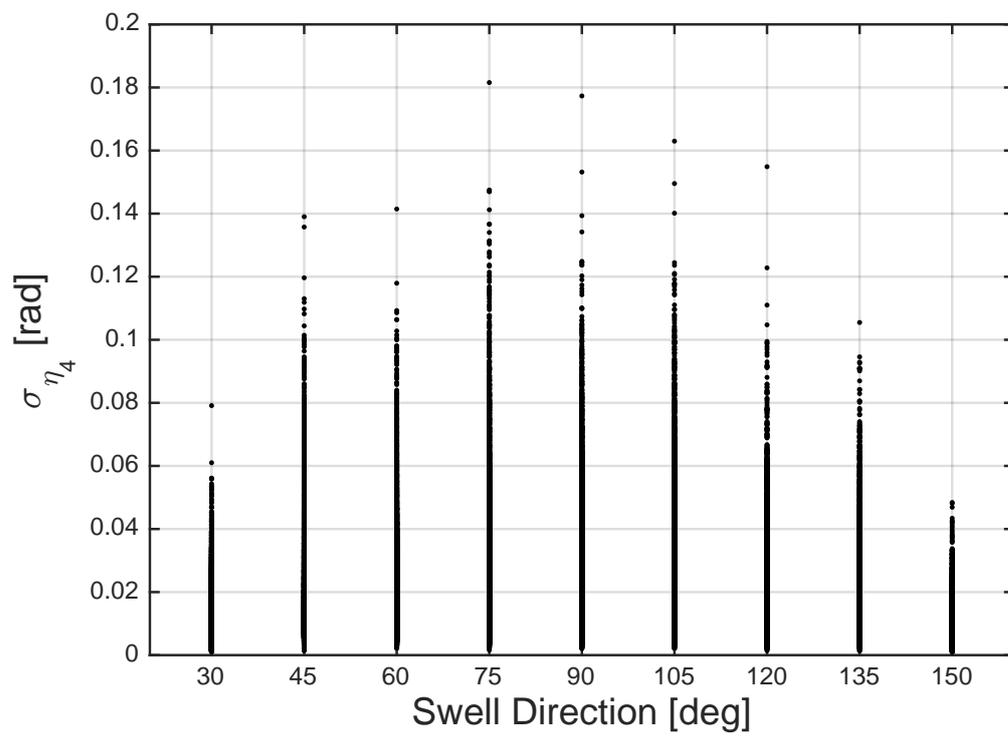


Figure 70: Adjusted swell direction versus  $\sigma_{\eta_4}$

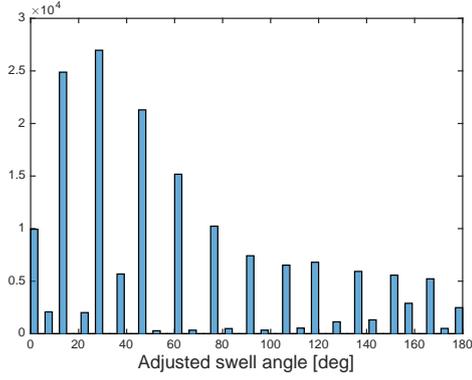


Figure 71: Distribution of adjusted swell sea direction

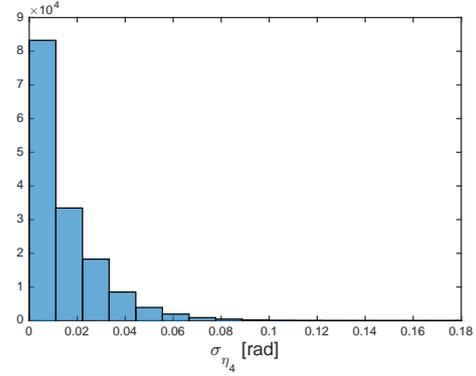


Figure 72: Distribution of  $\sigma_{\eta_4}$

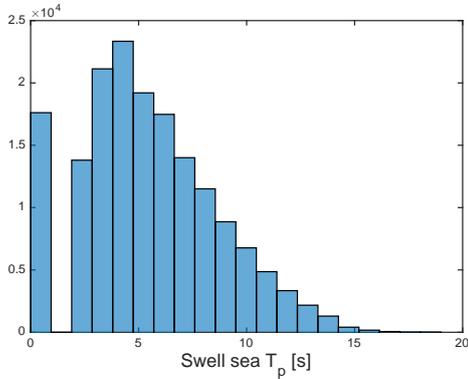


Figure 73: Distribution of swell sea  $T_p$

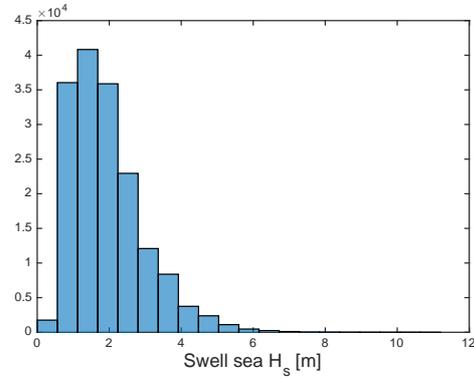


Figure 74: Distribution of swell sea  $H_s$

**Usability of good weather windows, taking roll response due two swell sea into consideration** The outline of the master thesis suggest investigating how often a good weather window is made unusable due to rolling caused by swell sea. The evaluation which is presented in the following is a prediction of a vessels ability to perform an operation in a particular month, based on two requirements, namely the significant wave height  $H_s$  (total sea) and the roll motion due to swell sea. The *MATLAB* script employs the following sequence in order to predict the usability of a good weather window:

$$if \quad H_s \leq H'_s \quad AND \quad \sigma_{\eta_4} \leq \frac{\eta_{4ac}}{\sqrt{-2 \ln [1 - (1 - q)(1/N)]}} \quad (84)$$

$\rightarrow$  sea state is acceptable

This check is performed for every observation in the Hindcast data (each row). Sequences of observations fulfilling or not fulfilling the requirements above are then established in the same manner as for the calms in Section 2.8.1. The average duration of these operational windows, taking roll into account, is then found by taking the total number of hours where the criterias are fulfilled and divided by the total number of sequences.

It should be pointed out that  $\sigma_{\eta_4}$  is calculated by using the swell sea together with the *RAO* (i.e. not the total sea).

The MATLAB script *rolling\_calm.m*, located in the folder "Rolling due to Swell Sea", was used to solve the task. The algorithm of the script can be described by the following steps:

1. The hindcast data which is needed is fetched:
  - (a)  $H_s$ , total sea
  - (b)  $H_s$ , swell sea
  - (c)  $T_p$ , swell sea
  - (d) Directions for wind sea and swell sea

These values are read and stored by the function *years\_with\_swell.m*.

2. *RAO*'s are fetched.
3. A *for*-loop begins: The direction of the swell sea in terms of the wind sea is determined. The *for*-loop loops through every entry in the Hindcast data.
4. Swell directions are mirrored due to the symmetry around the x-axis of the vessel.
5. The *RAO* to be used is chosen by considering which sector the swell direction lies in.
6. A wave spectrum is established. This is calculated using the swell  $H_s$  and  $T_p$ . The response spectrum for roll, due to swell, is then established from  $S_{\eta_4}(\omega) = RAO(\omega)^2 \cdot S(\omega)$ .

7. The standard deviation of the roll spectrum  $\sigma_{\eta_4}$ , and number of up zero up crossing cycles  $N$  is determined.
8. If  $H_s \leq H'_s$  and  $\sigma_{\eta_4} \leq \frac{\eta_{4ac}}{\sqrt{-2\ln[1-(1-q)^{(1/N)]}}}$ , the operational criterias are fulfilled, meaning that this observations is registered as a calm. A fixed probability of  $q = 0.1$  and a critical roll response of  $\eta_{4ac} = 4^\circ$  has been used in this case.
9. This evaluation is carried out for every observation in the Hindcast data. The observations are either calm or stormy values, and the length and number of calms are established. The calms are determined in the same manner as in section 2.8.1.
10. The average calm of every month is established by taking the total number of calm hours and dividing them by the total number of calms in each month.

The swell  $T_p$  which is used to establish the wave spectrum  $S(\omega)$  (item no.6) is modified in the same manner as the  $T_p$  values for total sea, explained in Section 2.3.2. The second equation in item no. 8 is established by using the same theory as in Section 3.1.2: The distribution function of 3-hour maximum roll is established, and if the standard deviation is below or equal to the term to the right in the equation in 8, the operational criteria is fulfilled.

A flowchart for the script which performs the analysis, *rolling\_calm.m*, is found appendix D.3.

**Discussion of results** Results are displayed in Figures 75, 76 and 77. The RAO with an anti-roll tank was used. It might seem strange to present the results as average duration of calms, because the the duration of a calm is a weather statistic, while the roll response of a vessel is not. A better description could be "usability of good weather windows". Nonetheless, it has been chosen to present the results in this manner in order make it clear how the results compare to the average duration of calms which is presented in Section 2.8.1, where the roll response due to swell sea was not considered. The thresholds which were used in these calculations were  $H'_s = 2$  metres and  $\eta_{4ac} = 4$  degrees. These choices are based on Table 10. A probability of  $q$  equal to 0.1 was used, meaning that the roll amplitude can exceed the critical roll response  $\eta_{4ac}$  10 % of the

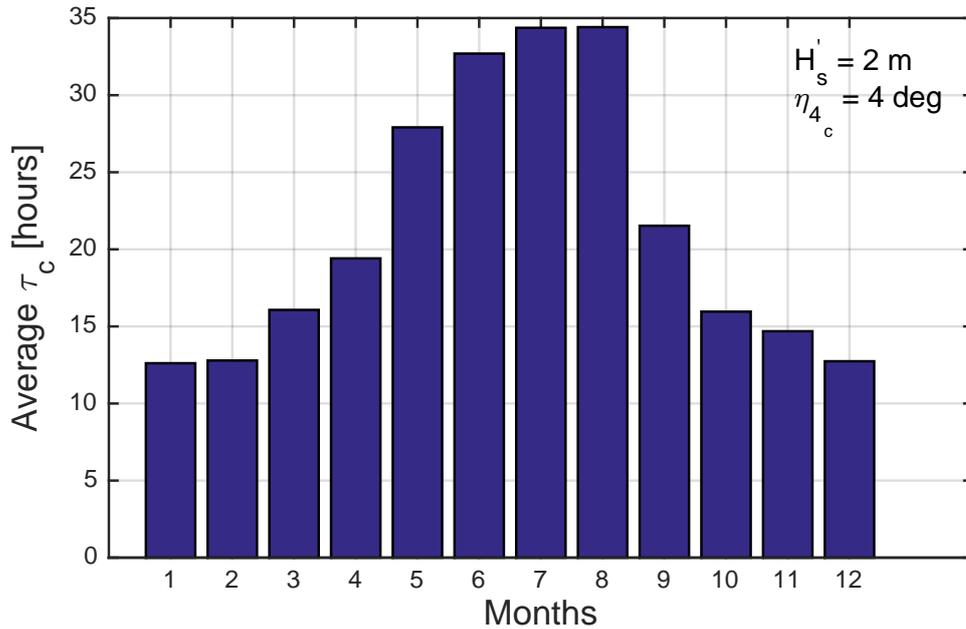


Figure 75: Calms, total sea and roll motion considered

time.

It can be seen that the results have drastically changed. For example, the average duration of a calm in July has decreased from 110 to a 34.4 hours, i.e. a reduction of roughly 70 %. In January, the average calm has been reduced from 24.5 to 12.5, 51 %. By this, one can conclude with the following: given the assumptions which have been made, the swell sea produces a roll response which has a significant effect on the ability to perform an operation which has the thresholds (limits) of  $H'_s = 2$  metres and  $\eta_{4_{ac}} = 4$  degrees.

**Lack of damping** The results are of such magnitude that they would appear to be dubious, and this is very likely due to the fact that the response spectrum method is not the best for analyzing the roll response of a vessel such as a *PSV*. The method which has been used assumes that there is a linear relationship between the input (waves) and the output (roll response) (see Section 3.1.2), which is a poor assumption, in particular for large roll amplitudes Haver [13, p. 21]. In reality, the damping increases nonlinearly when the roll amplitude is large. This is due to both viscous effects from the hull and the

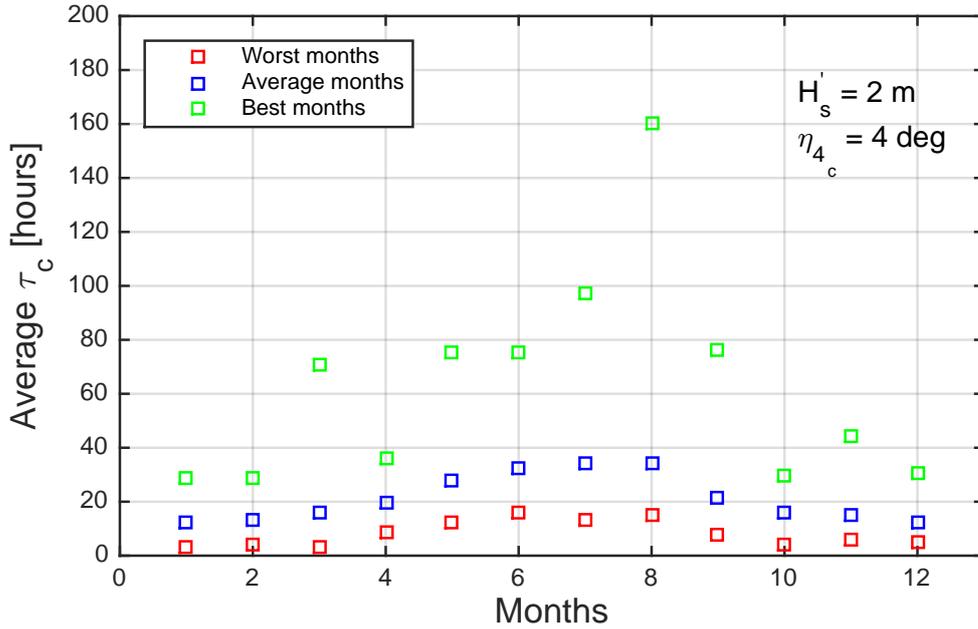


Figure 76: Worst, average and best calms, total sea and roll motion considered

fact that the vessel is generating larger outgoing waves from the vessel. The uncoupled roll equation is sometimes expressed as

$$(I_{44} + A_{44})\ddot{\eta}_4 + B_{44}\dot{\eta}_4 + B_v\dot{\eta}_4|\dot{\eta}_4| + C_{44}\eta_4 = F_4 \quad (85)$$

As we can see, the viscous damping ( $B_v$ ) is non-linear. Viscous damping is, as previously mentioned, due to skin friction and vortex shedding.

By this, one can understand that the largest roll amplitudes which have been established should be lower. If these roll amplitudes were lower, the operational criteria would be fulfilled more often, giving larger monthly average duration of calms. The results may therefore be considered as conservative.

**Critical values of  $\sigma_{\eta_4}$**  If we consider the values of  $\sigma_{\eta_4}$  which are of such magnitude that the criteria is not fulfilled (Equation 86), we can investigate these critical values

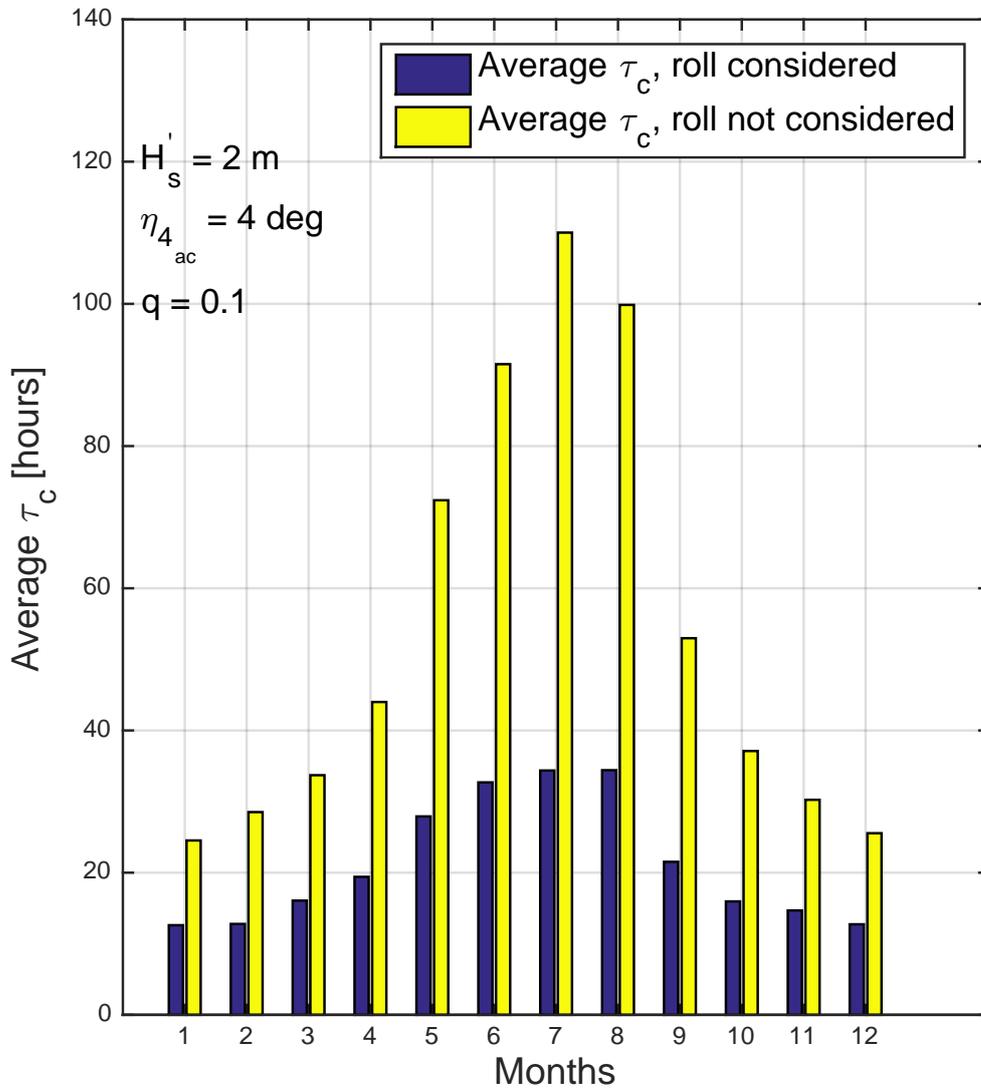


Figure 77: Average duration of a calm, both with and without roll response taken into consideration

further in order to determine any regularity or tendencies.

$$\sigma_{\eta_4} \leq \frac{\eta_{4ac}}{\sqrt{-2 \ln [1 - (1 - q)^{(1/N)}]}} \quad (86)$$

There are 46469 critical values of  $\sigma_{\eta_4}$  (values that are larger than the term to the right in the equation). This is  $\frac{46469}{166053} = 28\%$  of all hindcast values. By this, one might say that during one year, the ship will experience critical roll amplitudes due to swell 28 % of the time. Table 27 shows the distribution of the adjusted swell angle, and how often each *RAO* has been used.

Typically, the largest response of a system will occur when the frequency of the input is in the vicinity of the natural frequency of the system. It is therefore relevant to investigate the spectral frequency  $\omega_p$  of the wave spectrums  $S(\omega)$  (swell sea) which correspond to the critical values of  $\sigma_{\eta_4}$ . Figure 78 shows a histogram of  $\omega_p$  for swell sea, corresponding to critical values of  $\sigma_{\eta_4}$ . The mean value is 1.28 radians/seconds. If we compare this to the natural frequencies of the *RAO*'s (see Figure 69), roughly  $\omega_n = 1.5$  radians/seconds, these are quite close. By natural frequency of a *RAO* we mean the natural frequency in roll of the *PSV*. Since the critical values of  $\sigma_{\eta_4}$  are determined by  $\sigma_{\eta_4} = \sqrt{\int_0^\infty S_{\eta_4}(\omega) d\omega}$ , and  $S_{\eta_4}(\omega) = RAO(\omega)^2 \cdot S(\omega)$ , we can understand that *RAO*( $\omega$ ) and  $S(\omega)$  must coincide sufficiently in order to produce critical response spectrums  $S_{\eta_4}(\omega)$ . In other words, the peaks of  $S(\omega)$  and *RAO*( $\omega$ ) must lie close to each other.

Another important factor is the size of  $H_s$ . This variable decides the size of the wave spectrum  $S(\omega)$ , and a difference of one metres changes the spectrum drastically, see Figure 79. Figure 80 shows a histogram of  $H_s$  for swell sea, corresponding to critical values of  $\sigma_{\eta_4}$ . The mean of all swell sea  $H_s$  is 1.95 metres, while the mean for swell sea  $H_s$  corresponding to critical values of  $\sigma_{\eta_4}$  is equal to 2.38 metres, suggesting that it is the larger portion of swell sea waves in the hindcast data that produce critical roll amplitudes.

In summary, critical values of  $\sigma_{\eta_4}$  are produced by one of the following or the combinations of these:

Table 27: Distribution of adjusted swell angles for large values of  $\sigma_{\eta_4}$

Adjusted Swell Direction [deg]	30	45	60	75	90	105	120	135	150	Sum
Number of occurrences	2506	10700	8755	7173	5231	4657	3733	3142	572	46469
<i>RAO</i> [deg]	30	60	90	120	150					
Number of occurrences	2506	19455	17061	6875	572					46469

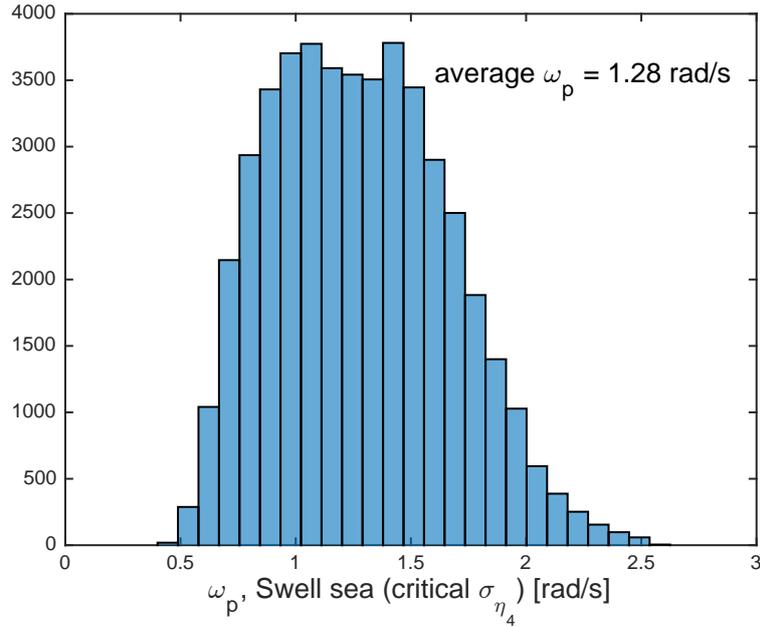


Figure 78: Swell Sea  $\omega_p$ , corresponding to critical values of  $\sigma_{\eta_4}$

1. The size of  $H_s$  is sufficiently large
2. Spectral frequency  $\omega_p$  of swell sea wave spectrum  $S(\omega)$  is sufficiently close to the natural frequency of *RAO*,  $\omega_n$
3. The direction of swell sea relative to the direction of wind sea is close to  $90^\circ$

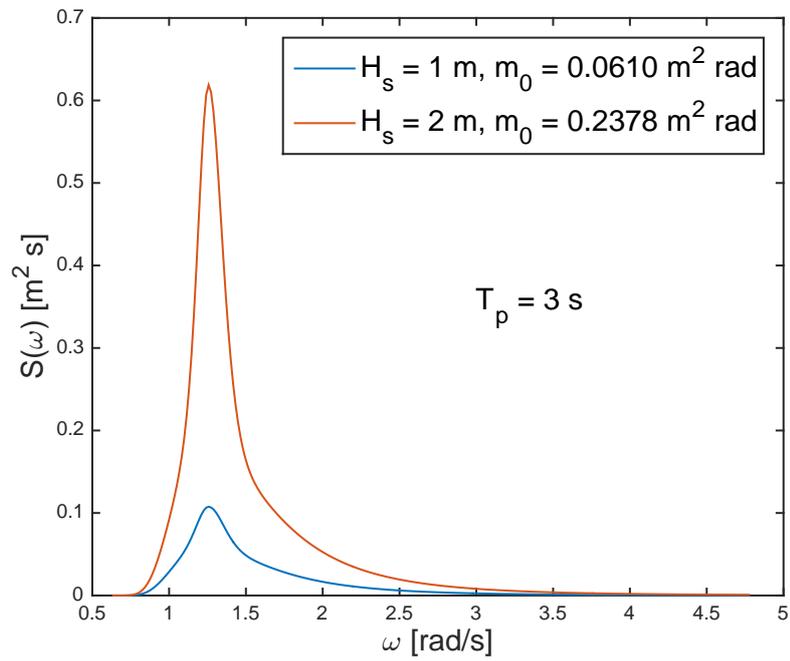


Figure 79: The effect of the size of  $H_s$  on the wave spectrum

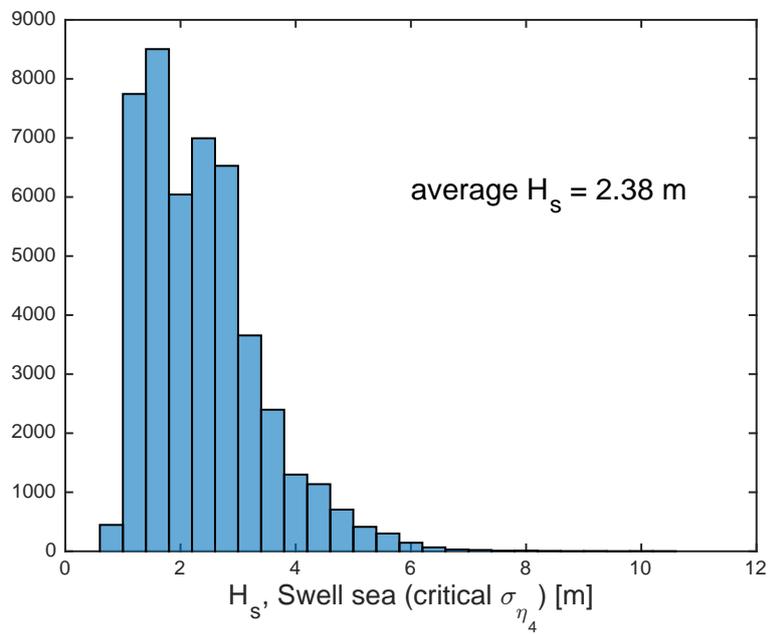


Figure 80: Swell Sea  $H_s$ , corresponding to critical values of  $\sigma_{\eta_4}$

## 4 Conclusion

The thesis has dealt with evaluation of marine operations, and these have partly been based on a Metocean Design Basis. The evaluations have been carried out partly by utilizing well known theory in terms of wave spectrums, response amplitude operators and response spectrums, while some of the theory is some what unorthodox.

**Part 1: Metocean Design Basis** Scatter diagrams were created in order to investigate tendencies of the areas of Haltenbanken and the Barents Sea. The distribution of waves in terms of direction is more even for the Barents Sea than for Haltenbanken. A short and long term description of the wave climate was established by probability distribution functions. The method of moments yielded the best results for the marginal distribution of  $H_s$ . Contour plots were also established. Finally, the duration of good and bad weather windows were produced. These were also described by a 2-parameter Weibull distribution. Almost all of the models have been established by the method of moments, which is a suitable method considering the large data sample. The results show that the climate is more severe for Haltenbanken than for Barents Sea. Both the lower and the upper range of  $H_s$  is described well, by the LoNoWe distribution and the 3 parameter Weibull distribution, respectively.

It is difficult to validate the results, especially considering that the access to other reports of relevant areas is limited. In total, no large discrepancies have been detected by the author, and the results appear satisfactory. A large amount of time has been spent on creating the *MATLAB* scripts and making sure that they do not make errors which lead to inaccurate results. There have been performed verifications at crucial points in most scripts. A deeper understanding of theory, in particular statistics and probability, and more experience is needed in order to better discuss the results.

**Part 2: Marine Operations** The procedure of determining limiting sea states was discussed by evaluating the heave response spectrum of a drill ship, operating in Haltenbanken. A plot of acceptable sea states together with relevant severe sea states was established. Here, an area of unacceptable sea states was established.

The feasibility of marine operations was investigated by simulation, where two different methods were tested. The first method employs the distribution of the duration of calms and storms. Even though the method shows potential, there are uncertainties regarding employing the distributions of the duration of calms and storms together with Monte Carlo simulation. The method with the largest accuracy is most likely the second method, which utilizes the hindcast data directly. This method is a good alternative when investigating the feasibility of an operation at an early stage.

Lastly, it was investigated what kind of impact the swell sea has on the roll response of a platform supply vessel. Results were quite noticeable. They show that the usability of good weather windows is reduced by more than 50 %. Results appear dubious, and this is most likely due to the fact that the method assumes a linear relationship between the waves and the response. By doing this we neglect the nonlinear behaviour of the roll damping. In other words, the roll damping should have been larger, yielding smaller roll amplitudes and thereby having a smaller influence on the usability of good weather windows. Although the results are inaccurate, they strongly suggest that the swell sea has significant influence on sea states which otherwise would seem more than acceptable.

## 5 Recommendations for Further Work

The Metocean report lacks information concerning wind, current and duration of weather windows in terms of the wave period. This should be established in further work. Additionally, results should be more thoroughly verified, employing statistical hypothesis tests. Further work and increased understanding of the subject on probability and statistics is needed in order to better evaluate results.

Simulation of marine operations has been particularly interesting. The method which is assumed to give the most accurate results is rather simple, while the other one, which is not a common method, could possibly have a lot of potential. The latter uses the distribution of the duration of calms and storms together with Monte Carlo simulation. Using Monte Carlo simulation in this context is interesting, and further work on this subject is exciting. One of the challenges is to incorporate the possibility of simulating with different thresholds.

The effect that the swell sea has on the roll response under seemingly suitable conditions is noticeable. Further analysis of this should be done, e.g. through computer simulation software. It is important that the software is able to fully account for the roll damping. The analysis in this project suggests that the swell sea and the effect that it has on the roll response, is a quantity which is not considered well enough during preparation of marine operations.

Lastly, there is generally a potential in terms of improving the *MATLAB* scripts. Throughout the project, the knowledge concerning programming in *MATLAB* has increased, thereby producing more accurate scripts along the way. Several of the scripts could be improved in terms of simplicity. By making them more simple, there is a smaller chance of errors. Lastly, there is also more room for stepwise verification in the scripts.

## References

- [1] Andersen, Odd Jan, (2009), *The peak period in the WAM10 hindcast archive*, Stavanger, Statoil
- [2] Baniela, Santiago I., (2008), *Roll Motion of a Ship and the Roll Stabilising Effect of Bilge Keels* In: *The Journal Of Navigation*, 2008, pp. 667-686
- [3] Bury, Karl V., (1975), *Statistical models in applied science*, London, Wiley
- [4] Bækkedal, Eivind, (2014), *Alternative methods of realizing the sea spectrum for time-domain simulation of marine structures in irregular seas*, Trondheim, Department of Marine Technology (NTNU)
- [5] Eik, Kenneth J. and Nygaard, Einar, (2003), *Statfjord Late Life Metocean Design Basis*, Stavanger, Statoil
- [6] Faltinsen, Odd, (1980), *Forelesningskompendium for FAG 81527 "Sjøbelastninger og bevegelser av skip"* Trondheim, Institutt for Marin Teknikk (NTNU)
- [7] Faltinsen, Odd, (1990), *Sea Loads*, Cambridge University Press
- [8] Faltinsen, Odd M. and Timokha, Alexander N., (2009), *Sloshing*, Cambridge University Press
- [9] Haver, Sverre (sverrekhaver@gmail.com), 17th of July, 2015, *Problems installing deck at Kvitebjorn*
- [10] Haver, Sverre, (2011), *Prediction of Characteristic Response for Design Purposes (PRELIMINARY VERSION)*, Stavanger, Statoil
- [11] Haver, Sverre, (-), *BB 6-1 Characteristic environmental load for quasi-static behaving jacket*, Trondheim, Department of Marine Technology (NTNU)
- [12] Haver, Sverre, (-), *BB 6-3 Prediction of q annual probability wave height*, Trondheim, Department of Marine Technology (NTNU)
- [13] Haver, Sverre, (2014), *Description of Metocean Characteristics for Planning of Marine Operations*,

- [14] Himeno, Yoji, (1981), *Prediction of ship roll damping - state of the art*, Michigan, The Department of Naval Architecture and Marine Engineering
- [15] Hindcast, *Backtesting* [Internet], Wikipedia, Available at <http://en.wikipedia.org/wiki/Backtesting#Hindcast> [Read: 20.07.2015]
- [16] Ikeda, Yoshiho, (1978), *On roll damping force of ship - Effect of Friction of Hull and Normal force of Bilge Keels*, In: Journal of The Kansai Society of Naval Architects, No. 161, Japan
- [17] Ikeda, Yoshiho, (1979), *On roll damping force of ship - effect of hull surface pressure created by bilge keels*, In: Journal of The Kansai Society of Naval Architects, No. 165, Japan
- [18] Larsen, Carl M., (2011), *Lecture notes for use in the course MAS128 Design for marine environment*, Trondheim, Department of Marine Technology (NTNU)
- [19] Laverton, Edward, (2014), *Metocean Description of Haltenbanken and Barents Sea*, Trondheim, Department of Marine Technology (NTNU)
- [20] Leira, Bernt J., (2010), *TMR4235 Stochastic Theory of Sealoading: Probabilistic modelling and estimation*, Trondheim, Department of Marine Technology (NTNU)
- [21] Metocean, *Metocean* [Internet], Definition.of, Available at <http://www.definition-of.com/Metocean> [Read: 23.06.2015]
- [22] Moments of 2 parameter Weibull distribution, *Weibull distribution* [Internet], Wikipedia, Available at [https://en.wikipedia.org/wiki/Weibull\\_distribution](https://en.wikipedia.org/wiki/Weibull_distribution) [Read: 8.06.2015]
- [23] Myrhaug, Dag, (2007), *TMR 4180 Marin Dynamikk, Uregelmessig sjø*, Trondheim, Institutt for Marin Teknikk (NTNU)
- [24] Nielsen, Finn Gunnar, (2007), *Lecture Notes in Marine Operations*, Trondheim/Bergen, Department of Marine Hydrodynamics (NTNU)

- [25] NORSOK standard N-003, (2008), *Action and Action Effects, Edition 2, September 2007*, The Society of Naval Architects and Marine Engineers
- [26] Oljefakta, *Kvitebjorn feltet* [Internet], Petro Media News, Available at <http://oljefakta.petro.no/felt/kvitebjorn> [Read: 14.07.2015]
- [27] Pettersen, Bjørnar, (2007), *TMR 4247, Marin teknikk, Hydrodynamikk*, Trondheim, Institutt for Marin Teknikk (NTNU)
- [28] Resonance, *Resonance* [Internet], Wikipedia, Available at <https://en.wikipedia.org/wiki/Resonance> [Read: 11.06.2015]
- [29] Walpole, Myers, Myers, Ye, (2007), *Probability & Statistics for Engineers and Scientists*, Pearson

# Appendices

A Outline of Master Thesis

Title: **Modelling of Metocean Conditions for the Purpose of Planning Marine Operations**

Student: Edward Laverton

## **Background**

A safe execution of a marine operation requires that governing load effects are kept well below the critical values. Governing load effects can be the hook load of a crane operation, it can be motions of vessel used for the operation or it can be load in the crane structure. Common for these load effects is that they are caused by the waves. This means that all cases we can replace the criteria regarding critical load effect by a critical sea condition, e.g. requiring that the significant wave height to be lower than a certain value during the length of the operation. The criteria can be optimized by also including spectral peak period in addition to the significant wave height. In principle wind can also represent a limiting quantity regarding the execution of an operation, but in this theses focus will be a wave governed operation.

The aim of the theses is to present a metocean description being convenient for the planning of a marine operation where significant wave height,  $h_s$ , is lower than a certain threshold  $h_0(t_p)$  for at least a duration  $d_0$ .

Available weather data will be data from the Norwegian hindcast data base, NORA10. For the theses data from Haltenbanken and Barents Sea are made available.

Below a possible division into sub-tasks is given.

1. Discuss a particular operation where the critical variable is heave 20m aft of midship and indicate how one can establish a limiting pair of  $h_s$  and  $t_p$  from the critical heave motion.
2. Introduce the available metocean data and present a summary of the metocean condition for the selected area. Base this on the work done in the project.
3. Define good weather window and estimate the average duration of good weather windows for various limiting values of  $h_s$ . Do this for all months. Find a proper distribution function of the duration events fulfilling the requirement to  $h_s$  and  $t_p$ . Investigate the sensitivity of the distribution parameters to the limiting values of  $h_s$  and  $t_p$ .

Determine also a probabilistic modelling of the duration of “bad” weather windows. Do this for all months and for various limiting conditions. Investigate sensitivity of distribution parameters to the limiting levels.

4. Is it possible to establish a simple tool for considering the feasibility of a generic marine operation based on a monthly scatter diagram for  $h_s$  and  $t_p$  and the duration statistics for good and bad weather windows established above
5. Investigating the feasibility of the generic operation simulating the execution of the operation in the hindcast data series starting in September 1957. Do this on a monthly basis, i.e. the first day of each month. Find the total time including waiting time for each month and each year. Discuss the year to year scatter and compare feasibility with what is done in 4).
6. Rolling is often a problem in connection with marine operations. Discuss how rolling can be minimized. Is a transfer function for rolling for a vessel with anti-rolling devices available? If so assume vessel is heading towards the wind sea and calculate rolling due to the swell component. Select Haltenbanken for this study. Is it important to account for the difference in direction between wind sea and swell. How often is a good weather window made unusable due to rolling.
7. Summarize the investigation in conclusions pointing out major learnings of this investigation.

The candidate may of course select another scheme as the preferred approach for solving the requested problem. He may also other subjects than those mentioned above.

The work may show to be more extensive than anticipated. Some topics may therefore be left out after discussion with the supervisor without any negative influence on the grading.

The candidate should in his report give a personal contribution to the solution of the problem formulated in this text. All assumptions and conclusions must be supported by mathematical models and/or references to physical effects in a logical manner. The candidate should apply all available sources to find relevant literature and information on the actual problem.

The report should be well organised and give a clear presentation of the work and all conclusions. It is important that the text is well written and that tables and figures are used to support the verbal presentation. The report should be complete, but still as short as possible.

The final report must contain this text, an acknowledgement, summary, main body, conclusions, suggestions for further work, symbol list, references and appendices. All figures, tables and equations must be identified by numbers. References should be given by author and year in the text, and presented alphabetically in the reference list. The report must be submitted in two copies unless otherwise has been agreed with the supervisor.

The supervisor may require that the candidate should give a written plan that describes the progress of the work after having received this text. The plan may contain a table of content for the report and also assumed use of computer resources. As an indication such a plan should be available by end of November.

From the report it should be possible to identify the work carried out by the candidate and what has been found in the available literature. It is important to give references to the original source for theories and experimental results.

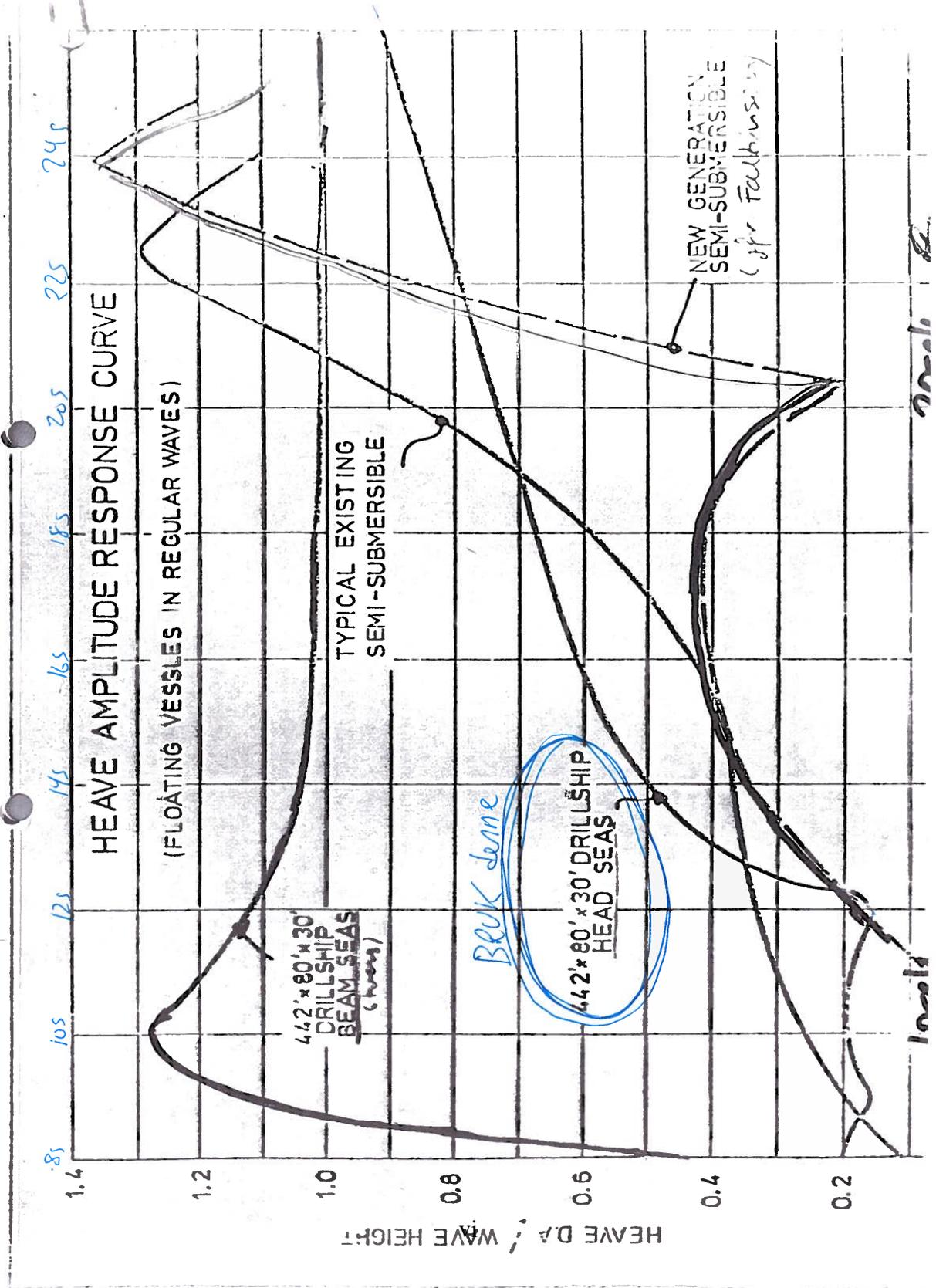
The report must be signed by the candidate, include this text, appear as a paperback, and - if needed - have a separate enclosure (binder, diskette or CD-ROM) with additional material.

Supervisor: Sverre Haver, NTNU.

Co-supervisors:

## B Response Amplitude Operators

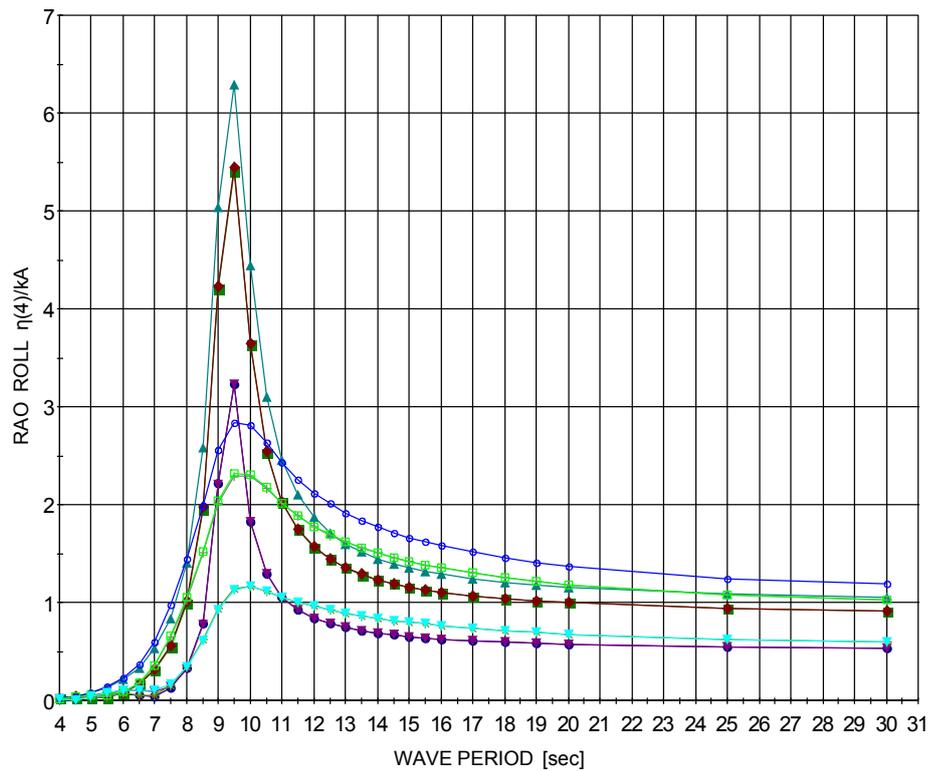
B.1 RAO, heave, drill ship



## B.2 RAO, roll, PSV

<b>RESPONSE AMPLITUDE OPERATORS</b>		ENCL.
		REPORT
		DATE 10:35:18
		REF

### DISPLACEMENTS



- For Edward - no roll tank; 0.00kn 30.0°
- For Edward - no roll tank; 0.00kn 60.0°
- ▲ For Edward - no roll tank; 0.00kn 90.0°
- ◆ For Edward - no roll tank; 0.00kn 120.0°
- ▼ For Edward - no roll tank; 0.00kn 150.0°
- \* For Edward - with roll tank; 0.00kn 30.0°
- † For Edward - with roll tank; 0.00kn 60.0°
- For Edward - with roll tank; 0.00kn 90.0°
- For Edward - with roll tank; 0.00kn 120.0°
- ▽ For Edward - with roll tank; 0.00kn 150.0°

Project: For Edward

ShipX - 09.06.2015 - 13:06:20 - Licensed to: Steen (NTNU)

## C Matlab scripts

*MATLAB* has been used throughout the whole project. All tasks have been solved partly by using scripts and functions. Some scripts use several functions created by the author. Most folders contain a script which the reader should use, named *RUN.m*. The heading of each script explains what the script does and which functions it runs. Some scripts take several minutes to run. It is important that the hindcast files in the folder "Hindcast" are added to the current path in *MATLAB*. All scripts are located in *vedlegg.zip*. The structure of the file is

1. Part 1:
  - (a) Modifications of Hindcast data
  - (b) Scatter Diagrams
  - (c) Long term distribution
  - (d) Monthly long term distributions
  - (e) 3 par Wei f\_Hs
  - (f) Contour Plot
  - (g) Weather Windows
2. Part 2:
  - (a) Establishing a Limiting Sea State
  - (b) Feasibility of Op Longest Calm
  - (c) Generic Marine Op
  - (d) Rolling due to Swell Sea
3. Hindcast:
  - (a) Heidrun (Haltenbanken)
  - (b) Barents Sea



## D.2 Flowchart for *mar\_op\_weibull.m*

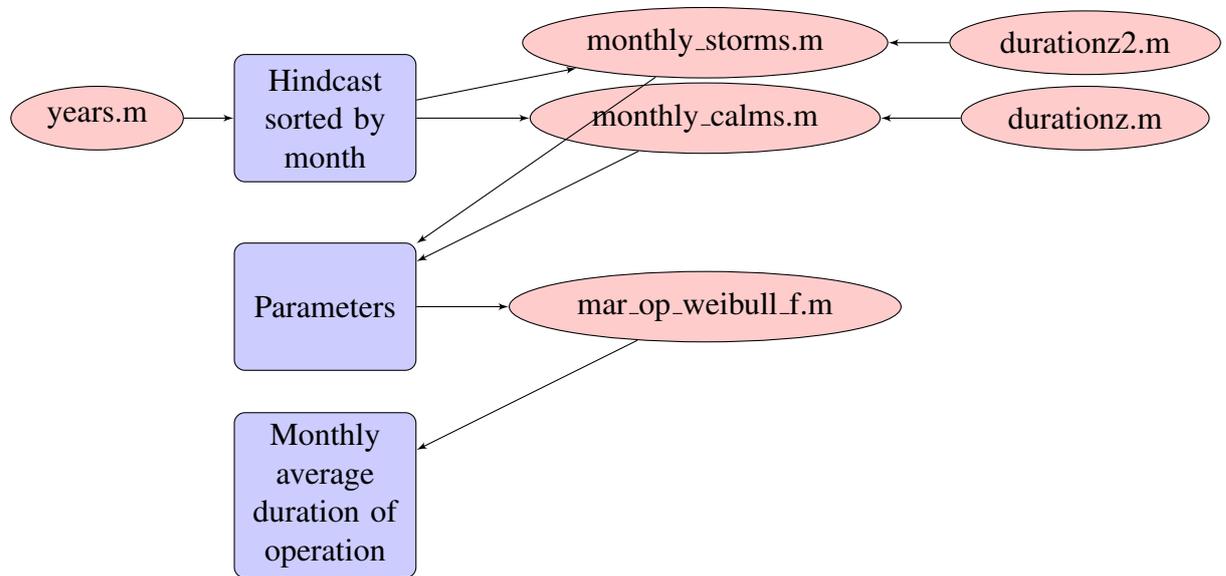


Figure 82: Flowchart for script *mar\_op\_weibull.m*

### D.3 Flowchart for *rolling\_calm.m*

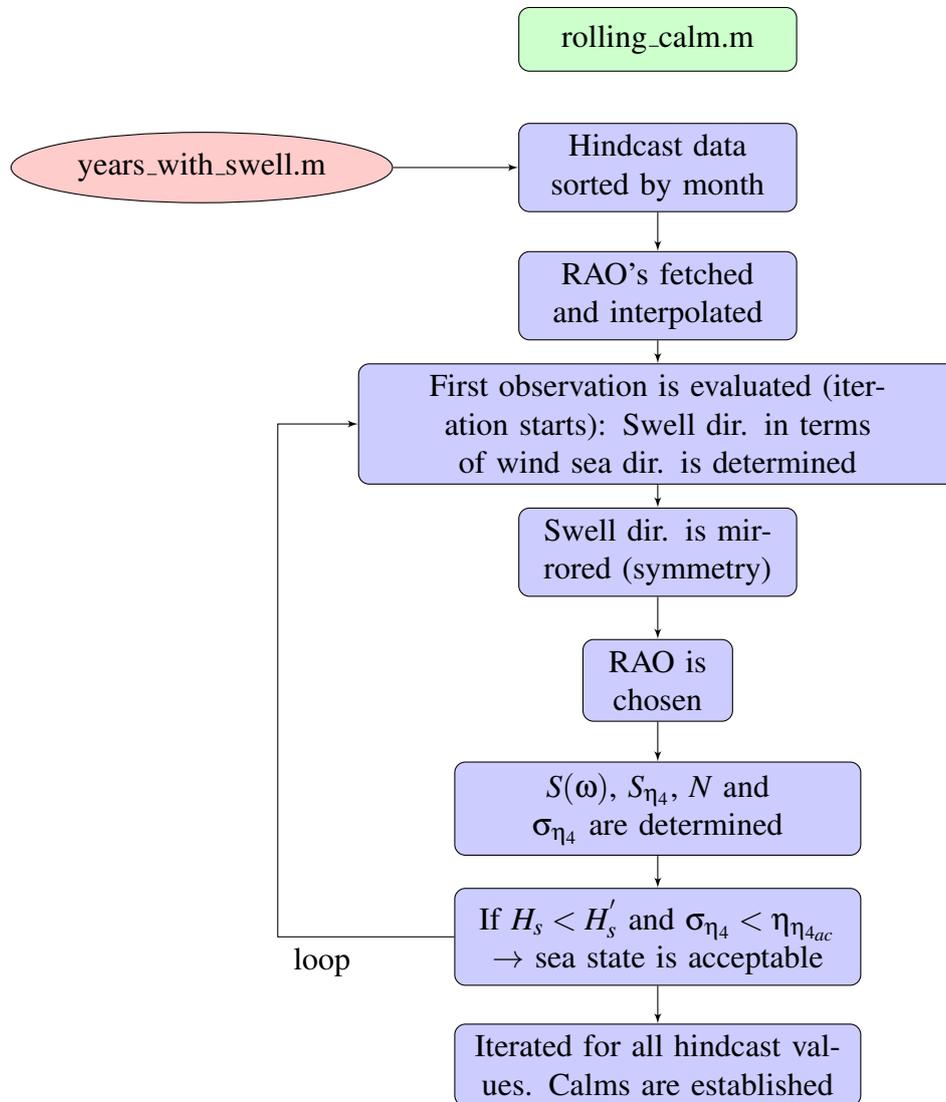


Figure 83: Flowchart for script *rolling\_calm.m*

## E Confidence Interval

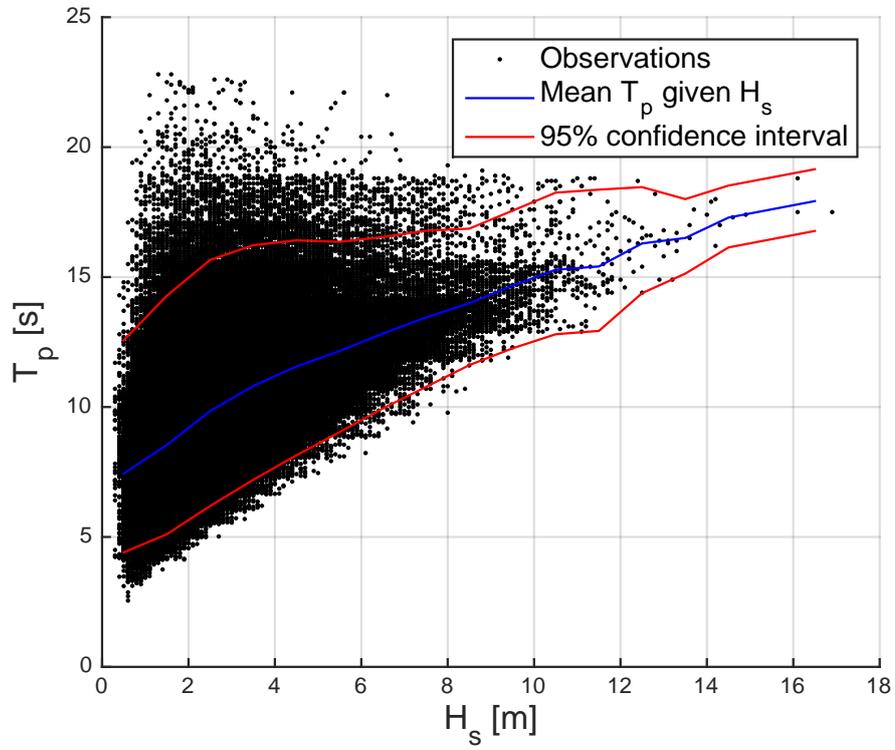


Figure 84: Confidence Intervals

## F Scatter Diagrams

Table 28: Omni Directional Scatter Diagram for Haltenbanken

		Omni Directional Scatter Diagram Haltenbanken																				SUM	
		Spectral peak period, $T_p$																					
$H_s$		2-3	3-4	4-5	5-6	6-7	7-8	8-9	9-10	10-11	11-12	12-13	13-14	14-15	15-16	16-17	17-18	18-19	19-20	20-21	21-22	22-23	
0-1	2	148	1044	1946	3106	3072	2479	1852	898	433	260	109	47	44	25	13	8	4	4	0	0	0	15494
1-2	0	13	1180	4715	7178	9004	11033	9280	6148	4131	2507	1272	623	382	228	104	75	36	22	14	4	4	57949
2-3	0	0	7	454	2930	5062	5755	6786	6413	4886	3528	2114	1140	726	361	168	103	29	21	10	7	7	40500
3-4	0	0	0	4	260	1399	3378	4241	4040	3750	3007	1869	1128	731	383	181	133	21	26	5	3	3	24559
4-5	0	0	0	0	6	85	928	2024	2599	2494	1892	1326	922	551	254	155	102	13	6	2	0	0	13359
5-6	0	0	0	0	0	1	95	562	1286	1650	1445	782	495	332	192	90	66	3	6	3	0	0	7008
6-7	0	0	0	0	0	0	0	11	61	300	829	1050	612	308	213	121	71	44	4	2	0	1	3627
7-8	0	0	0	0	0	0	1	10	31	223	571	550	244	133	62	51	39	1	0	0	0	0	1916
8-9	0	0	0	0	0	0	0	0	4	48	147	364	190	107	22	21	24	1	0	0	0	0	928
9-10	0	0	0	0	0	0	0	0	0	6	27	120	135	83	28	21	11	2	0	0	0	0	433
10-11	0	0	0	0	0	0	0	0	0	0	4	25	61	41	21	14	10	0	0	0	0	0	176
11-12	0	0	0	0	0	0	0	0	0	0	0	6	20	19	9	4	5	0	0	0	0	0	63
12-13	0	0	0	0	0	0	0	0	0	0	0	0	1	10	8	2	1	0	0	0	0	0	22
13-14	0	0	0	0	0	0	0	0	0	0	0	0	0	4	3	3	0	0	0	0	0	0	10
14-15	0	0	0	0	0	0	0	0	0	0	0	0	0	1	1	2	2	0	0	0	0	0	6
15-16	0	0	0	0	0	0	0	0	0	0	0	0	0	0	0	0	0	0	0	0	0	0	0
16-17	0	0	0	0	0	0	0	0	0	0	0	0	0	0	0	1	2	0	0	0	0	0	3
SUM	2	161	2231	7119	13480	18623	23680	24816	21719	18450	14438	9149	5314	3377	1718	901	625	114	87	34	15	15	166053

Table 29: Omni Directional Scatter Diagram for Barents Sea

$H_s$		Omni Directional Scatter Barents Sea																							SUM
		Spectral peak period, $T_p$																							
		2-3	3-4	4-5	5-6	6-7	7-8	8-9	9-10	10-11	11-12	12-13	13-14	14-15	15-16	16-17	17-18	18-19	19-20	20-21	21-22	22-23			
0-1	12	672	4690	7825	5719	2718	1450	1268	918	666	401	274	159	110	67	29	25	12	10	4	2	27031			
1-2	0	41	2089	9685	16046	14329	8291	4729	2891	2339	2014	1386	794	575	341	168	145	61	55	24	16	66019			
2-3	0	0	14	584	5752	10089	7376	4873	2979	2107	1677	1326	756	537	325	186	114	49	55	16	8	38823			
3-4	0	0	0	0	277	2374	5440	3940	2061	1467	1084	863	534	394	215	108	79	11	18	7	8	18880			
4-5	0	0	0	0	2	73	1313	2592	1758	974	690	545	342	247	140	52	48	7	6	3	2	8794			
5-6	0	0	0	0	0	1	95	674	1027	744	460	315	229	129	79	30	27	3	4	0	0	3817			
6-7	0	0	0	0	0	0	2	85	279	353	375	225	160	93	47	19	19	1	0	0	0	1658			
7-8	0	0	0	0	0	0	2	37	102	165	149	99	63	17	14	3	0	0	0	0	0	651			
8-9	0	0	0	0	0	0	0	2	15	43	80	42	25	13	6	4	0	0	0	0	0	230			
9-10	0	0	0	0	0	0	0	0	0	1	7	32	17	21	7	5	8	0	0	0	0	98			
10-11	0	0	0	0	0	0	0	0	0	1	0	7	8	5	4	6	1	0	0	0	0	32			
11-12	0	0	0	0	0	0	0	0	0	0	0	0	0	4	3	1	1	0	0	0	0	9			
12-13	0	0	0	0	0	0	0	0	0	0	0	0	0	2	0	1	3	0	0	0	0	6			
13-14	0	0	0	0	0	0	0	0	0	0	0	0	0	0	0	2	2	0	0	0	0	4			
14-15	0	0	0	0	0	0	0	0	0	0	0	0	0	0	0	1	0	0	0	0	0	1			
15-16	0	0	0	0	0	0	0	0	0	0	0	0	0	0	0	0	0	0	0	0	0	0			
16-17	0	0	0	0	0	0	0	0	0	0	0	0	0	0	0	0	0	0	0	0	0	0			
SUM	12	713	6793	18094	27796	29584	23967	18163	11952	8769	6916	5202	3140	2205	1258	628	479	144	148	54	54	166053			

Table 30: Scatter Diagram, sector 1(north),  $-15^\circ$  to  $15^\circ$ , for Haltenbanken

		Scatter Diagram, Haltenbanken, Northern Sector																						SUM
		Spectral Peak Period, $T_p$																						
$H_s$		2-3	3-4	4-5	5-6	6-7	7-8	8-9	9-10	10-11	11-12	12-13	13-14	14-15	15-16	16-17	17-18	18-19	19-20	20-21	21-22	22-23		
0-1	0	19	159	477	836	723	336	145	61	30	12	7	3	0	2	0	0	0	1	1	0	0	2812	
1-2	0	0	95	516	1335	2081	2428	1865	755	259	104	56	32	22	10	1	3	0	0	0	2	0	9564	
2-3	0	0	0	11	140	510	899	1233	1202	793	290	48	35	22	13	6	3	1	0	0	1	0	5207	
3-4	0	0	0	0	1	33	238	489	556	480	324	92	37	10	6	4	2	0	0	0	0	0	2272	
4-5	0	0	0	0	0	0	0	24	158	261	277	213	83	28	4	6	2	0	0	0	0	0	1056	
5-6	0	0	0	0	0	0	0	0	16	82	121	118	59	16	3	1	0	0	0	0	0	0	416	
6-7	0	0	0	0	0	0	0	0	1	13	49	72	26	4	1	1	0	0	0	0	0	0	167	
7-8	0	0	0	0	0	0	0	0	0	1	9	36	20	5	1	1	0	0	0	0	0	0	73	
8-9	0	0	0	0	0	0	0	0	0	0	1	1	8	8	2	1	0	0	0	0	0	0	21	
9-10	0	0	0	0	0	0	0	0	0	0	1	0	3	2	1	0	0	0	0	0	0	0	7	
10-11	0	0	0	0	0	0	0	0	0	0	0	0	1	2	1	1	0	0	0	0	0	0	5	
11-12	0	0	0	0	0	0	0	0	0	0	0	0	0	3	1	0	0	0	0	0	0	0	4	
12-13	0	0	0	0	0	0	0	0	0	0	0	0	0	0	0	0	0	0	0	0	0	0	0	
13-14	0	0	0	0	0	0	0	0	0	0	0	0	0	0	0	0	0	0	0	0	0	0	0	
14-15	0	0	0	0	0	0	0	0	0	0	0	0	0	0	0	0	0	0	0	0	0	0	0	
15-16	0	0	0	0	0	0	0	0	0	0	0	0	0	0	0	0	0	0	0	0	0	0	0	
16-17	0	0	0	0	0	0	0	0	0	0	0	0	0	0	0	0	0	0	0	0	0	0	0	
SUM	0	19	254	1004	2312	3347	3925	3907	2931	2020	1170	403	175	68	42	13	8	2	1	3	0	0	21604	

Table 31: Scatter Diagram, sector 7(south), 165° to 195°, for Haltenbanken

		Scatter Diagram, Haltenbanken, Southern Sector																						SUM
		SPECTRAL PEAK PERIOD, $T_p$																						
$H_s$		2-3	3-4	4-5	5-6	6-7	7-8	8-9	9-10	10-11	11-12	12-13	13-14	14-15	15-16	16-17	17-18	18-19	19-20	20-21	21-22	22-23		
0-1	0	10	25	35	26	43	43	39	25	12	14	0	0	1	1	1	1	0	0	0	0	0	275	
1-2	0	0	56	148	128	87	114	172	178	157	96	67	24	14	11	8	3	1	1	1	1	0	1266	
2-3	0	0	1	41	159	181	62	110	123	120	136	81	46	15	13	5	3	2	2	1	0	0	1101	
3-4	0	0	0	1	39	153	110	44	53	84	84	83	60	27	10	9	8	1	2	0	1	0	769	
4-5	0	0	0	0	1	28	118	54	22	24	37	48	58	24	6	10	3	1	1	1	0	0	436	
5-6	0	0	0	0	0	1	22	41	11	8	22	12	17	9	10	2	3	0	0	0	0	0	158	
6-7	0	0	0	0	0	0	8	9	8	6	9	12	7	7	6	2	3	0	0	0	0	0	77	
7-8	0	0	0	0	0	0	1	4	4	0	1	6	3	1	1	0	0	0	0	0	0	0	21	
8-9	0	0	0	0	0	0	0	0	2	0	0	1	0	0	0	0	1	0	0	0	0	0	4	
9-10	0	0	0	0	0	0	0	0	0	0	0	0	0	0	1	0	0	0	0	0	0	0	1	
10-11	0	0	0	0	0	0	0	0	0	0	0	0	0	0	0	0	0	0	0	0	0	0	0	
11-12	0	0	0	0	0	0	0	0	0	0	0	0	0	0	0	0	0	0	0	0	0	0	0	
12-13	0	0	0	0	0	0	0	0	0	0	0	0	0	0	0	0	0	0	0	0	0	0	0	
13-14	0	0	0	0	0	0	0	0	0	0	0	0	0	0	0	0	0	0	0	0	0	0	0	
14-15	0	0	0	0	0	0	0	0	0	0	0	0	0	0	0	0	0	0	0	0	0	0	0	
15-16	0	0	0	0	0	0	0	0	0	0	0	0	0	0	0	0	0	0	0	0	0	0	0	
16-17	0	0	0	0	0	0	0	0	0	0	0	0	0	0	0	0	0	0	0	0	0	0	0	
SUM	0	10	82	225	353	493	478	473	426	411	399	310	215	99	58	37	24	5	6	3	1	4108		

Table 32: Scatter Diagram, sector 4(east), 75° to 105°, for Haltenbanken

		Scatter Diagram, Haltenbanken, Eastern Sector																						SUM
		Spectral Peak Period, $T_p$																						
$H_s$		2-3	3-4	4-5	5-6	6-7	7-8	8-9	9-10	10-11	11-12	12-13	13-14	14-15	15-16	16-17	17-18	18-19	19-20	20-21	21-22	22-23		
0-1	0	12	100	45	7	11	20	14	5	5	1	0	0	0	0	0	0	0	0	1	0	0	221	
1-2	0	4	132	490	170	40	34	45	25	25	13	9	2	3	4	1	1	1	1	1	1	0	1001	
2-3	0	0	2	75	319	131	14	13	26	21	14	5	3	4	3	0	1	0	0	0	0	0	631	
3-4	0	0	0	1	33	114	29	3	4	7	3	4	0	1	0	0	0	0	0	0	0	0	199	
4-5	0	0	0	0	0	13	14	2	0	0	0	1	1	1	0	0	0	0	0	0	0	0	32	
5-6	0	0	0	0	0	0	3	6	0	0	0	0	0	1	0	0	0	0	0	0	0	0	10	
6-7	0	0	0	0	0	0	0	0	0	0	0	0	0	0	0	0	0	0	0	0	0	0	0	
7-8	0	0	0	0	0	0	0	0	0	0	0	0	0	0	0	0	0	0	0	0	0	0	0	
8-9	0	0	0	0	0	0	0	0	0	0	0	0	0	0	0	0	0	0	0	0	0	0	0	
9-10	0	0	0	0	0	0	0	0	0	0	0	0	0	0	0	0	0	0	0	0	0	0	0	
10-11	0	0	0	0	0	0	0	0	0	0	0	0	0	0	0	0	0	0	0	0	0	0	0	
11-12	0	0	0	0	0	0	0	0	0	0	0	0	0	0	0	0	0	0	0	0	0	0	0	
12-13	0	0	0	0	0	0	0	0	0	0	0	0	0	0	0	0	0	0	0	0	0	0	0	
13-14	0	0	0	0	0	0	0	0	0	0	0	0	0	0	0	0	0	0	0	0	0	0	0	
14-15	0	0	0	0	0	0	0	0	0	0	0	0	0	0	0	0	0	0	0	0	0	0	0	
15-16	0	0	0	0	0	0	0	0	0	0	0	0	0	0	0	0	0	0	0	0	0	0	0	
16-17	0	0	0	0	0	0	0	0	0	0	0	0	0	0	0	0	0	0	0	0	0	0	0	
SUM	0	16	234	611	529	309	114	83	60	58	31	19	6	10	7	1	2	1	1	2	1	0	2094	

Table 33: Scatter Diagram, sector 10(west), 235° to 265°, for Haltenbanken

$H_s$		Scatter Diagram, Haltenbanken, Western Sector																							SUM
		Spectral Peak Period, $T_p$																							
		2-3	3-4	4-5	5-6	6-7	7-8	8-9	9-10	10-11	11-12	12-13	13-14	14-15	15-16	16-17	17-18	18-19	19-20	20-21	21-22	22-23			
0-1	0	1	23	124	349	473	575	526	298	97	73	32	13	11	10	0	0	0	1	0	0	2606			
1-2	0	1	46	211	574	927	1440	1668	1367	1038	654	339	136	95	72	25	19	7	2	2	0	8623			
2-3	0	0	0	26	191	551	676	862	809	817	800	527	276	195	92	50	24	1	3	0	3	5903			
3-4	0	0	0	0	7	78	384	550	481	625	625	445	244	147	86	38	23	4	2	1	0	3740			
4-5	0	0	0	0	0	3	61	258	392	354	345	269	202	121	41	28	20	1	2	0	0	2097			
5-6	0	0	0	0	0	0	5	52	177	263	254	173	120	67	30	16	16	0	0	1	0	1174			
6-7	0	0	0	0	0	0	0	2	32	128	183	111	79	62	19	15	7	0	0	0	0	638			
7-8	0	0	0	0	0	0	0	1	0	26	72	119	69	39	17	6	7	0	0	0	0	356			
8-9	0	0	0	0	0	0	0	0	0	11	19	59	61	30	9	4	9	0	0	0	0	202			
9-10	0	0	0	0	0	0	0	0	0	0	1	22	31	24	11	8	2	0	0	0	0	99			
10-11	0	0	0	0	0	0	0	0	0	0	0	2	16	9	3	6	5	0	0	0	0	41			
11-12	0	0	0	0	0	0	0	0	0	0	0	2	5	2	3	3	1	0	0	0	0	16			
12-13	0	0	0	0	0	0	0	0	0	0	0	0	0	3	4	0	0	0	0	0	0	7			
13-14	0	0	0	0	0	0	0	0	0	0	0	0	0	1	1	2	0	0	0	0	0	4			
14-15	0	0	0	0	0	0	0	0	0	0	0	0	0	1	0	0	1	0	0	0	0	2			
15-16	0	0	0	0	0	0	0	0	0	0	0	0	0	0	0	0	0	0	0	0	0	0			
16-17	0	0	0	0	0	0	0	0	0	0	0	0	0	0	0	0	0	0	0	0	0	0			
SUM	0	2	69	361	1121	2032	3141	3919	3556	3359	3026	2100	1252	807	398	201	134	13	10	4	3	25508			

Table 34: Scatter Diagram, sector 1(north),  $-15^\circ$  to  $15^\circ$ , for Barents Sea

		Scatter Diagram, Barents Sea, Northern Sector																							SUM
		Spectral Peak Period, $T_p$																							
$H_s$		2-3	3-4	4-5	5-6	6-7	7-8	8-9	9-10	10-11	11-12	12-13	13-14	14-15	15-16	16-17	17-18	18-19	19-20	20-21	21-22	22-23			
0-1	1	41	477	903	493	204	31	45	53	50	32	29	12	4	6	1	4	0	0	2	1	1	2390		
1-2	0	1	104	860	1660	1401	606	266	108	60	86	45	42	29	25	12	10	5	2	0	0	1	5323		
2-3	0	0	0	11	349	959	733	403	145	41	29	38	26	15	11	8	4	6	3	0	0	0	2781		
3-4	0	0	0	0	5	113	402	332	112	54	22	13	8	3	4	2	2	0	1	0	0	0	1073		
4-5	0	0	0	0	0	6	48	206	105	37	10	5	5	3	2	0	0	0	0	0	0	0	427		
5-6	0	0	0	0	0	0	0	2	43	69	55	9	0	1	3	1	0	0	0	0	0	0	183		
6-7	0	0	0	0	0	0	0	0	4	22	22	7	4	3	0	0	0	0	0	0	0	0	62		
7-8	0	0	0	0	0	0	0	0	0	5	7	14	2	0	0	0	0	0	0	0	0	0	28		
8-9	0	0	0	0	0	0	0	0	0	0	1	2	3	0	0	0	0	0	0	0	0	0	6		
9-10	0	0	0	0	0	0	0	0	0	0	0	1	2	1	0	0	0	1	0	0	0	0	5		
10-11	0	0	0	0	0	0	0	0	0	0	0	0	1	0	0	0	0	0	0	0	0	0	1		
11-12	0	0	0	0	0	0	0	0	0	0	0	0	0	0	0	0	0	0	0	0	0	0	0		
12-13	0	0	0	0	0	0	0	0	0	0	0	0	0	0	0	0	0	0	0	0	0	0	0		
13-14	0	0	0	0	0	0	0	0	0	0	0	0	0	0	0	0	0	0	0	0	0	0	0		
14-15	0	0	0	0	0	0	0	0	0	0	0	0	0	0	0	0	0	0	0	0	0	0	0		
SUM	1	42	581	1774	2507	2683	1822	1299	619	327	212	142	98	57	49	23	21	11	8	1	1	2	12279		

Table 35: Scatter Diagram, sector 7(south), 165° to 195°, for Barents Sea

		Scatter Diagram, Barents Sea, Southern Sector																							SUM
		Spectral Peak Period, $T_p$																							
$H_s$		2-3	3-4	4-5	5-6	6-7	7-8	8-9	9-10	10-11	11-12	12-13	13-14	14-15	15-16	16-17	17-18	18-19	19-20	20-21	21-22	22-23			
0-1	0	35	267	470	178	60	49	55	38	27	18	9	6	2	1	0	0	0	0	0	0	0	1215		
1-2	0	6	194	1023	1322	634	229	146	142	138	103	72	29	33	25	6	5	3	3	1	2	2	4116		
2-3	0	0	3	95	821	979	264	127	72	71	55	70	38	29	22	16	9	7	6	0	0	0	2684		
3-4	0	0	0	0	53	524	595	140	46	40	27	30	20	25	15	8	3	1	2	1	0	0	1530		
4-5	0	0	0	0	0	15	275	244	44	7	13	16	12	8	10	9	5	0	2	0	1	0	661		
5-6	0	0	0	0	0	0	24	119	74	1	0	5	6	0	0	3	3	0	0	0	0	0	235		
6-7	0	0	0	0	0	0	0	22	42	11	0	0	2	1	2	2	2	0	0	0	0	0	84		
7-8	0	0	0	0	0	0	0	0	4	10	0	0	0	0	0	1	1	0	0	0	0	0	16		
8-9	0	0	0	0	0	0	0	0	0	0	0	0	0	0	0	0	0	0	0	0	0	0	0		
9-10	0	0	0	0	0	0	0	0	0	0	0	0	0	0	0	0	0	0	0	0	0	0	0		
10-11	0	0	0	0	0	0	0	0	0	0	0	0	0	0	0	0	0	0	0	0	0	0	0		
11-12	0	0	0	0	0	0	0	0	0	0	0	0	0	0	0	0	0	0	0	0	0	0	0		
12-13	0	0	0	0	0	0	0	0	0	0	0	0	0	0	0	0	0	0	0	0	0	0	0		
13-14	0	0	0	0	0	0	0	0	0	0	0	0	0	0	0	0	0	0	0	0	0	0	0		
14-15	0	0	0	0	0	0	0	0	0	0	0	0	0	0	0	0	0	0	0	0	0	0	0		
SUM	0	41	464	1588	2374	2212	1436	853	462	305	216	202	113	98	75	45	28	11	13	2	2	3	10541		

Table 36: Scatter Diagram, sector 4(east), 75° to 105°, for Barents Sea

$H_s$		Scatter Diagram, Barents Sea, Eastern Sector																						SUM
		Spectral Peak Period, $T_p$																						
		2-3	3-4	4-5	5-6	6-7	7-8	8-9	9-10	10-11	11-12	12-13	13-14	14-15	15-16	16-17	17-18	18-19	19-20	20-21	21-22	22-23		
0-1	3	95	521	605	546	248	70	10	6	11	14	9	8	5	2	2	1	0	0	0	0	0	2156	
1-2	0	9	271	958	1272	1278	713	250	96	45	39	26	15	9	6	4	7	0	0	0	0	0	4998	
2-3	0	0	2	58	506	748	623	496	209	49	14	21	14	9	11	4	3	1	0	0	2	2770		
3-4	0	0	0	0	20	217	391	344	156	49	7	4	5	5	1	0	1	0	0	0	0	0	1200	
4-5	0	0	0	0	0	7	98	193	144	73	10	3	1	2	0	0	1	0	0	0	0	0	532	
5-6	0	0	0	0	0	1	7	41	71	43	13	0	0	0	0	0	0	0	0	0	0	0	176	
6-7	0	0	0	0	0	0	1	8	13	15	10	0	0	0	0	0	0	0	0	0	0	0	47	
7-8	0	0	0	0	0	0	0	0	6	6	14	3	1	0	0	0	0	0	0	0	0	0	30	
8-9	0	0	0	0	0	0	0	0	0	2	5	0	0	0	0	0	0	0	0	0	0	0	7	
9-10	0	0	0	0	0	0	0	0	0	0	0	0	0	0	0	0	0	0	0	0	0	0	0	
10-11	0	0	0	0	0	0	0	0	0	0	0	0	0	0	0	0	0	0	0	0	0	0	0	
11-12	0	0	0	0	0	0	0	0	0	0	0	0	0	0	0	0	0	0	0	0	0	0	0	
12-13	0	0	0	0	0	0	0	0	0	0	0	0	0	0	0	0	0	0	0	0	0	0	0	
13-14	0	0	0	0	0	0	0	0	0	0	0	0	0	0	0	0	0	0	0	0	0	0	0	
14-15	0	0	0	0	0	0	0	0	0	0	0	0	0	0	0	0	0	0	0	0	0	0	0	
SUM	3	104	794	1621	2344	2499	1903	1342	701	293	126	66	44	30	20	10	13	1	0	0	0	0	11916	

Table 37: Scatter Diagram, sector 10(west), 235° to 265°, for Barents Sea

$H_s$		Scatter Diagram, Barents Sea, Western Sector																							SUM
		Spectral Peak Period, $T_p$																							
		2-3	3-4	4-5	5-6	6-7	7-8	8-9	9-10	10-11	11-12	12-13	13-14	14-15	15-16	16-17	17-18	18-19	19-20	20-21	21-22	22-23			
0-1	0	23	229	570	702	513	498	426	282	177	87	63	39	30	20	7	5	3	1	0	0	3675			
1-2	0	1	82	458	1109	1507	1562	1175	856	679	535	319	160	129	66	25	34	7	7	2	0	8713			
2-3	0	0	1	24	266	641	844	832	758	693	521	378	181	127	47	31	21	7	11	3	0	5386			
3-4	0	0	0	0	6	86	413	568	496	506	397	276	157	103	55	21	19	0	1	0	1	3105			
4-5	0	0	0	0	0	1	52	242	388	353	330	247	148	82	40	6	12	2	1	0	0	1904			
5-6	0	0	0	0	0	0	2	46	153	204	225	162	109	56	24	10	8	0	1	0	0	1000			
6-7	0	0	0	0	0	0	0	1	23	101	188	146	89	58	25	9	5	0	0	0	0	645			
7-8	0	0	0	0	0	0	0	0	0	21	63	95	72	45	11	7	1	0	0	0	0	315			
8-9	0	0	0	0	0	0	0	0	0	2	11	37	25	10	8	4	1	0	0	0	0	98			
9-10	0	0	0	0	0	0	0	0	0	1	2	13	10	10	5	4	4	0	0	0	0	49			
10-11	0	0	0	0	0	0	0	0	0	0	0	2	5	4	2	1	1	0	0	0	0	15			
11-12	0	0	0	0	0	0	0	0	0	0	0	0	0	4	3	0	1	0	0	0	0	8			
12-13	0	0	0	0	0	0	0	0	0	0	0	0	0	2	0	1	3	0	0	0	0	6			
13-14	0	0	0	0	0	0	0	0	0	0	0	0	0	0	0	2	1	0	0	0	0	3			
14-15	0	0	0	0	0	0	0	0	0	0	0	0	0	0	0	1	0	0	0	0	0	1			
SUM	0	24	312	1052	2083	2748	3371	3290	2956	2737	2359	1738	995	660	306	129	116	19	22	5	1	24923			